Effects of Cholesterol on the Bending Modulus of Membranes and the Electroporation Induced Pore Formation of Vesicles

by

Nadia Akter Mokta

MASTER OF PHILOSOPHY IN PHYSICS

Department of Physics

BANGLADESH UNIVERSITY OF ENGINEERING AND TECHNOLOGY

July, 2021

The thesis titled "Effects of Cholesterol on the Bending Modulus of Membranes and the Electroporation Induced Pore Formation of Vesicles" Submitted by Nadia Akter Mokta, Roll No. 1018143002 F, Session: October/2018, has been accepted as satisfactory in partial fulfillment of the requirement for the degree of MASTER OF PHILOSOPHY IN PHYSICS on 31 July, 2021.

BOARD OF EXAMINERS

1.	**Dr. Mohammad Abu Sayem Karal** (Supervisor) Professor Department of Physics, BUET, Dhaka	Chairman
2.	**Dr. Md. Rafi Uddin** Professor and Head Department of Physics, BUET, Dhaka	Member (Ex-officio)
3.	**Dr. Md. Forhad Mina** Professor Department of Physics, BUET, Dhaka	Member
4.	**Dr. Muhammad Samir Ullah** Associate Professor Department of Physics, BUET, Dhaka	Member
5.	**Dr. Muhammad Abdul Kadir** Associate Professor Department of Biomedical Physics & Technology University of Dhaka, Dhaka	Member (External)

CANDIDATE'S DECLARATION

It is hereby declared that this thesis or any part of it has not been submitted elsewhere for the award of any degree or diploma.

Nadia Akter Mokta

Roll No. 1018143002

Session: October, 2018

Dedicated

To

My Beloved Parents

And Teachers

Acknowledgement

Firstly, I would like to convey my utmost appreciation to my respected supervisor Professor Dr. Mohammad Abu Sayem Karal, Department of Physics, Bangladesh University of Engineering and Technology (BUET), Dhaka for choosing me as a M.Phil. thesis student and giving me the chance for doing research on membrane biophysics. In the last two years, his constant encouragement inspired me to be a better researcher and hard-working person. It was a great experience to be a part of his research team.

It is my great honor to convey my gratitude to Professor Prof. Dr. Md. Rafi Uddin, Head of the Department of Physics, BUET for his great support to move through the academic course during this degree program. I would like to express my profound appreciation to Professor Dr. Jiban Podder, Professor Dr. Md. Feroz Alam Khan, Professor Dr. A. K. M. Akther Hossain, Professor Dr. Md. Mostak Hossain, Professor Dr. Afia Begum, Professor Dr. Md. Forhad Mina, Professor Dr. Nasreen Akter, and Professor Dr. Mohammed Abdul Basith for their valuable suggestions during the submission of my research proposal in CASR, BUET. I am thankful to all other respected teachers of the Department of Physics for their kind co-operation.

I acknowledge to all my lab mates, specially Md. Kabir Ahamed, Marzuk Ahmed, Shareef Ahammed, Tawfika Nasrin, Sabrina Sharmin, Malay Kumar Sarkar Urbi Shyamolima Orchi, Md. Towhiduzzaman, Salma Akter and Sharif Hasan for their continuous encouragement and support.

I am also thankful to the authority of Department of Physics, BUET for providing me the logistic supports for this thesis work. Sincere acknowledgement to the CASR, BUET for granting funds to carry out this research. I would like to acknowledge the Prime Minister's Education Assistance Trust, Bangladesh for providing the fellowship during my M.Phil. study.

Finally, I would like to express my appreciation to my beloved parents and family members who always supported and encouraged me in my work and inspired me to do my best.

Abstract

The effects of cholesterol (chol) in the membranes of giant unilamellar vesicles (GUVs) on the size distribution of vesicles and the irreversible electroporation (IRE)-induced pore formation in GUVs were investigated. Dioleoylphosphatidylcholine (DOPC)/chol-GUVs and dioleoylphosphatidylglycerol (DOPG)/DOPC/chol-GUVs were prepared using the natural swelling method. The average sizes of GUVs were obtained from the size distribution histograms of vesicles, which were fitted by the lognormal distribution. The size of GUVs increased with the increase of chol in neutral and charged membranes. Using the theorical approach, the values of bending modulus (K_{ben}) were obtained 19.1 ± 0.1, 23.1 ± 0.1, 28.6 ± 0.01 and 31.0 ± 0.1 k_BT (here k_B is the Boltzmann constant and T is the absolute temperature) for DOPC/chol-GUVs ratios of 100/0, 85/15, 71/29 and 60/40, respectively. The values of K_{ben} were also found to increase with chol for charged membrane. IRE signal (pulsating direct current) induced lateral electric tension in the membranes of GUVs. The time dependent fraction of intact GUVs among all the examined GUVs was fitted to a single exponential decay function from where the rate constant (k_p) of pore formation was obtained. The values of k_p were obtained $(1.0 \pm 0.1)\times10^{-2}$ s^{-1} at 7.0 mN/m, $(2.9 \pm 0.3)\times10^{-2}$ s^{-1} at 8.0 mN/m, $(11.0 \pm 0.3)\times10^{-2}$ s^{-1} at 9.0 mN/m for ratio of DOPG/DOPC/chol-GUVs as 46/39/15. Similar increase of k_p was also obtained for other chol content. The estimated line tension was observed to increase from 12.9 to 14.6 pN with the corresponding increase of chol from 15 to 40 mole%. The increased energy barrier in the prepore state, due to the increase of chol, was the main factor for decreasing the k_p. Hence, the increase of K_{ben} due to chol controlled the k_p of IRE-induced pore formation in GUVs.

Contents

CHAPTER 3

MATERIALS AND METHOD

CHAPTER 4

RESULTS AND DISCUSSION

List of Figures

List of Tables

List of Symbols and Abbreviation

IRE	-	Irreversible Electroporation
GUV	-	Giant Unilamellar Vesicle
LUV	-	Large Unilamellar Vesicle
SUV	-	Small Unilamellar Vesicle
MD	-	Molecular Dynamics
AC	-	Alternating Current
DC	-	Direct Current
SCF	-	Self-Consistent Field
POPC	-	1-palmitoyl-2-oleoyl-*sn*-glycero-3-phosphocholine
POPG	-	Phosphatidylethanolamine-phosphatidylglycerol
DOPC	-	1, 2-dioleoyl-*sn*-glycero-3-phosphocholine
DOPG	-	1, 2-dioleoyl-*sn*-glycero-3-phospho-(1́-*rac*-glycerol)
EGTA	-	Ethyleneglycol- *N*,*N*,*N*′,*N*′,-tetraacetic Acid
BSA	-	Bovine Serum Albumin
PIPES	-	1,4-Piperazinediethanesulfonic Acid

CHAPTER 1

INTRODUCTION

1.1 Background

When lipid molecules disperse in aqueous solution, the self-assembled system changes into the aggregates of different sizes and shapes [1-3]. Such aggregates form bilayer vesicles after some specific processes [4-5]. Vesicles are basically closed and spherical structures formed by a lipid bilayer ranging from nano to micrometer in size (diameter). Such vesicles are used in several researchers as they used model of real cells [6-7]. There are various methods for preparing the unilamellar vesicles with different sizes. Among these vesicles, giant unilamellar vesicles (GUVs) of diameters 10 μm or more have attracted special attention as their size and shape can be visualized using an optical microscope [8-12]. Such GUVs can be synthesized using the well-known natural swelling method [13-15, 11]. The size along with the shape of GUVs gives the opportunity to study the phenomena occurring at the single individual vesicle. The GUVs have been used for investigating the membrane's elasticity [14, 16], rupture/pore formation in membranes using mechanical/electrical stress [17-20], pore formation due to peptides and nanoparticles [21-23] etc. Such vesicles are potentially used for delivering the drug to a specific body organ [24-27].

The natural swelling method is a well-accepted process to obtain the oil-free different sizes GUVs [11]. In vesicle's population the size distribution analysis gives important information for the processes of the formation of GUVs. Several experimental and theoretical investigations dealing with this problem which explained the fundamental principles of the spontaneous lipid vesiculation [28]. The equilibrium size distribution of vesicles and the stability of each vesicle in the population are determined by a competition between total curvature energy of all vesicles and various sources of entropy of the system (i.e., vesicle translation and bilayer undulation). In addition, membrane bending modulus is one of the important factors for determining the size distribution of vesicles.

As it has been known that cholesterol is a basic element of cell membranes which varies up to 50 mol% of the total lipid content. Hence, such cholesterol plays important role in functioning of real biological system [29]. For example, cholesterol inhibits the formation of pores in membranes and increases the line tension of membranes [30-31]. On the other

hand, pore forming toxin, lysenin, induces pore formation in the lipid membranes of GUVs in presence of cholesterol [32]. The cholesterol has some ordering effects on lipids, the effect of cholesterol on the mechanical properties of lipid membranes is controversial, leaving open questions about the interaction mechanism between cholesterol and lipids.

The bending modulus is a most important parameter for determining the mechanical property of lipid bilayer. There are many experimental techniques such as micromanipulation, tether pulling, vesicle deformation induced by electric fields, nuclear magnetic resonance and X-ray diffraction are commonly used to determine the mechanical property of cholesterol containing membranes [33, 34]. Among those huge bulk studies, till to date there is no commonly accepted theoretical approach that how cholesterol influences on the bending modulus of lipid bilayer. From one side, some studies indicated that cholesterol rises the membrane bending rigidity [35-41]. In particular, addition of 50 mole% cholesterol in the membranes of vesicles, the bending modulus increase upto 3-4 times [42]. But from other side, the effect of cholesterol on bending modulus is not universal rather it depends on the types of lipid [43, 44]. Particularly, it was reported that that the bending modulus of DOPC membrane does not change significantly with the addition of cholesterol, but the sphingomyelin membrane shows higher flexibility [45]. Possible causes for such variations are discussed in the reported paper [46]. An illustration is provided for showing the structure of cholesterol and the cholesterol containing lipid bilayer in Fig. 1.1.

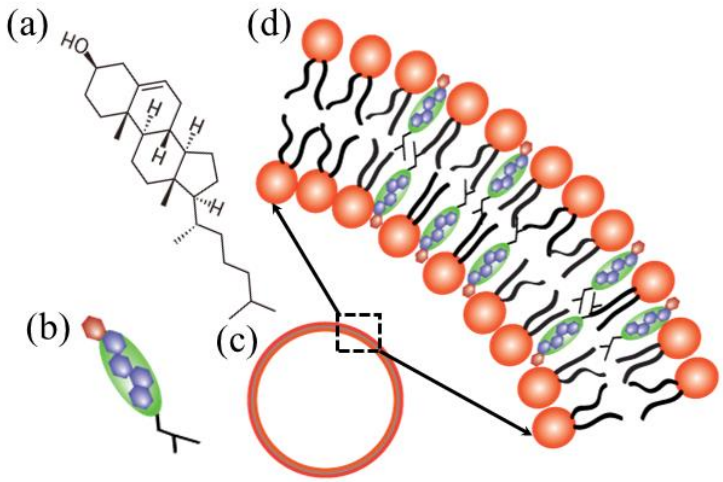

Fig. 1.1 (a) Structure of cholesterol (b) illustration of cholesterol (c) lipid membrane of GUV and (d) cholesterol-rich lipid membrane. [31]

Plasma membranes of mammalian cells contain 15-50% cholesterol depending on the types of organism [47], which is an important element of lipid rafts involved in signal transduction and endocytosis [48, 49]. Cholesterol modulates the physicochemical activities of plasma membranes [50], kinetics of voltage-gated ion channels [51], function of G-protein coupled receptors [52], rate of motion of hydrophobic tails [53] etc. Cholesterol also influences the mechanical stability of membranes, enhancing the mechanical strength, affecting membrane elasticity, and increasing packing density of lipids by means of the so called 'condensing and ordering' effects [54-56]. For the reason of the above modification, membranes are less permeable to water, small molecules, and ions [57-59]. Incorporation of cholesterol influences the bending rigidity of membranes and stiffens them [60].

Recently, irreversible electroporation (IRE) technique has been used for the ablation of certain tumor and cancer cells. Cell ablation occurred due to the permanent permeabilization of the membranes through the application of electric pulses of micro to millisecond duration [61, 62]. In order to model cell membranes, bilayers can be prepared as vesicle or liposome, which are closed, spherical systems ranging in diameter from nanometers to micrometers. The unilamellar vesicles are extensively investigated in medical researches for delivering the drug to a specific body organs [63-65, 27]. Among the various unilamellar vesicles, giant unilamellar vesicles (GUVs) of diameters 10 μm or more have attracted special interest because the size and shape of GUVs can be visualized using optical microscopes [10, 66-67]. As a mimic of cells, such GUVs are used to investigate quite several biophysical phenomena, for example the elasticity of lipid membranes [60], rupture/pore formation of vesicles [18, 23, 68, 69], molecular diffusion through nano-sized pore [22] and size distribution of vesicles [11, 33]. Artificial permeabilization due to transient pore or transmembrane pore in plasma membranes is used for various medical and bioengineering purposes [70-72].

A theoretical model describes the continuous trajectory of pore formation in lipid membranes subjected to applied lateral tension or electrical stress. The waiting time of pore formation followed a nonmonotonous function of the lateral tension, falling from infinity at zero tension to a minimum at several mN/m. On the contrary, electrical stress caused the waiting time to decrease monotonously [73]. The kinetics, statistics, and energetics of pore formation in lipid membrane studied by molecular dynamics (MD) simulations show a linear dependency of the activation energy for prepore formation under applied field [74]. The electropore life cycle describes the pore initiation, construction and resealing. The pore

creation time depends strongly on the electric field gradient across the membrane interface and that the pore annihilation time is weakly dependent on the pore-initiating electric field. The pore annihilation time is much longer than the pore creation time [75]. The MD simulations of a bare bilayer, a bilayer containing a peptide nanotube channel and a system with a peripheral DNA double strand has been performed under a high transverse electrical field. In all systems, the applied electric fields induce an electroporation in the lipid membrane manifested by the formation of water wires and water channels across the membranes. The results suggest the evidence of lateral stress on the bilayer under electric field [76]. The pore formation begins with the formation of single-file like water defects penetrating into the bilayer under the electric field [77]. The metastability of small hydrophilic pore in the lipid membranes is investigated by MD simulations. The metastability is due to compensating positive and negative curvature effects at the pore edge [78]. Hence, the research on pore formation in the membranes due to electroporation is rapidly growing due to its potential applications in biology, biotechnology and medicine [79, 80]. The constant-current (chronopotentiometric) measurements of planar bilayer lipid membrane demonstrated the constant-intensity current flow through bilayer membranes generated fluctuating pores in their structure. The presence of cholesterol in the lipid bilayer caused an increase in the value of the breakdown potential. The greater stability of the membrane with cholesterol can result from an increased critical pore radius [81]. MD simulations shows that the rate of pore formation is much slower at cholesterol containing DOPC membranes subjected to a transverse electric field because of the substantial increment of membrane cohesion [82]. The MD simulation study of the electroporation of lipid bilayers at different cholesterol contents indicated that the addition of cholesterol in concentrations of lipid: sterol ranging from 20 to 50 mol% increases substantially the membrane cohesion, which is manifested by an increase of the electroporation threshold [83]. The increase of the electroporation threshold upon addition of cholesterol, often linked to the increase of the stiffness of the bilayer, was studied [84]. The question thus arises how cholesterol influences the size distribution of vesicles and the IRE-induced rate constant of pore formation in membranes. Exactly this is the focus of this study.

1.2 Aims and Objectives

(a) Synthesis of cholesterol-rich neutral and charged membranes of GUVs using the well-known natural swelling method.

(b) Purification of GUVs using the membrane filtering method.

(c) Investigations on the size distribution of vesicles for estimating the bending modulus of membranes.

(d) Investigations of IRE-induced pore formation in GUVs for different cholesterol in charged membranes.

(e) Statistical analysis for obtaining the probability of pore formation and the rate constant of pore formation of GUVs.

(f) Correlation between the bending modulus of membranes and the rate constant of pore formation in vesicles.

.

1.3 Outline of Thesis

The thesis paper has been divided into five chapters.

Chapter one contains general introduction of the size distribution of vesicles, bending modulus of membranes, IRE-induced pore formation in GUVs in presence of various concentration of cholesterol.

Chapter two describes the literature review and theoretical aspects. It also includes the basic structure of biomembranes, lipid membranes and vesicles.

Chapter three describes the materials and method which contains the preparation and observation of GUVs using optical microscope.

Chapter four describes the results and discussion. The effects of cholesterol on the bending modulus and the IRE-induced rate constant of pore formation in GUVs are described here with theoretical explanations.

Chapter five describes the conclusions of thesis.

At last, references are included.

Chapter 2

LITURATURE REVIEW AND THEORETICAL ASPECTS

2.1 Previous Study on Bending Modulus

Claessens *et al*. [85] investigated the ionic strength dependent sizes of large unilamellar vesicles (LUVs) formed by DOPG and DOPC. Self-consistent field (SCF) calculations on charged bilayers show that the mean bending modulus k_c and the Gaussian bending modulus $|k|$ have opposite sign and $|k| > k_c$; especially at low ionic strength. Fig. 2.1 presents the result obtained for DOPG in NaCl, NaBr and NaI solution. The initial size of vesicles decreases with ionic strength and it was comparable for all three types of salt. However, at high ionic strength, the size of vesicles in NaI was always smaller than that of vesicles in NaBr, and these were in turn smaller than those in NaCl. The stronger the ion is hydrated, the more the bilayer membrane is dehydrated.

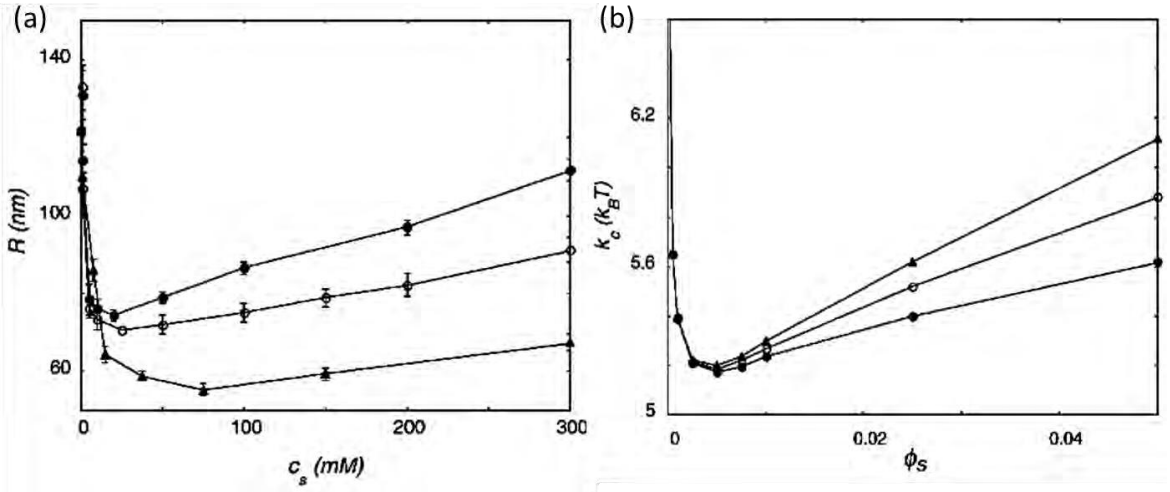

Fig. 2.1 (a) Radius R of DOPG vesicles as a function of ionic strength. Vesicles were prepared by freeze-thawing DOPG vesicles 15 times in NaCl (●), NaBr (○), and NaI (▲). (b) Bending modulus, k_c versus ionic strength. Data are shown for $\chi_{w\text{-anion}} = 0$ (●), $\chi_{w\text{-}\ anion} = -1$ (○), and $\chi_{w\text{-}\ anion} = -2$ (▲); in all cases, $\chi_{w\text{-}\ cation} = -2$.

The experiments show that vesicles in salt solution made by freeze-thaw experiments are very likely close to their entropically stabilized size. When vesicles are subjected to the freeze-thaw method, the initial size of the vesicles has no influence on the vesicle radius. Ion hydration is considered by the choice of the Flory-Huggins interaction parameters $\chi_{w\text{-}cation} = -2$ and $\chi_{w\text{-}anion} = -1$. In the high ionic strength regime, the radii of the DOPG vesicles in NaCl also increase faster with ionic strength than similar vesicles in the other salt solutions. Also, for this situation, k_c from the calculations and the experimentally determined vesicle radius show the same trends in their behavior as a function of ionic strength. As the experiments performed here on LUVs diameter of each vesicle cannot possible to measure.

Claessens *et al.* [86] obtained that large negative Gaussian bending modulus associated with charged membranes results in an overall curvature energy that is so low that entropic stabilization is possible. In Self-consistent field (SCF) calculations, DOPG and DOPC lipid molecules were modeled as linear chains with segment sequence $C_{18}X_2C_2X_2C_{18}$ and $C_{18}Y_2C_2Y_2C_{18}$, respectively. The phospholipid mixtures show a dependence of radius (R) on the NaBr concentration that is comparable to what is observed for the pure components (Fig. 2.2a).

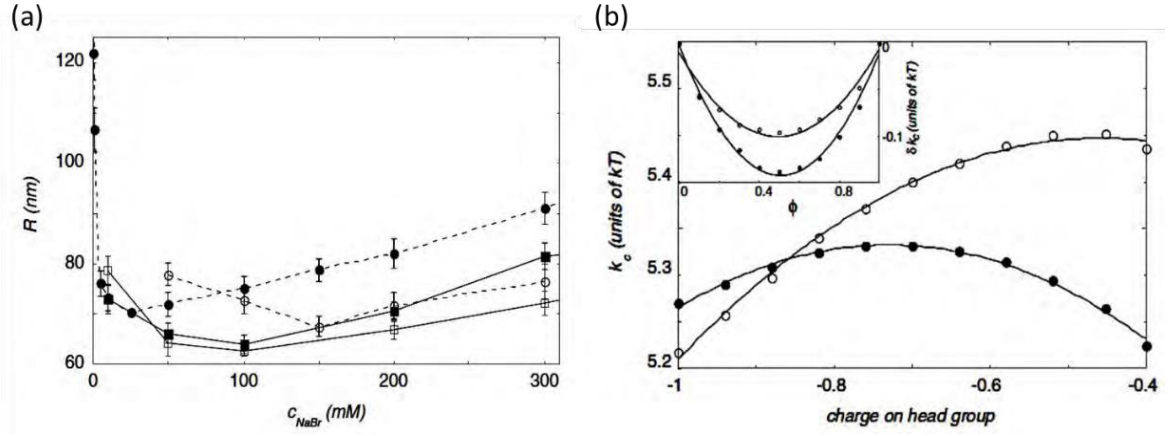

Fig. 2.2 (a) The radius of stable DOPG (●), DOPC (○) and mixed DOPG/DOPC vesicles (ϕ_{DOPC} = 0.1, ■; ϕ_{DOPC} = 0.2, □) as a function of NaBr concentrations; (b) The mean bending modulus k_C of a charged $C_{18}X_2C_2X_2C_{18}$ at ϕ_S = 0.0025 (○) and ϕ_S = 0.01 (●) as a function of the charge (in units of e) on the headgroup, Inset: The dependence of k_C that results from lipid mixing as a function of $C_{18}Y_2C_2Y_2C_{18}$ in the bilayer.

An initial decrease in R is followed by a slight increase of the vesicle radius with C_{NaBr}. In phospholipid mixtures, the minimum in R is observed at NaBr concentrations that lie between those seen for pure DOPG and DOPC vesicles. The shift in the position of the minimum in R (C_{NaBr}) probably results from changes in the surface charge density with composition. When the charge on the surfactant head group is decreased from −1e to −2/5e, a maximum in k_c is observed (Fig. 2.2b). At low ionic strength the maximum occurs at a high surface charge, but with increasing ionic strength the maximum is observed to shift to lower surface charges. The difference between the two calculated k_c curves (Fig. 2.2a and 2.2b) is expected to be related to mixing of lipids within the bilayer. As a result, such vesicles can be stabilized by some translational entropy, most likely assisted by some undulation entropy. They collected evidence that the size of the vesicles as produced by repetitive freeze-thaw cycles is correlated to the membrane persistence length which is related to the mean bending modulus. It was estimated by molecularly realistic SCF calculations. The bilayers composed of a mixture of lipids typically do have a lower rigidity than expected from the rigidities of the pure lipid bilayers. This relatively low rigidity results in a relatively low membrane persistence length. They argue that the sizes of the entropically stabilized vesicles composed of DOPC/DOPG mixtures are relatively small.

Karal *et al.* [87] investigated the effects of salt concentrations (C) and DOPG mole fraction (X) on the size distribution of DOPG/DOPC-GUVs prepared by the natural swelling method. The average size of the vesicles (D_{ave}) was determined using equation (2.2) by analyzing the size distribution histograms which was fitted by the theoretical equation (2.1). The lognormal distribution is expressed as follows [88]:

$$f(D) = \frac{1}{D}\frac{1}{\sigma\sqrt{2\pi}}\exp\left[-\frac{\{ln(D)-\mu\}^2}{2\sigma^2}\right]$$
$$= \frac{1}{D}\frac{1}{\sigma\sqrt{2\pi}}\exp\left[-\frac{\{ln(D)/\rho\}^2}{2\sigma^2}\right] \qquad (2.1)$$

where $f(D)$ indicates the frequency of GUVs with diameter D (probability density function), the dimension median ρ (or dimensionless μ lnρ) and σ^2 are the distribution parameters, and μ is the mean of the distribution of ln$D$. The value of D_{ave} is expressed as follows,

$$D_{\text{ave}} = \int_0^\infty Df(D)\,dD = \exp\left(\mu + \frac{1}{2}\sigma^2\right) = \rho\exp\left(\frac{\sigma^2}{2}\right) \tag{2.2}$$

The size distribution of GUVs was also fitted using the following equation from where the bending modulus of membranes (K_{ben}) was obtained.

$$f(D_m) = \frac{n_m(D_m)}{\Delta D_m} = \left(\frac{L}{\Delta K_{\text{ben}}}\right)\left(\frac{D_{\text{freq}}}{D_m}\right)^2 \exp\left[-\left(\frac{D_{\text{freq}}}{D_m}\right)^2\right] \tag{2.3}$$

where, D_{m} = 2 μm in our case) and $L = N_{\text{init}}\varphi/4\pi\Delta D_{\text{m}}$. Equation (2.3) has two fitting parameters, D_{freq} and K_{ben} (L is normalized parameter).

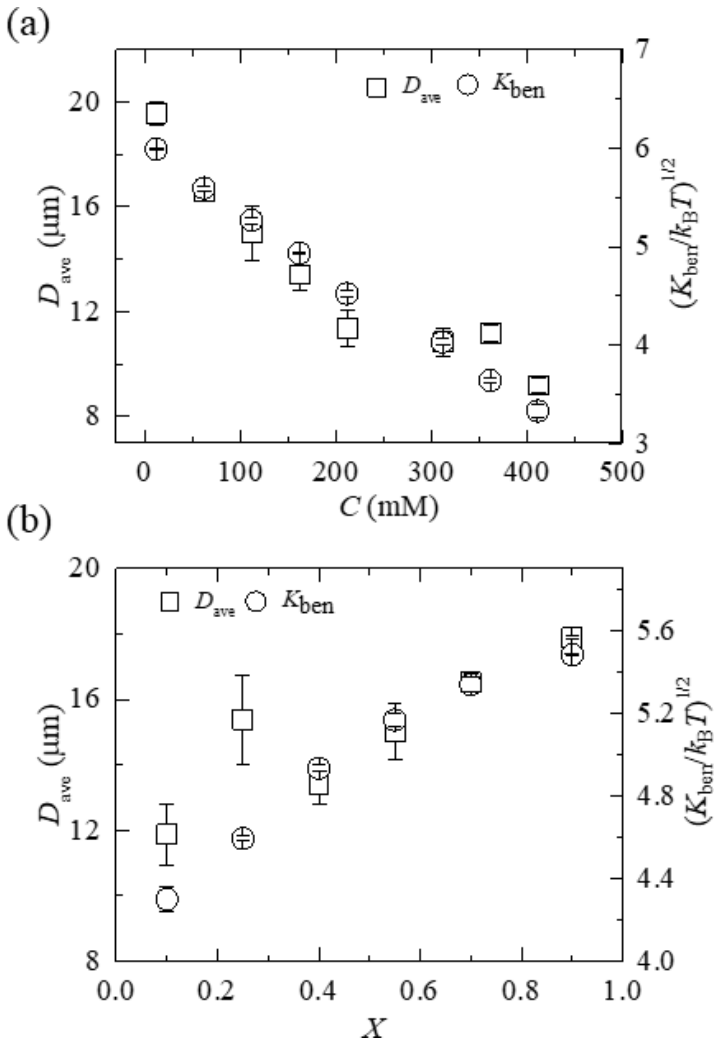

Fig. 2.3 Relationship between the average size (D_{ave}) and the bending modulus of bilayer (K_{ben}). (a) Effects of C on D_{ave} and K_{ben} for DOPG mole fraction X = 0.40. (b) Effects of X on D_{ave} and K_{ben} at C = 162 mM.

Fig. 2.3 shows that both the D_{ave} and K_{ben} decreased with the increase of C in buffer for 40%DOPG/60%DOPC-GUVs (here, X = 0.40). On the other hand, the values of D_{ave} and K_{ben} increased with the increase of X for C = 162 mM NaCl in buffer. If the K_{ben} decreases, D_{ave} in the system also decreases. If K_{ben} decreases the bending energy of small vesicles also decreases, therefore the fraction of such vesicles in assemble increases as result the average size of all vesicles decreases.

Rawicz *et al.* [89] investigated the effect of chain length and unsaturation on lipid bilayers. They used micropipette aspiration technique for measuring the bending modulus (k_c) and area compressibility modulus (K_A) of phosphatidylcholine (PC) membranes. Fig. 2.4 shows the change of area expansion of GUVs with applied tension. Bending modulus was derived from measurements of apparent expansion in vesicle surface area under very low tensions (0.001– 0.5 mN/m), which was dominated by smoothing of thermal bending undulations.

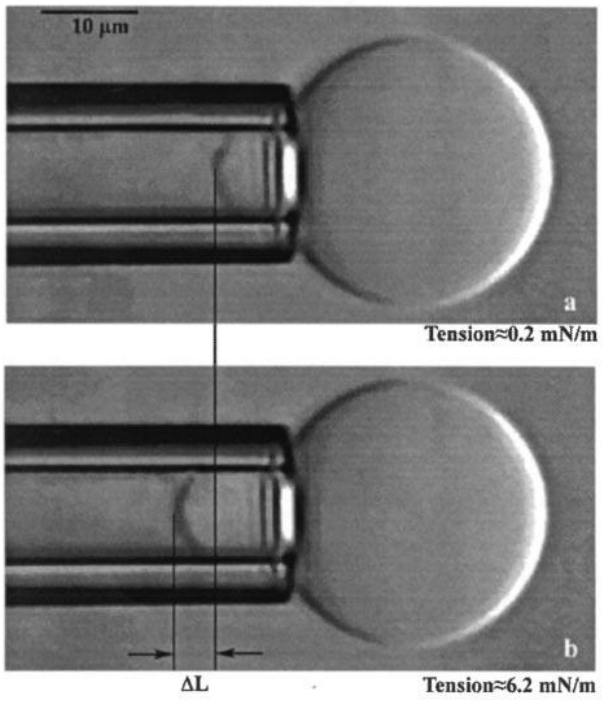

Fig. 2.4 Video micrograph of a vesicle area expansion test. (a) The vesicle at low tension. (b) The vesicle at high tension. The change in projection length is proportional to the change in apparent surface area.

Area stretch modulus was obtained from measurements of vesicle surface expansion under higher tension (0.5 mN/m and above), which involve an increase in area per molecule and a

small-but important contribution from smoothing of residual thermal undulations. Though the elastic modulus was same for all PC membranes, however, bending rigidity with polyunsaturation decreased significantly. The tension dependent change of area for different membranes is shown in Fig. 2.5.

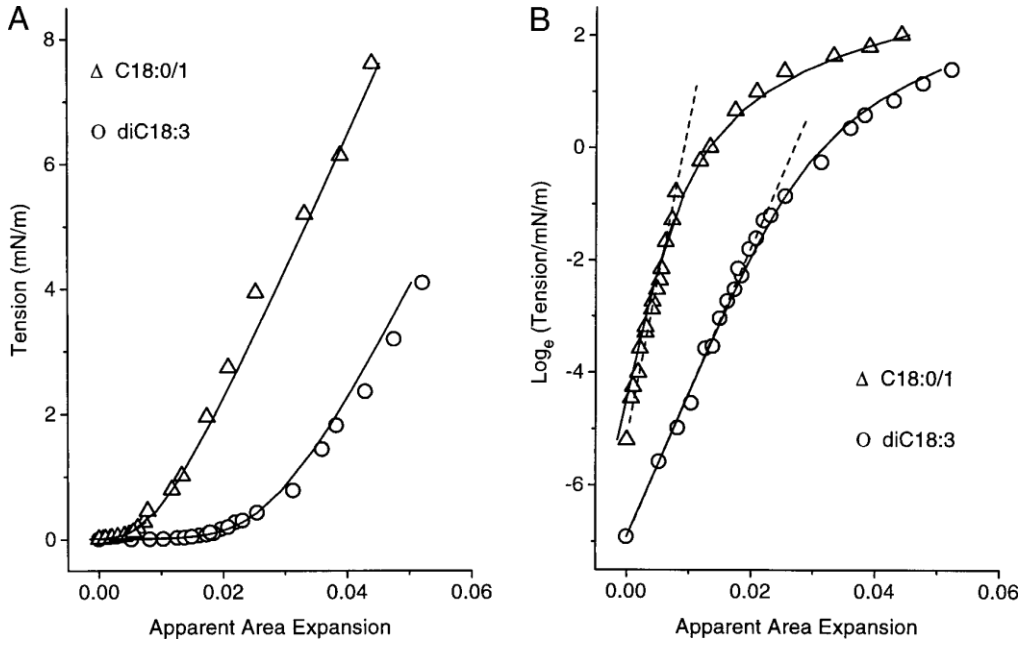

Fig. 2.5 (A) Linear plot of tension versus apparent area expansion. (B) Semilog plot of tension versus apparent area expansion. Slopes of the linear fits (dashed lines) applied to the range of very low tensions yield elastic bending moduli k_c ($\times 8\pi/k_BT$) for each bilayer ($k_c = 0.9 \times 10^{-19}$ J for C18:0/1 and $k_c = 0.4 \times 10^{-19}$ J for diC18:3).

Pan *et al.* [90] investigated the effect of cholesterol on structural and mechanical properties of membranes (Fig. 2.6). They have shown the effects of cholesterol on membrane bending modulus K_C, membrane thickness D_{HH}, the partial and apparent areas of cholesterol and lipid and the order parameter S_{xray} are depend upon the number of saturated hydrocarbon chains in the lipid molecules. Particularly striking is the result that up to 40% cholesterol does not increase the bending modulus K_C of membranes composed of phosphatidylcholine lipids with two *cis* monounsaturated chains, although it does have the expected stiffening effect on membranes composed of lipids with two saturated chains. They have used five sample of lipid such as DOPC, SOPC, DMPC, DPPC and diC22:1PC. In their result, they have shown that as cholesterol concentration c increases, K_C for DMPC

increases rapidly and at c = 0.3, it is already more than fourfold larger than at c = 0. Increasing K_C decreases the intensity of the diffuse scattering required for the method, which is why only K_C up to c = 0.3 for DMPC is obtained. For SOPC K_C also increases, but not as dramatically as for DMPC, and above c = 0.3 it levels off. The results for SOPC are like results for POPC which has two fewer carbons in its saturated *sn*-1 chain. The leveling off K_C has also been observed for SOPC/cholesterol and POPC/ergosterol. Their more surprising result is that both DOPC and diC22:1PC have essentially constant K_C for c up to 0.4.

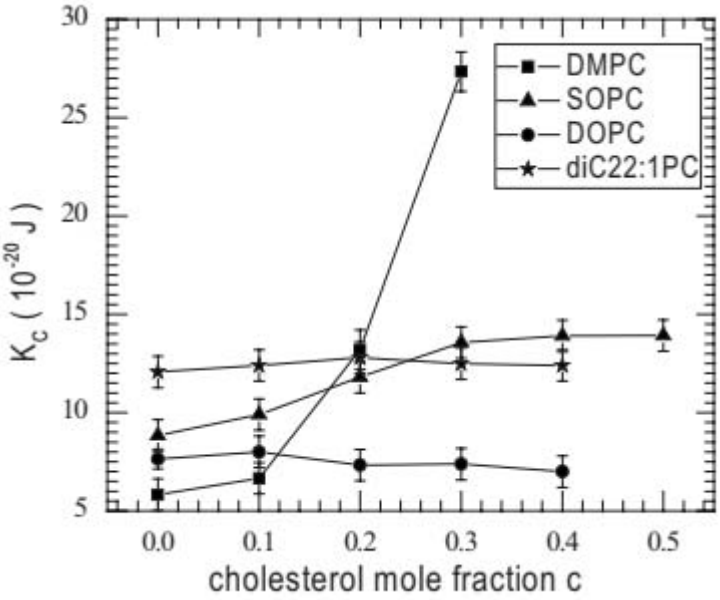

Fig. 2.6 Bending modulus K_C for bilayers of four lipids with cholesterol mole fraction c at 30 °C.

However, it had not been emphasized that the overall phenomenological description is that the effect of cholesterol on K_C increases dramatically with the number of saturated chains. Since cholesterol does not increase K_C in DOPC has been thrice confirmed using entirely different techniques on giant unilamellar vesicles. Quantitatively, the polymer brush theory predicts that the area modulus K_A is the same for all lipid bilayers. These K_C results motivate a theory of elastic moduli in the high cholesterol limit and they challenge the relevance of universality concepts. Although most of the results were obtained at 30 °C, additional data at other temperatures to allow consideration of a reduced temperature variable do not support universality for the effect of cholesterol on all lipid bilayers. If the concept of universality is to be valid, different numbers of saturated chains must be considered to create different universality classes.

Genova *et al*. [91] investigated the influence of cholesterol on the bending modulus of SOPC membrane throughout a considerably wide interval of concentrations. Thermally induced shape fluctuations of giant quasi-spherical lipid vesicles were used to study the influence of cholesterol on the bending modulus (k_c) of membrane. At low concentration of cholesterol, a decrease of the bending elasticity modulus is observed and compared to pure SOPC membrane. At high cholesterol content, a two-fold increase of bending modulus is also obtained. The data for k_c for mixed SOPC- cholesterol membrane is compared to the results obtained by different methods on different lipid matrices. Table 2.1 represents the cholesterol dependent bending modulus of SOPC membranes.

Table 2.1 Bending modulus of SOPC-GUVs containing different concentration of cholesterol.

Cholesterol concentration (mol %)	Bending modulus $k_c \times 10^{-19} (J)$
0	1.70 ± 0.10
10	1.56 ± 0.05
20	1.98 ± 0.11
30	2.02 ± 0.09
50	2.67 ± 0.13

2.2 Previous Study on Electroporation

Electroporation or electropermeabilization is a technique in which an electrical field is applied to cells in order to increase the permeability of cell membrane, allowing chemicals, drugs or DNA into the cells [92, 93]. IRE is a soft tissue ablation technique using short but strong electrical fields to create permanent and hence lethal nanopores in the cell membrane, to disrupt cellular homeostasis. The cell death results from induced apoptosis or necrosis induced by either membrane disruption or secondary breakdown of the membrane due to transmembrane transfer of electrolytes and adenosine triphosphate [94-106]. The first generation of IRE for clinical use, in the form of the NanoKnife System, became commercially available for research purposes in 2009, solely for the surgical ablation of soft tissue tumors [97]. Cancerous tissue ablation via IRE appears to show

significant cancer specific immunological responses which are currently being evaluated alone and in combination with cancer immunotherapy [98-102].

Rubinsky *et al.* [103] investigated to treat the hepatocarcinomas by means of IRE. They reported an experimental study on pig livers where the electrodes were inserted percutaneously, without exposing the liver, and the histological samples were analyzed with apoptotic markers. Equivalent observations were obtained (lesion manifestation by ultrasonography and sharp transition zone between ablated and normal tissue). They investigated in their report that the IRE pulse parameters were bipolar electroporation 2.5 kV pulse applied in a train of eight 100 microsecond pulses separated by 100 milliseconds. Fig. 2.7 shows the treatment planning and surgical protocol for IRE ablation in pig liver. Four electrodes 18 gage stainless steel electrodes with 1.5 cm distance between probes were used in the investigations. In Fig. 2.7(A), the results of mathematical analysis of two electrode system showing constant electrical field. The numbers on the figures indicate the magnitude of the electrical field in increments of 100 V/cm starting from 100 V/cm (outer isoline). The power delivered during each pulse is 1.2 J per cm depth of electrode. In Fig. 2.7(B), the results of mathematical analysis of four electrode system show constant electrical field magnitude isolines due to the superposition of the application of the IRE pulses between the four pairs of IRE electrodes. The numbers on the figures indicate the magnitude of the electrical field in increments of 100 V/cm starting from 600 V/cm (outer isoline). Experiments have shown that 600 V/cm induces irreversible electroporation in liver. In Fig. 2.7(C), the photograph of application of electroporation probes with ultrasound and in Fig. 2.7(D), insertion of a set of four electrodes are shown. They found the results from these parameters because the sequence of eight 100 microsecond pulses separated by 100 milliseconds was conventionally used in reversible data and previous information was available for the electrical field magnitude that separated between reversible and irreversible electroporation.

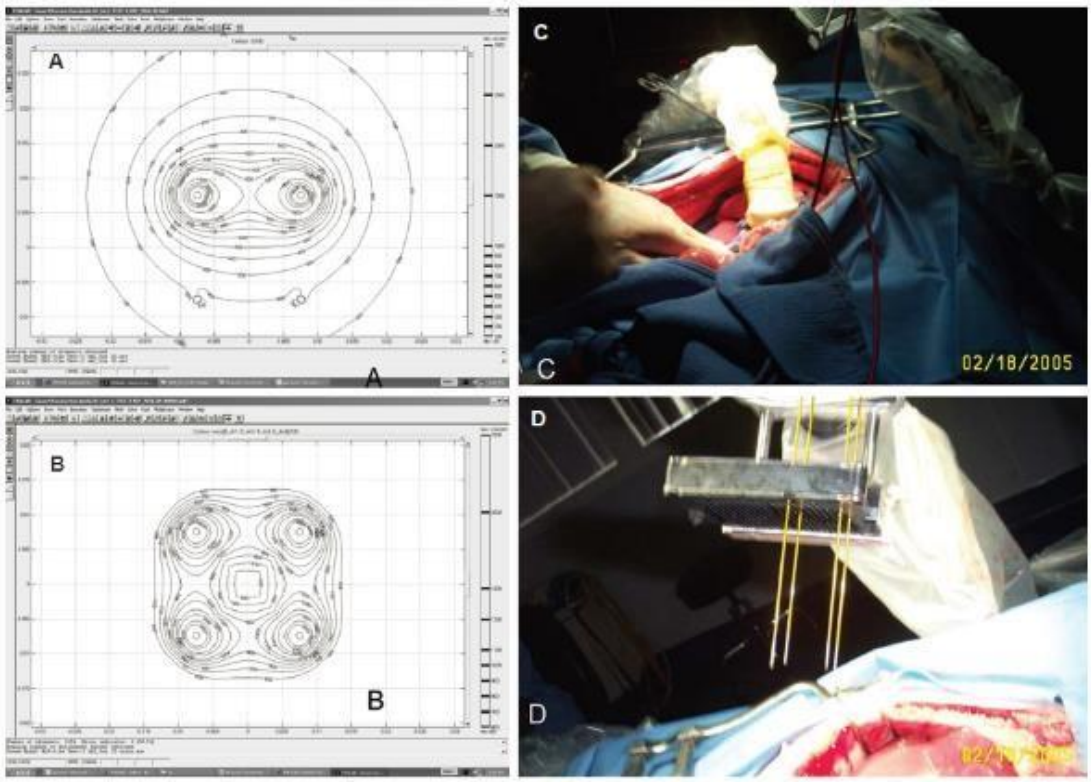

Fig. 2.7 Treatment planning and surgical protocol for irreversible electroporation ablation in the pig liver. [103]

In Fig. 2.8(A), margin of ablated area (bottom half) and unaffected area (top half) are shown. Focal dark areas are necrotic hepatocytes with calcification. In Fig. 2.8(B), margin of ablated area (left) and unaffected area (right) are shown. Focal dark areas are necrotic hepatocytes with calcification. In Fig. 2.8(C), central area of ablation is shown. Hepatocytes have hypereosinophilic cytoplasm and pyknotic nuclei. Sinusoids are congested. Scale bar 100 micron. In Fig. 2.8(D), normal area of hepatic parenchyma for comparison to ablated region. In Fig. 2.8(E), area of hepatic necrosis with hypereosinophilic cytoplasm and pyknotic nuclei is shown. Aggregate of hepatocytes at bottom also contain calcium. In Fig. 2.8(F), area of hepatic necrosis with hypereosinophilic cytoplasm and pyknotic nuclei are shown. Hepatocytes are separated by hemorrhage. In Fig. 2.8(G), brown granular pigment is calcium in areas of hepatic necrosis of ablated region is shown.

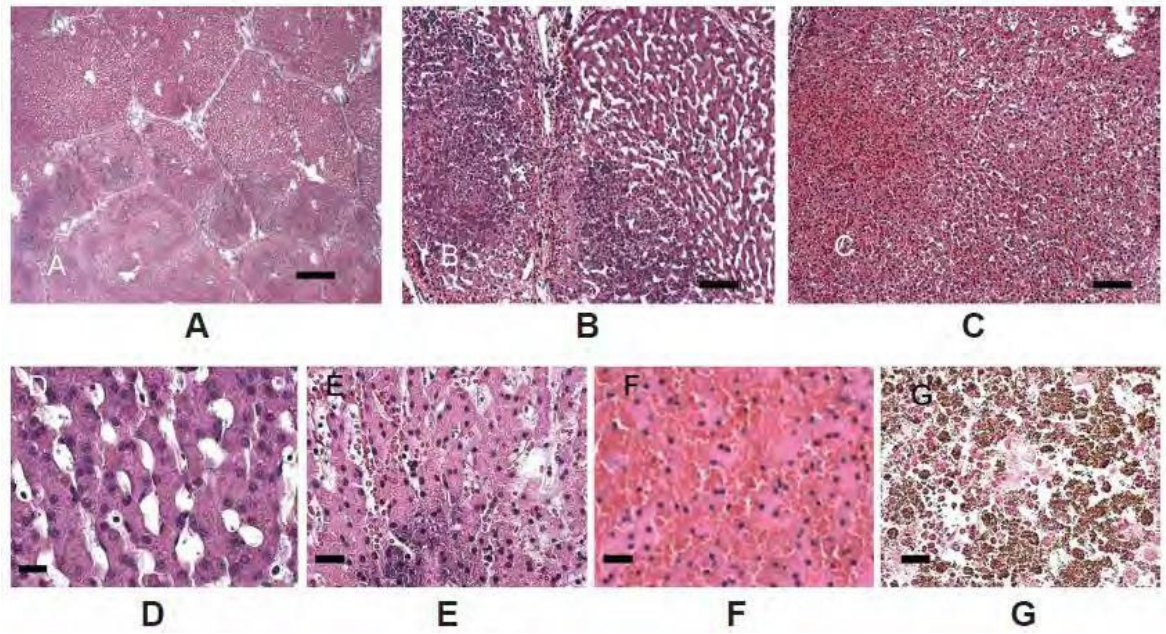

Fig. 2.8 Microscopic histology of IRE ablation in the pig liver, 24 hours post IRE. Scale bar in (A) 500 μm (B, C) 100 μm, and (C, D, E) 25 μm. [103]

Riske *et al.* [104] investigated the rupture of charged 50%POPG/50%POPC-GUVs (% indicates mole %) subjected to high electric filed. Strong electric pulses applied to GUVs induce the formation of pores, which reseal within milliseconds. They studied the response of GUVs to such pulses. Vesicles composed of charged membranes in a buffer solution of HEPES and EDTA exhibited the same behavior as observed with neutral GUVs. Surprisingly, when the medium was changed to a nonbuffered solution with or without salt, the vesicles bursted and disintegrated to tubular structures after the pulse is applied. A fast-digital camera and confocal microscopy were used to observe the dynamics of vesicle rupture and the membrane reorganization after the applied pulse as shown in Fig. 2.9. The experiments suggested that the membrane charge plays a significant role for the rupturing of GUVs. Vesicles made of lipid extract from human plasma membranes behave the same fashion, implying that the reported bilayer reorganization may also occur to a certain degree in the membrane of electroporated cells.

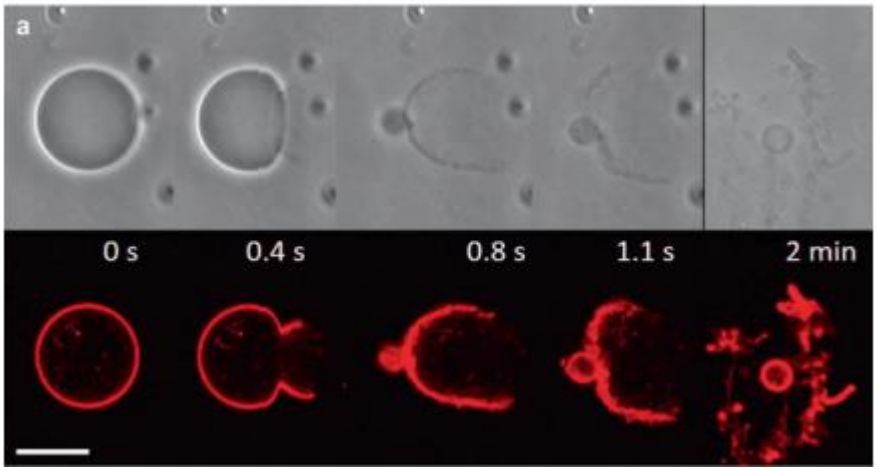

Fig. 2.9 Bursting vesicles. (a) Pulse-induced bursting of a 50%POPG/50%POPC-GUVs. The images were obtained with phase contrast (top) and confocal microscopy (bottom). The DC pulse applied was 1.4 kV/cm and 200 μs. The approximate time after the beginning of the pulse is marked; note that the scanning speed is 2.62 fps. The last image is a magnified fraction (refocused). The scale bars correspond to 15 μm.

Karal *et al.* [105] investigated the effects of electrostatic interactions on the rate constant (k_p) for mechanical tension induced pore formation in GUVs. The mechanical tension was applied by the micropipette aspiration technique. They changed the salt concentration (C) of buffer solution as well as the DOPG mole fraction (X) in lipid membranes. They obtained the results that with the decrease of salt concentration and increased the DOPG mole fraction, the rate constant of pore formation increases.

Using the mean first passage time approach the rate constant of the formation of pore in membranes was determined as follows [106],

$$k_p = A_F\left(\sigma_c + B\right)\exp\left[-\frac{\pi\Gamma^2}{k_B T\left(\sigma_c + B\right)}\right] \tag{2.4}$$

where $A_F = \left(\frac{D_r\sqrt{3}}{k_B T}\right)$ is the pre-exponential factor. The fitting parameters of equation (2.4) are A_F and Γ. The electrostatic effect, B is defined as follows

$$B \approx \left\{4\Omega\left[\frac{1-q}{p} + \ln\left(p+q\right)\right]\frac{k_B T}{e} - \frac{\Omega^2}{\varepsilon_w \varepsilon_0}\omega^2\frac{h}{2}\right\} \tag{2.5}$$

where h is the thickness of membrane, Ω is the membrane surface charge density, ε_w is the relative dielectric constant of water, ε_0 is the permittivity of free space, $p = 2\pi\lambda_B X/\kappa A_0$

and $q = \sqrt{1+p^2}$, $1/\kappa$ is the Debye length (0.76 nm), Bjerrum length in water at 25 °C is $\lambda_B = e^2/4\pi kT\varepsilon_0\varepsilon_W = 0.716$ nm , k_B is Boltzmann constant, T is absolute temperature, and ω is the fitting parameter. Fig. 2.10 shows the obtained results from the study. At 12 mM NaCl concentration (C) in buffer solution, the rate constant of pore formation increased with the applied tension [Fig. 2.10(a), open squares]. The similar results were also obtained for C = 162 (with Debye length 0.76 nm and 312 mM NaCl in buffer. Fig. 2.10(a) shows that with a decrease in C, the tension required to induce pores decreased. Electrostatic interactions in buffer increase with a decrease in salt concentration because shielding of the membrane surface charge by counterions decreases (i.e., the Debye length increases**)** [107]. Hence, Fig. 2.10(a) indicates that k_p increases with an increase in the extent of electrostatic interaction.

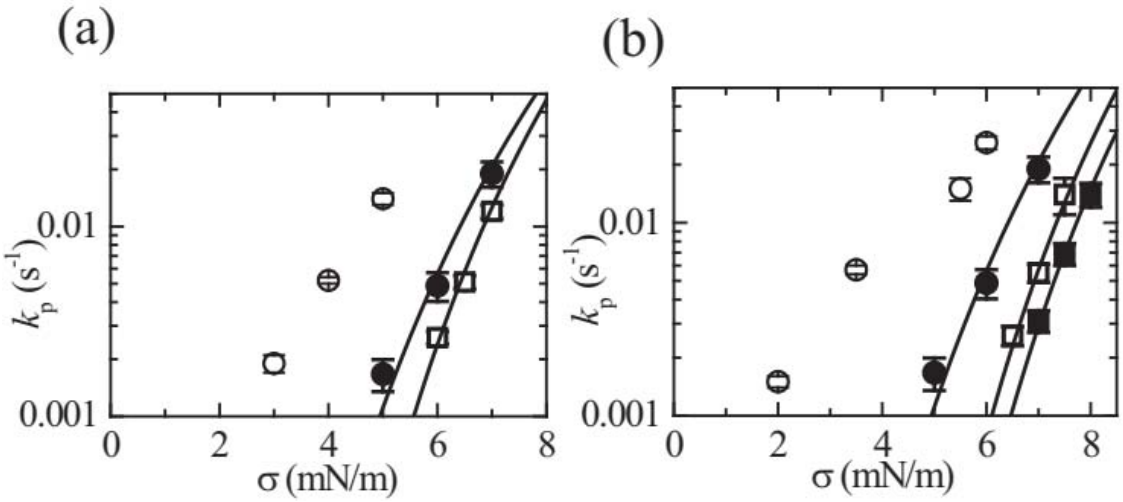

Fig. 2.10 Tension dependence of rate constant of pore formation (k_p) for DOPG/DOPC-GUVs for different DOPG mole fraction (X) and NaCl concentration (C). The solid lines show the best-fit theoretical curves of equation (2.4) with D_r = 165 nm^2/s and ω = 0.45. (a) Effect of C for 40%DOPG/60%DOPC-GUVs (i.e., X = 0.40). C = 12 mM (open circle), 162 mM (closed circle), and 312 mM (open square). (b) Effect of X at C = 162 mM. X = 0.70 (open circle), X = 0.40 (closed circle), X = 0.10 (open square) and X = 0.0 (closed square).

They also investigated the effects of surface charge density, which is controlled by DOPG mole fraction (X) in membranes, on the rate constant of pore formation. Fig. 2.10(b) shows that with an increase in X, the tension required to induce pores decreased. Comparing the data for the same tension, but for different X, k_p increases with an increase in X. Therefore,

the results in figure clearly show that k_p increases with the increase of electrostatic interactions in the membranes of vesicles.

Karal *et al.* [108] investigated the electrostatic effects on the electrical tension (σ_c)-induced irreversible rate constant (k_p) of pore formation in GUVs. The DOPG/DOPC-GUVs were prepared using the natural swelling method. The rate constant of pore formation increased with the decrease of salt concentration in buffer along with the increased of surface charge density of membranes (Fig. 2.11). Fig. 2.11(A) shows the σ_c dependent k_p values for C = 62, 162 and 262 mM using 40%DOPG/60%DOPC-GUVs. Similarly, Fig. 2.11(B) shows the σ_c dependent k_p values for X = 0.60, 0.40, 0.20 and 0.10 at C = 162 mM. In both systems, the value of k_p increases with the increase of σ_c. The experimental results of σ_c vs k_p was fitted with the theoretical equation (eq. 2.4) and obtained the line tension of membranes. The solid lines show the best fitted theoretical curves corresponding to equation (2.4). The decrease in energy barrier of a prepore due to electrostatic interaction was the key factor causing an increase of rate constant of pore formation.

As is known, ions of solution in colloidal systems shield the surface charges of membrane lipids and hence reduce the effects of electrostatic interactions. The higher the concentration of salt in the solution, the weaker the electrostatic effects in the system. Again, as the surface charge density in membrane increases the repulsive force between the lipid molecules also increases and hence increase the electrostatic effects. These statements support our investigations that as the electrostatic interaction increases in the membranes (decrease of salt concentration or increase of surface charge density) the probability of pore formation and the rate constant of pore formation increase. Therefore, the results presented in Fig. 2.11 clearly indicate that electrostatic interactions play an important role in processes of the formation of pores in the membranes of GUVs.

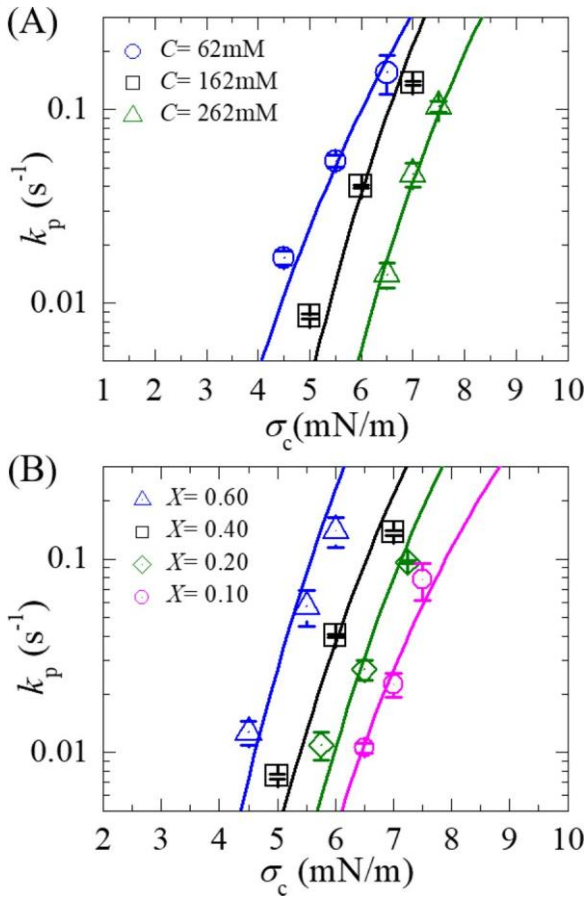

Fig. 2.11 The electric tension (σ_c) dependent k_p for different salt concentrations (C) and DOPG mole fraction (X). (A) The σ_c dependent k_p value for C = 62 mM (open circle), C = 162 mM (open square) and C = 262 mM (open triangle) using 40%DOPG/60%DOPC-GUVs (i.e., X = 0.40). (B) The σ_c dependent k_p for X = 0.60 (open triangle), 0.40 (open square), 0.20 (open diamond) and 0.10 (open circle) at C = 162 mM. The solid lines show the best fitted theoretical curves corresponding to equation (2.4).

2.3 Membrane Curvature and Bending

Mechanical property of membranes is two types. One is bending modulus or bending rigidity, and another is elastic modulus or area compressibility modulus. Bending modulus is defined as a quantity in which strain due to stress is not change proportionally. It generally occurred at lower (0.001 - 0.5 mN/m) applied tension. Cell can easily bend due to this modulus. The bending modulus is one of the most important properties of lipid membranes, playing an important role in several biological processes including exo- and endocytosis, vesicle fusion, and the regulation of membrane protein activity. Elastic modulus of membrane is defined as a quantity in which stress and strain changes

proportionally. It generally occurred at relatively higher (0.5 mN/m and above) applied tension. Cell can easily expand due to this modulus. The bilayer obeys a simple continuum theory characterized by a very small number of effective material parameters. The bending modulus is a mechanical macroscopic constant that describes the tendency of a certain material to resist bending. In the case of a lipid membrane, it is defined as the energy required for deforming the bilayer from its intrinsic curvature to some other curvature and is undoubtedly one of the most important properties of bilayer. It plays an important role in many biological situations, including endocytosis [109], the organization of membrane trafficking [110], and membrane fusion [111]. According to the theory of Helfrich [112], if the membrane is modeled as a two-dimensional elastic sheet, the curvature energy per unit area can be expressed as,

$$E = \frac{K_c}{2}(c_1 + c_2 - c_0)^2 + \bar{k}K \qquad (2.6)$$

where $c_1 = 1/R_1$ and $c_2 = 1/R_2$ are the two main curvatures, c_0 is the spontaneous curvature, K the gaussian curvature, $\bar{k}$ the gaussian modulus and K_c the bending modulus. If the membrane topology is fixed, the second term is a constant, and if the bilayer is symmetric c_0 is equal to zero. Thus, in the simplest case, the only parameter characterizing membrane rigidity is the bending modulus K_c, and the optimum configuration is the flat one. However, thermal undulations lead to local displacements. It has been considered $u(r)$ the vertical displacement of each point of the membrane, identified by r, with respect to the horizontal plane of the flat membrane. These displacements can be expressed in terms of plane waves. Considering the membrane surface tension γ, and working in the reciprocal space, the power spectrum $\langle u_q^2 \rangle$ dependence on the wave vector q can be derived, using the equipartition theorem [113].

$$< |u|^2 >= \frac{k_B T}{A(K_c q^4 + \gamma q^2)} \qquad (2.7)$$

where, A is the area of a squared piece of membrane. Thus, in the case of vanishing (or negligible) surface tension, simple q^{-4} dependence is found. Since the only parameter left is K_c, this result gives origin to the most common experimental and numerical methods to determine the bending modulus from the thermal undulation spectrum.

2.4 Biomembranes

Biomembranes are one of the most important elements of cells (Fig. 2.12). It represents an envelope of the cell with unique barrier function that provides directional transport of species into the cell and waste and toxic compounds out of the cell. In addition, channel proteins maintaining non-equilibrium ion distribution between the extra cellular and cytoplasmic of cells. Hence, biomembranes provide not only structural and barrier functions but also contain integral and peripheral proteins that are responsible for communication of the cell with surrounding environment. They have receptor function and are responsible also for transfer of the signals into the cell by means of sophisticated signaling pathways. In a membrane, there are several catalytical processes are concentrated, for example the energy transduction connected with synthesis of energetically reaches molecule adenosine triphosphates (ATP) [114].

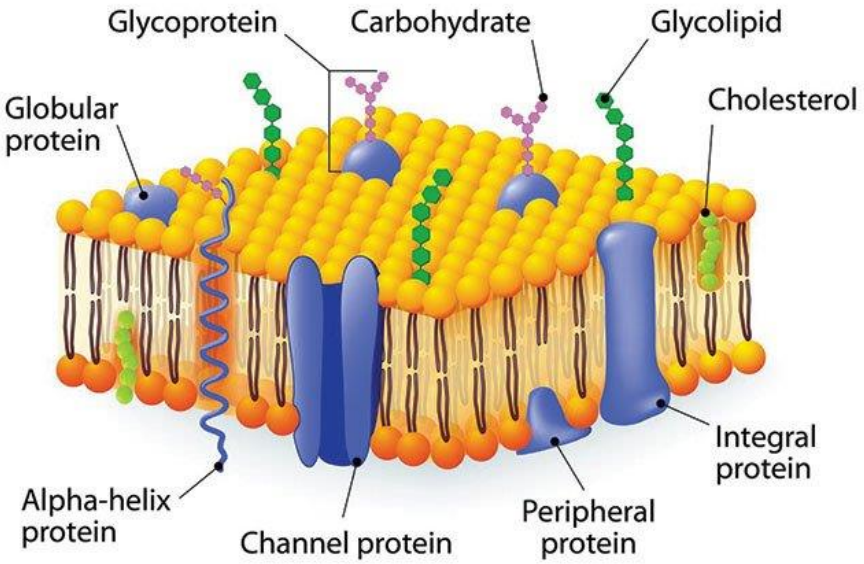

Fig. 2.12 The structure of biomembrane.

Biomembranes are permeable only to very small molecules like water, oxygen and carbon dioxide and to a very small degree of polar compounds of hydrophobic molecules. These molecules are either transported into the cell via endocytosis or through membrane proteins that allow a controlled carriage through pores and channels or by active transport. Under physiological conditions the cell keeps chemical gradients for Na^+ and K^+ across the cell membrane to facilitate the membranepotential that is vital to many cellular functions. Most cellular reactions are controlled by the Ca^{2+} signaling

system and the concentration of free Ca^{2+} in the cytoplasm is under strict control. It is kept very low (~0.1 μm) inside the cell, while the outside concentrations of free Ca^{2+} are multifold higher (~1.3 mM). High levels of intracellular ATP entertain the different active ports that maintain these gradients and sustain the energy-dependent cellular processes which the cell integrity depends on.

2.5 Lipid Membranes

Lipids are nonpolar compounds which are soluble in nonpolar solvents. It is the major component of all types of biomembranes [115]. Based on chemical structure and constitution, lipids are broadly classified into simple lipids and complex lipids. Simple lipids containa trihydric alcohol, glycerol and long chain fatty acids. The carboxyl groups of the fatty acids are ester-linked to the hydroxyl groups of glycerol. The fatty acids present in simple lipids have generally 16 or 18 carbon atoms and they may be saturated or unsaturated. The lipid molecules are oriented in such a manner that the hydrophilic glycerol moieties remain in contact with water, while the fatty acid tails project inward to build a compact hydrophobic central zone [116]. Hence, in a bilayer membrane, lipids form the middle hydrophobic layer and glycerol and protein remain on two sides facing the outer and inner aqueous environment [117]. Fig. 2.13 shows the schematic illustrations of a lipid molecule and its molecular structure.

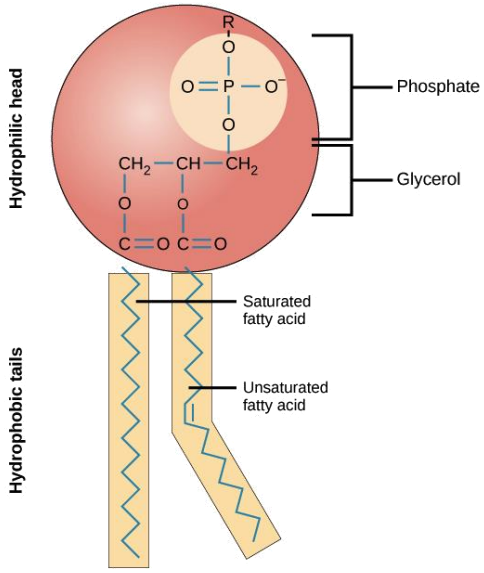

Fig. 2.13 Lipid molecule and molecular structure of lipid molecule. [118]

In a phospholipid molecule, two hydroxyl groups of glycerol are esterified with carboxyl groups of long chain fatty acids as in case simple lipids, while the third hydroxyl group of glycerol is esterified with phosphoric acid. Such a lipid is called a phosphatide. In most of the phospholipids, phosphoric acid is further linked to an organic group. Another group of complex lipids are steroids which are quite different in chemical structure from simple lipids [119]. The steroid nucleus contains three 6- membered and one 5-membered carbon rings. Steroids having an alcoholic (OH) group attached to one of the rings are known as sterols, e.g. cholesterol. Sterols are widely distributed in the plasma membranes of animals, plants and fungi, but not in bacteria. The structure of a lipid molecule and the structure of lipid membrane are illustrated in Fig. 2.14. Phospholipids with certain head groups can alter the surface chemistry of a bilayer and can serve as signals as well as "anchors" for other molecules in the membranes of cells [120]. Just like the heads, the tails of lipids can also affect membrane properties, for instance by determining the phase of the bilayer. The bilayer can adopt a solid gel phase state at lower temperatures but undergo phase transition to a fluid state at higher temperatures, and the chemical properties of the lipids' tails influence at which temperature this happens. The packing of lipids within the bilayer also affects its mechanical properties,including its resistance to stretching and bending. Many of these properties have been studied with the use of artificial "model" bilayers produced in a lab.

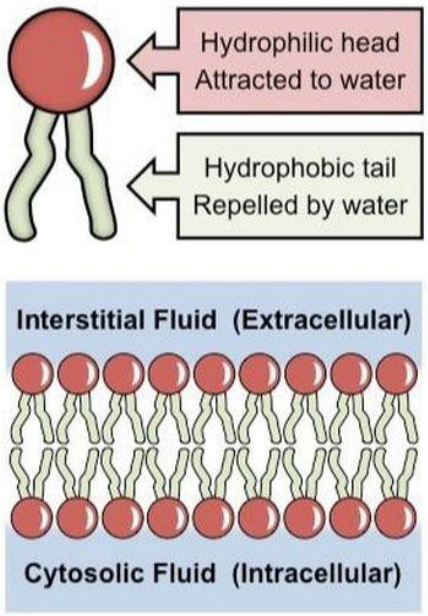

Fig. 2.14 Schematic diagram of lipid bilayer. [121]

2.6 Cholesterol

Cholesterol strengthens the bilayer and decreases its permeability. It also regulates the activity of certain integral membrane proteins. Cholesterol is biosynthesized by all animal cells and is an essential structural component of animal cell membranes. Cholesterol composes about 30% of all animal cell membranes. It is required to build and maintain membranes and modulates membrane fluidity over the range of physiological temperatures. The hydroxyl group of each cholesterol molecule interacts with water molecules surrounding the membrane, as do the polar heads of the membrane phospholipids and sphingolipids, while the bulky steroid and the hydrocarbon chain are embedded in the membrane, alongside the nonpolar fatty-acid chain of the other lipids. Through the interaction with the phospholipid fatty-acid chains, cholesterol increases membrane packing, which both alters membrane fluidity [122] and maintains membrane integrity so that animal cells do not need to build cell walls (like plants and most bacteria). The membrane remains stable and durable without being rigid, allowing animal cells to change shape and animals to move. The chemical structure of cholesterol is shown in Fig. 2.15.

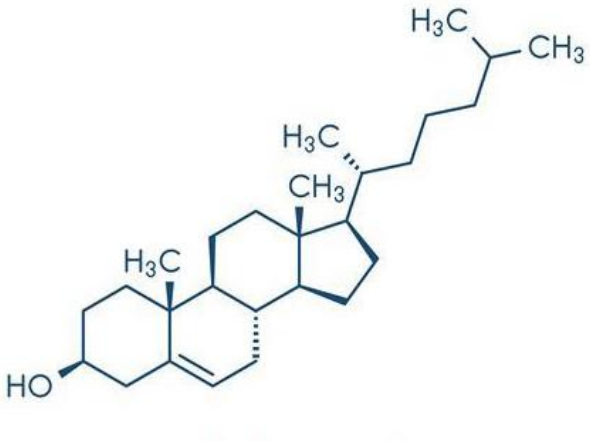

Fig. 2.15 Chemical structure of cholesterol.

2.6.1 Types of cholesterol

Cholesterol moves throughout the body carried by lipoproteins in the blood. These lipoproteins include:

- Low-density lipoprotein (LDL). LDL is often called “the bad cholesterol.”
- High-density lipoprotein (HDL). HDL is often called “the good cholesterol.”
- Very-low-density lipoproteins (VLDL) are particles in the blood that carry triglycerides.

2.6.2 Sources of cholesterol

Since all animal cells manufacture cholesterol, all animal-based foods contain cholesterol in varying amount. Major dietary sources of cholesterol include cheese, egg yolks, beef, pork, poultry, fish, and shrimp. Human breast milk also contains significant quantities of cholesterol. However dietary cholesterol intake does not correlate well with blood plasma cholesterol levels. There is a correlation between saturated fat intake and cholesterol levels but most of the circulating plasma level of cholesterol is of endogenous origin (i.e. produced by the liver).

2.6.3 Advantages and disadvantages of cholesterol

Cholesterol itself isn't bad. Body needs some cholesterol to make hormones, vitamin D, and digestive fluids. Cholesterol also helps the organs function properly. Yet having too much LDL cholesterol can be a problem. High LDL cholesterol over time can damage the arteries, contribute to heart disease, and increase the risk for a stroke.

2.7 Vesicles

Vesicles made by model bilayers have also been used clinically to deliver drugs. Biological membranes typically include several types of molecules other than phospholipids [123]. In cell biology, a vesicle is a structure within or outside a cell, consisting of liquid or cytoplasm enclosed by a lipid bilayer. Vesicles can be prepared artificially in the laboratory using lipids and cholesterol. Depending on the sizes unilamellar vesicles are categorize into three types: 1) Small Unilamellar Vesicles (SUVs) which size range is 20-100 nm, 2) Large Unilamellar Vesicles (LUVs) which size range is 100-1000 nm and 3) Giant Unilamellar Vesicles (GUVs) which size range is 1-80 μm. The different types of unilamellar vesicles are illustrated in Fig. 2.16.

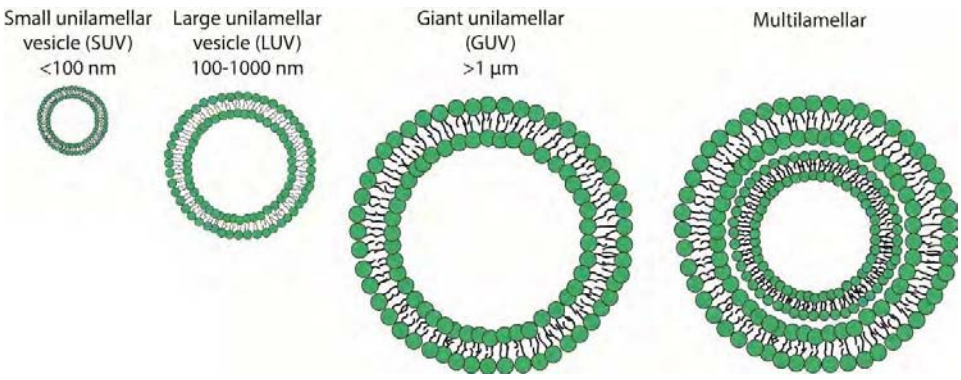

Fig. 2.16 Different classes of vesicles. [123]

CHAPTER 3

MATERIALS AND METHOD

3.1 Chemicals and Reagents

The chemicals and reagents used in this work are of analytical grade without further purification. The lipids 1, 2-dioleoyl-*sn*-glycero-3-phosphotigycerol (sodium salt) (DOPG) and 1, 2-dioleoyl-*sn*-glycero-3-phosphocholine (DOPC) were purchased from Avanti Polar Lipids Inc. (Alabaster, AL) and Cholesterol ($C_{27}H_{46}O$) was purchased from WAKO pharmaceuticals (Japan). Bovine serum albumin (BSA), Piperazine-1, 4-bis (2-ethanesulfonic acid) (PIPES), O, O′-bis (2-aminoethyl) ethyleneglycol-*N*,*N*,*N*′,*N*′,-tetraacetic acid (EGTA) and calcein were purchased from Sigma-Aldrich (Germany). Glucose, sucrose and sodium hydroxide were purchased from Mark Germany.

3.2 Structure of DOPG, DOPC and Cholesterol

The structure of DOPG, DOPC and cholesterol are described below.

DOPG: Phosphatidylglycerol is a glycerophospholipid found in pulmonary surfactant. The general structure of phosphatidylglycerol consists of a L-glycerol 3-phosphate backbone ester-bonded to either saturated or unsaturated fatty acids on carbons 1 and 2 (Fig. 3.1). It is found at high levels in the membranes of all cells and at low levels in fat stores. PG has two hydroxyl groups in its head group. The head group substituent glycerol is bonded through a phosphomonoester. It is an anionic lipid. Molecular weight of DOPG is 775.058 g/mol.

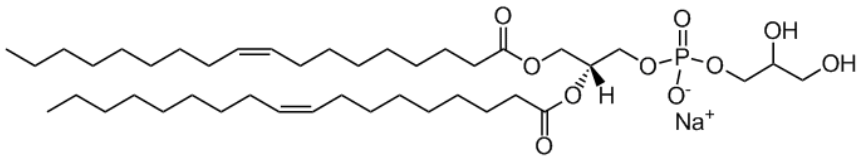

Fig. 3.1 Chemical structure of DOPG.

DOPC: 1,2-Dioleoyl-sn-glycero-3-phosphocholine (DOPC) is a phosphatidylcholine (36:2) in which the phosphatidyl acyl groups at positions 1 and 2 are both oleoyl. Phosphatidylcholine (PC) is generally the most abundant lipid in animal cell membranes providing structural framework with molecular weight 787.1 g/mol (Fig. 3.2). PC is more common in the outer leaflet where it functions as part of the permeability barrier. PC is also

the primary substrate of Phospholipase D enzymes which produce the signaling lipids - phosphatidic acid and lysophosphatidic acid.

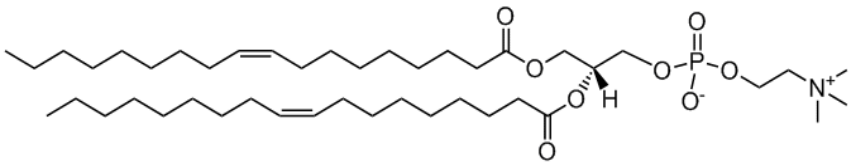

Fig. 3.2 Chemical structure of DOPC.

Cholesterol: Cholesterol is an organic molecule. It is a sterol, a type of lipid. It is biosynthesized by all animal cells and is an essential structural component of animal cell membranes (Fig. 3.3). The hydroxyl group of each cholesterol molecule interacts with water molecules surrounding the membrane, as do the polar heads of the membrane phospholipids and sphingolipids, while the bulky steroid and the hydrocarbon chain are embedded in the membrane, alongside the nonpolar fatty-acid chain of the other lipids. It is a yellowish crystalline solid. In this research, triglyceride was used.

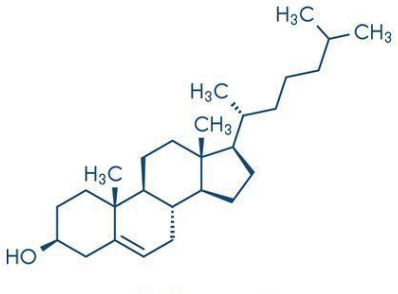

Fig. 3.3 Chemical structure of cholesterol.

3.3 Instruments used for the Synthesis and Purification of GUVs

The following instruments were used for synthesis and characterization.

1) Drying oven (Ecocell)
2) Nitrogen gas cylinder with multistage regulator
3) pH meter (BT675 Boeco, Germany)
4) Vortex mixture (Stuart SA8, UK)
5) Incubator (Phoenix TIN-IN35, Germany)
6) Analytical balance (Radwag, Poland)
7) Frezzer (Siemens)
8) Rotary vacuum pump
9) Centrifuge (NUVE NF 800R, Turkey)

3.4 Synthesis of Lipid Membranes of GUVs

There are several different methods for the formation of GUVs [124]. Here to prepare the population of lipid GUVs we used the natural swelling method [11, 13, 15]. At first, 200 μL of a mixture of 1 mM DOPC and cholesterol (or a mixture of 1 mM DOPG, DOPC and cholesterol) was taken into a 4.5 mL glass vial which was gently shacked and was kept without any motion for 40-60 s to get the compositionally homogeneous mixture of the lipids and cholesterol throughout the total suspension. It is known that due to high diffusion of lipid molecules in chloroform, they are distributed very quickly throughout the bulk of the sample. Then this mixture was dried with a gentle flow of N_2 gas to produce a thin, homogeneous lipid film followed by the vial was placed in a vacuum desiccator for 12 h. During this procedure the lipid bilayer stacks in the vial arise. After this a 20 μL MilliQ water was added into the vial and pre-hydrated for 8 min at 45 ºC following the sample was incubated for 3.5 h at 37 °C with 1 mL MilliQ containing 0.10 M sucrose (for neutral membrane) and 1 mL buffer (10 mM PIPES, 150 mM NaCl, pH 7.0, 1mM EGTA) containing 0.10 M sucrose (for charged membrane). As the result of this procedure, the GUVs contained sucrose in vesicle's interior with different size arise in solution. We have considered early the problem of the GUV's vesiculation [11, 22], and concluded that this time is enough for forming the thermodynamically equilibrium population of GUVs. To observe the population of GUVs in phase contrast microscope, an amount of 280 μL 0.10 M glucose containing MilliQ (for neutral membranes) and 0.10 M glucose containing buffer (for charged membranes) was added into the microchamber. Then 20 μL aliquot of GUVs suspension was introduced into the handmade microchamber and it was waited 20−25 min for achieving the equilibrium settle down of vesicles at the bottom of microchamber. The asymmetrical concentration of sugar between the inside and the outside of GUVs was created for the visualization of GUVs. For removing the strong attraction between the glass surface and the GUVs, the microchamber and the glass surface were coated with 0.10% (w/v) BSA dissolved in the same solution. An inverted phase contrast microscope (Olympus IX-73, Japan) with a 20× objective at 25 ± 1 ºC was used to observe the GUVs and the images were recorded using a charge-coupled device camera (Olympus DP22, Japan). Before going to the next section, it is necessary to clarify the notation used. In particular, the DOPG/DOPC/chol (46/39/15)-GUVs means that in the sample there were 46% of DOPG, 39% of DOPC and 15% of cholesterol (here, C_h is the mole percentage of cholesterol in GUVs), where % indicates the mole%.

The following block diagram (Fig. 3.4) and schematic diagram shows synthesis of GUVs using natural swelling method.

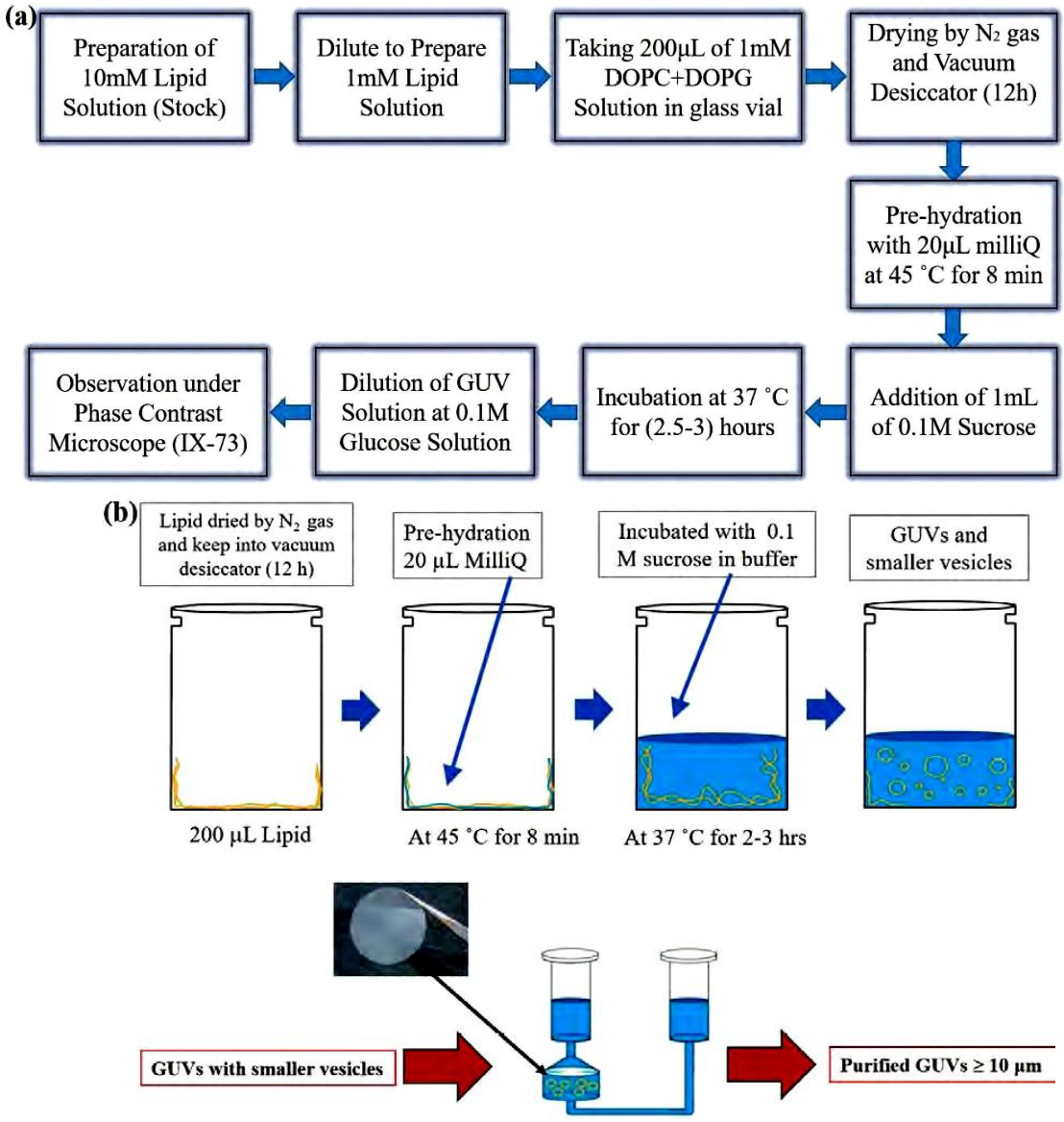

Fig. 3.4 Block diagram (a) and schematic diagram (b) showing steps of natural swelling method.

To prepare the cholesterol (i.e. chol, C_h)-rich neutral membranes, DOPC/chol (100/0, 100/0 indicates molar ratio), DOPC/chol (85/15), DOPC/chol (71/29) and DOPC/chol (60/40)-GUVs were prepared in MilliQ water containing 0.10 M sucrose as an internal solution. As for preparation of the GUVs with charged membranes containing cholesterol, it is necessary to make a note. Embedding in lipid monolayer cholesterol condenses it and

thereby changes the area per lipid molecule of this monolayer. To obtain GUVs with more or less same surface charge density in case of the charged GUVs with the different fractions of cholesterol (that is necessary for comparison of the results of different experiments) it is necessary to make some specific procedure. It is well reported that after addition of cholesterol in the lipid membranes its condensation occurs [125-128]. In the absence of cholesterol the cross sectional area of DOPG (a_{DOPG}) and DOPC (a_{DOPC}) lipid molecules is about 72.5 Å^2/molecule (Nagle and Tristram-Nagle 2000). However, in the presence of cholesterol the cross sectional area of these molecules decreases to about 50, 42 and 40 Å^2/molecule for 15, 29 and 40 mole% cholesterol, respectively [129-130]. The cross sectional area of cholesterol molecule is about half of DOPG or DOPC lipid one i.e. 33–38 Å^2/molecule [126]. The surface charge density of cholesterol-free DOPG/DOPC/chol (70/30/0)-GUVs, $\Omega_{\mathrm{PG}} = eX / a_{\mathrm{DOPG}}$ is – 0.154 C/m^2, where X is the DOPG mole fraction in the membranes and e is electronic charge. The surface charge density of cholesterol containing charged GUVs is determined by expression $\Omega_{\mathrm{ch}} = \dfrac{eX}{a_{\mathrm{DOPG}}\left(1-c_{\mathrm{h}}\right)+a_{\mathrm{ch}}c_{\mathrm{h}}}$, where X is the fraction of DOPG molecules in GUV and $c_{\mathrm{h}} = C_{\mathrm{h}}/100$ is the mole fraction of cholesterol in GUVs. Therefore, to obtain the cholesterol containing charged GUVs with more or less same surface charge density (≈ – 0.15 to – 0.16 C/m^2) for different fractions of cholesterol the GUVs with different composition (namely DOPG/DOPC/chol (46/39/15), DOPG/DOPC/chol (43/28/29) and DOPG/DOPC/chol (40/20/40)) were prepared in the buffer containing 0.10 M sucrose as an internal solution. The total salt concentration, C, in the buffer was 162 mM [30]. The values of X in the DOPG/DOPC/chol (70/30/0), DOPG/DOPC/chol (46/39/15), DOPG/DOPC/chol (43/28/29) and DOPG/DOPC/chol (40/20/40)-GUVs were 0.70, 0.46, 0.43 and 0.40, respectively. Hence all these GUVs with 15, 29 and 40 mole% cholesterol have approximately the same surface charge density (≈ – 0.15 to – 0.16 C/m^2), which is close to the surface charge density in the membranes of DOPG/DOPC/chol (70/30/0)-GUVs. Table 3.1 shows the values of surface charge density of different membranes.

Table 3.1 Surface charge density of cholesterol containing membranes.

Cholesterol, C_h (mole %)	Surface area of DOPG mole fraction, a_{DOPG} (m^2/molecule)	Surface area of cholesterol mole fraction, a_{ch} (m^2/molecule)	Surface charge density of membranes, Ω_{ch} (C/m^2)
0	72.5×10^{-20}	0	0.154
15	50.0×10^{-20}	34×10^{-20}	0.150
29	42.0×10^{-20}	35×10^{-20}	0.172
40	40.0×10^{-20}	37×10^{-20}	0.160

3.5 Purification Method of GUVs

After incubation, the GUVs suspension was centrifuged at 13,000×g for 20 min at 20 °C using a refrigerated centrifuge (NF 800R, NUVE, Turkey) and then the supernatant containing GUVs was filtered through a 10 μm diameter pores nuclepore polycarbonate membrane (Whatman® Nuclepore™ Track-Etched Membranes, UK) clamped in a polypropylene filter holder (Swinnex, ϕ = 25 mm, Millipore Co., Billerica, MA). The arrangement of the purification technique is depicted in Fig. 3.5.The upper end of the filter holder was connected with a 10 mL plastic (polypropylene) syringe 2 (JMI Syringes and Medical Devices Ltd. Bangladesh) and the lower end was connected with a tube containing three different types of polypropylene fittings (Luer fittings VRFE6, VRFC6, VRSC6; AS-ONE, Japan) having inner diameter 3 mm as shown in Fig. 3.5. In this case, the tube contains a total number of 11 fittings instead of 9 that was used in the membrane filtering method [11]. The other end of the tube was connected to syringe 1 having the same volume of 10 mL. The GUVs suspension in buffer containing 0.10 M glucose was added to syringe 1 where the flowing of buffer was continuously controlled due to the double headed peristaltic pump (CPPSP2, Shenchen, China) through a plastic tube of inner diameter 3 mm(JMI Syringes and Medical Devices Ltd. Bangladesh). Before starting the flow of buffer from beaker to syringe 1, the air bubbles were carefully removed from the polypropylene tube and filter holder.

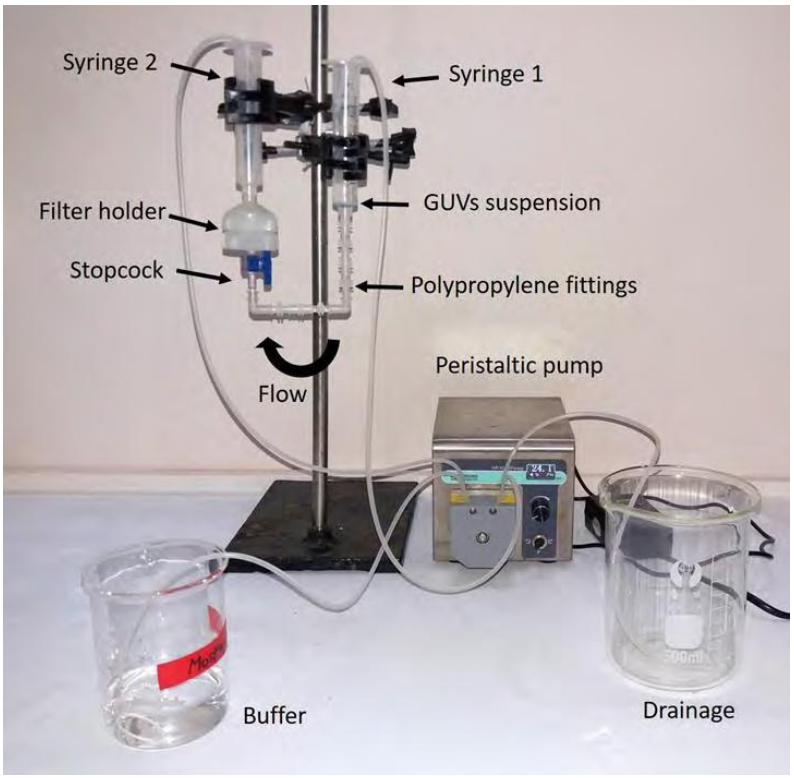

Fig. 3.5 Set-up of membrane filtering method.

The direction of the flow of buffer at the filter was from the bottom to the top, shown in Fig. 3.5, so the smaller vesicles passed through the filter into the upper syringe (syringe 2). After filtering for a definite time, the addition of buffer containing 0.1 M glucose to syringe 1 was stopped, and then the buffer inside syringe 2 was removed by the pump at the same flow rate. Finally, the suspension in the tube and the filter holder was collected and used as a purified GUV suspension.

3.6 Observations of GUVs

At first, 280 µL buffer containing 0.1 M glucose (external solution) was transferred into a handmade microchamber. Then 20 µL aliquot of GUVs suspension (0.1 M sucrose in buffer as the internal solution) was mixed into the buffer of microchamber (Fig. 3.6). To visualize the GUVs in the suspension, sugar asymmetry between the inside and the outside of GUVs is created. The GUVs were settled down at the bottom of the microchamber due to the density difference of sugar solution. The difference inrefractive indices of the sugar solution enhanced the contrast of GUVs during the observation. To remove the strong attraction between the glass surface and the GUVs, the microchamber along with the glass surface were coated with 0.10% (w/v) BSA dissolved in buffer containing 0.1 M glucose.

Fig. 3.6 GUVs suspension in microchamber.

Phase contrast microscopy is suitable for viewing colorless and transparent specimens and live cells. It utilizes the difference between light rays propagating directly from the light source and light rays refracted by the specimen when light passes through it to add bright/dark contrast to images of transparent specimens. The microscope is fitted with a phase-contrast objective and a condenser for observations. Specimens may be made to appear dark against a bright background (positive contrast) or bright against a dark background (negative contrast). The borders of images are surrounded by a characteristic bright "halo." The GUVs were observed using an inverted phase contrast microscope (Olympus IX-73, Japan) with a 20x objective at 25 ± 1 ºC and the images were recorded using a digital camera (Model: DP22, Olympus) shown in Fig. 3.7.

Fig. 3.7 Inverted phase contrast microscope (Olympus IX-73, Japan).

To investigate the effects of cholesterol of the size of vesicles and the IRE-induced pore formation in GUVs, both phase contrast and fluorescence microscope is used. Fig. 3.8 shows the images in optical microscope. The green color in the inside of GUVs shown in Fig. 3.8(b) indicates the encapsulated calcein solution.

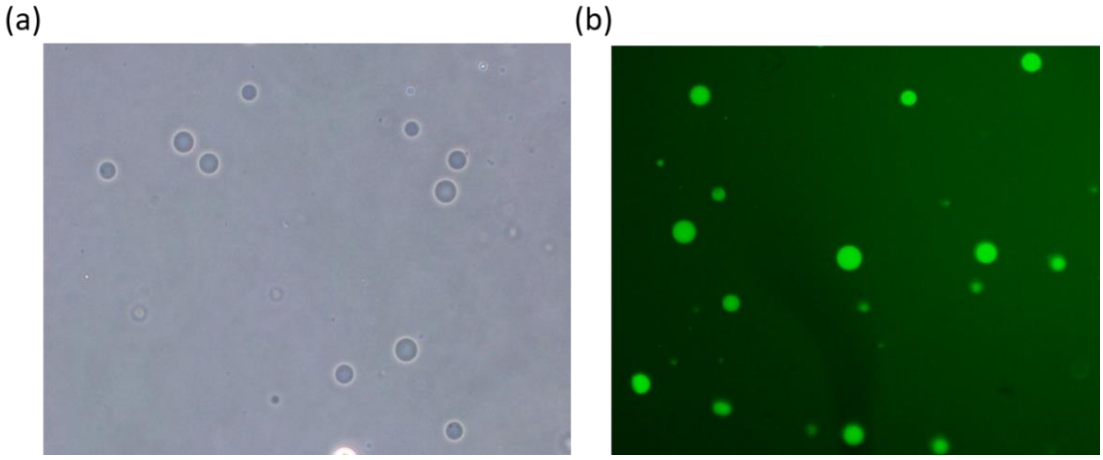

Fig. 3.8 (a) Phase contrast image and (b) Fluorescence GUVs images.

3.7 Method of Applying IRE Technique in GUVs

220V AC voltage was applied to a single-phase transformer for generating a variable secondary output of 0-800 V AC with minimum current of 5 A. Using a full wave rectifier, the secondary voltage was converted to DC voltage. A MOSFET (Metal–Oxide–Semiconductor Field-Effect Transistor) based switching circuit was used for getting the square pulses of 1.1 kHz frequency. A microcontroller is used to control the IRE signal. The gold coated electrode of length 17.0 mm and width 2.54 mm (Model: SH-17P-25.5, Hellotronics) was used for applying the signal on GUVs. To apply the IRE signal on GUVs, we initially keep the E at around 440 V/cm and focus a ‘single GUV’ between the electrodes. Then the value of E increases rapidly (~7 s) to reach a specific level and this E is held constant for a specific time (i.e. 60 s). The experimental setup for applying the IRE signal on GUVs is illustrated in Fig. 3.9. Pore formation time is defined as the time when the GUV was started to break, and had a time resolution of less than 1 s.

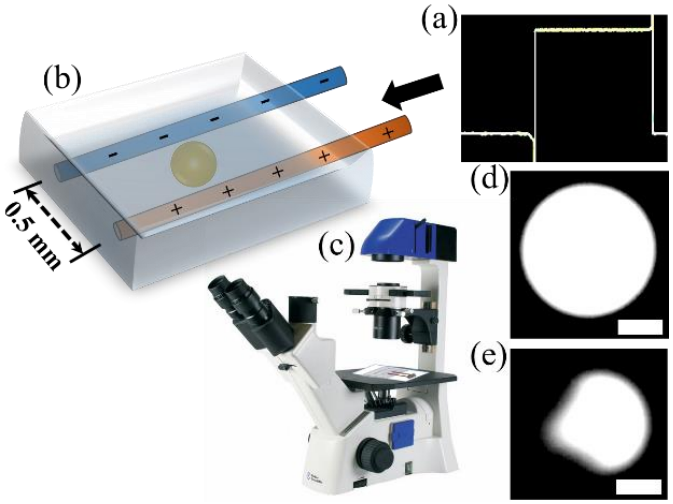

Fig. 3.9 Experimental setup for applying the IRE signal on GUVs. (a) IRE signal (b) Targeted GUV in IRE system (c) Microscopic system for observing the GUV (d) Intact GUV (fluorescence image) (e) Ruptured GUV. Bar corresponds to 10 μm.

Since the lipid membranes are impermeable to ions the electric field, E, polarizes the inner and outer free charges of buffer of GUV with radius R. The accumulation time of free charges is calculated by the Maxwell–Wagner equation [131]. The accumulation of free charges increases the membrane potential V_m, which induces the stretching of membranes. Such stretching induces lateral tension in the membranes of GUVs. The IRE-induced lateral tension, σ_c, is calculated by the following Maxwell stress tensor [131, 132-133].

$$\sigma_c = \varepsilon_m \varepsilon_0 \left(\frac{h}{2h_e{}^2}\right) V_m{}^2 \qquad (3.1)$$

where, ε_m is the permittivity of the membrane (~4.5 [134], ε_0 is the permittivity of free space, h is the membrane thickness (~4 nm) [89] and h_e the dielectric thickness of membrane (~2.8 nm) [135]. It is possible to employ a simple model in order to consider the uniform field on the GUV with negligible membrane conductivity. The induced membrane potential at each membrane point is defined as follows by considering the membrane charging time $\tau_{charg} \approx 0$ [131, 136].

$$V_m = 1.5\, RE \qquad (3.2)$$

Therefore, equation (3.1) can be simplified as follows.

$$\sigma_c = 22.86\, R^2 E^2 \text{ [mN/m]} \qquad (3.3)$$

Equation (3.3) shows that for a GUV with radius R, σ_c can be described as a function of E. In this experiment E = 350-560 V/cm electric field is applied. For R = 10 μm and E = 553 V/cm, V_m = 0.83 V. The membrane tension is considered as constant as it has been used a particular value of E for a specific R. By choosing the appropriate value of E, various constant tensions are applied on GUVs.

CHAPTER 4

RESULTS AND DISCUSSION

4.1 Size Distribution of Vesicles

4.1.1 Effects of cholesterol on the size distribution of GUVs of neutral membranes

To investigate the effects of cholesterol (chol, C_h) on the size distribution of GUVs in vesicle population, primarily it has been considered that the GUVs with neutral membranes using various molar ratios of C_h. Fig. 4.1 shows the experimental results of DOPC/chol (100/0, 100/0 indicates molar ratio) and DOPC/chol (71/29)-GUVs. The phase contrast image of DOPC/chol (100/0)-GUVs in the suspension (i.e., for $C_h = 0$) is shown in Fig. 4.1(a). After measuring the diameters, D, of $N = 350$ GUVs (i.e., N is the number of measured GUVs) from the several phase contrast images of DOPC/chol (100/0)-GUVs, a histogram of the size distribution of GUVs was obtained (Fig. 4.1(b)). In each experiment there were about 350 GUVs which were chosen arbitrary from the entire ensemble. It has been considered that this amount is quite enough to obtain a representative histogram. It is seen that the shape of histogram is asymmetric with positive skewness, indicating a large fraction of small GUVs with 3–10 μm diameters (which is smaller than GUVs of the average diameter) and a small fraction of more than 10 μm diameters GUVs. Note, the similar results were obtained for other systems (for DOPC-GUVs [30] and for POPC/cholesterol-GUVs [137]. One can assume that such a size distribution of vesicles is a characteristic property of populations of lipid GUVs. To get the average values of the distribution parameters it has been repeated the experiment and got the similar result (i.e., the total number of experiments was $n = 2$-3).

Then, it has been considered that the GUVs with membranes containing the cholesterol. The results of this experiment (phase contrast image for DOPC/chol (71/29), i.e., $C_h = 29$) is shown in Fig. 4.1(c). The histogram based on the 350 GUV's observations (i.e., $N = 350$) from several phase contrast images has been constructed (Fig. 4.1(d)). It is seen that as in case of DOPC/chol (71/29)-GUVs the shape of histogram is also asymmetric, indicating a large number of more than 11 μm diameters GUVs and a small number of 3–11 μm diameters GUVs. The similar results were also obtained in other independent experiments. It has been performed 2–4 independent experiments in each condition. But it has been

presented only one independent experiment in each condition for avoiding the redundant. The average value D_{ave} (i.e. the arithmetic mean over all measured GUVs) from these two experiments is shown in table 4.1. By comparing the histograms of Figs. 4.1(b) and 4.1(d) one can conclude that with the increase of C_h the size distribution of GUVs shifts in the range of larger vesicles, indicating the decrease of histogram asymmetricity. The GUVs size distribution for cholesterol-rich neutral GUVs was also analyzed for two other concentrations namely C_h = 15 and 40 (see results in Table 4.1).

To analyze the experimental results quantitatively, we use a well-known lognormal distribution [88]:

$$f(D) = \frac{1}{D}\frac{1}{\sigma\sqrt{2\pi}}\exp\left[-\frac{\{\ln(D)-\mu\}^2}{2\sigma^2}\right]$$
$$= \frac{1}{D}\frac{1}{\sigma\sqrt{2\pi}}\exp\left[-\frac{\{\ln(D/\rho)\}^2}{2\sigma^2}\right], \qquad (4.1)$$

where $f(D)$ indicates the probability density function (frequency of GUVs with diameter D), the dimension median ρ (or dimensionless $\mu = \ln\rho$) and σ^2 are the distribution parameters, more μ is mean of distribution of (ln$D$). The average value (diameter) of the distribution, D_{ave}, is calculated using equation 4.2 as follows [88]:

$$D_{ave} = \int_0^\infty Df(D)\,dD = \exp\left(\mu + \frac{1}{2}\sigma^2\right) = \rho\exp\left(\frac{\sigma^2}{2}\right) \qquad (4.2)$$

Note, the similar approach based on this distribution was used for the description of the distribution of GUVs suspension at various conditions [11, 87].

Figs. 4.1(a) and 4.1(b) show a phase contrast image and a size distribution histogram of DOPC/chol (100/0)-GUVs, respectively. Figs. 4.1(c) and 4.1(d) show a phase contrast image and a size distribution histogram of DOPC/chol (71/29)-GUVs, respectively. The blue lines show the best fitting curves of equation 4.1. The parameters in Fig. 4.1(b) are μ = 2.25, σ = 0.49, and in Fig. 4.1(d) are μ = 2.63, σ = 0.39. The values of the coefficient of determination, R^2, are obtained 0.91 in Fig. 4.1(b) and 0.95 in Fig. 4.1(d) from the fitted (blue) curves. The red lines show the best fitting theoretical curves corresponding to the equation 4.7. The fitting parameters in Fig. 4.1(b) are K_{ben} = 19.0 k_BT, D_{freq} = 6.4 μm, L = 3360, and in Fig. 4.1(d) are K_{ben} = 28.5 k_BT, D_{freq}= 9.1 μm and L = 4230. The values of R^2

in Fig. 4.1(b) and Fig. 4.1(d) are obtained 0.92 and 0.69, respectively from the fitted (red) curves.

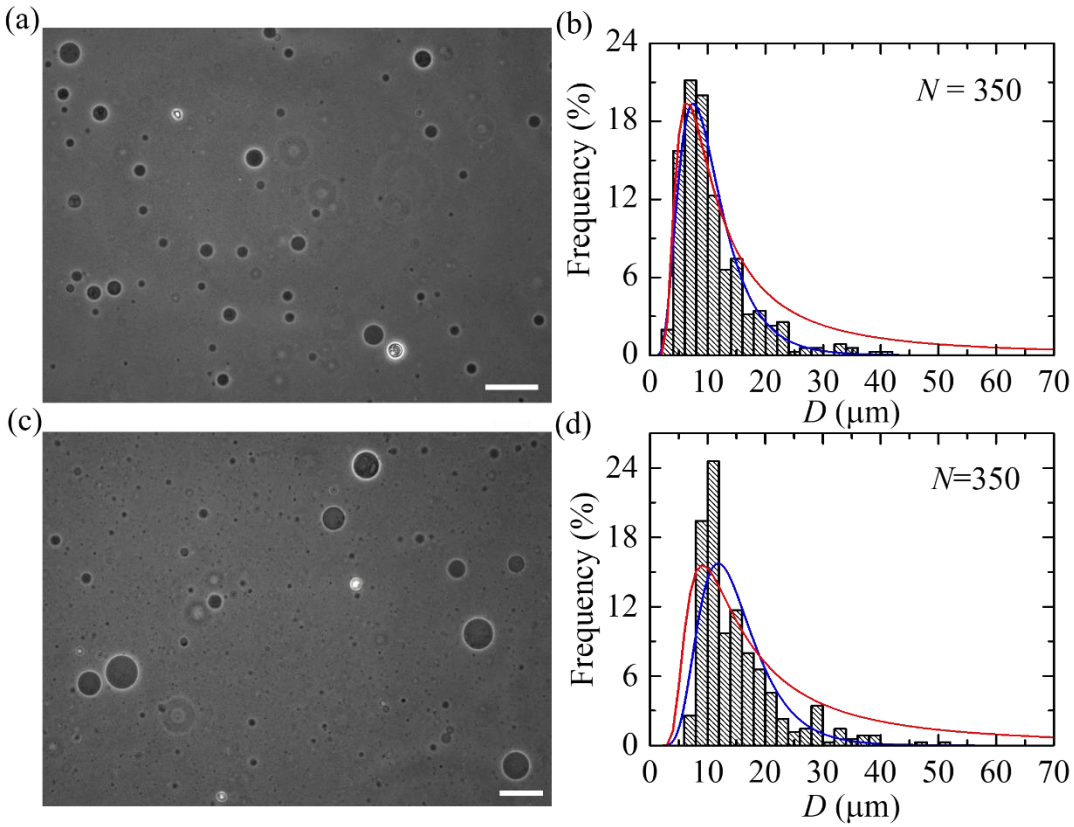

Fig. 4.1 Effects of cholesterol on the size distribution of GUVs containing neutral membranes. The bar in the images corresponds to 50 μm.

In the first independent experiment, the average sizes (diameters) of GUVs, D_{ave1}, were obtained 10.7 μm for DOPC/chol (100/0)-GUVs and 15.0 μm for DOPC/chol (71/29)-GUVs. Then the similar experiments were performed and the average sizes of GUVs, D_{ave2}, were obtained 9.9 μm for DOPC/chol (100/0)-GUVs and 14.9 μm for DOPC/chol (71/29)-GUVs from the second independent experiment. The arithmetic mean of the average sizes of GUVs, $D_{ave} = (D_{ave1} + D_{ave2})/2$, was calculated from the results of two independent experiments (i.e. $n = 2$) using $N = 350$ GUVs in each experiment. The D_{ave} were obtained (9.9 ± 0.8) and (14.9 ± 0.04) μm (± indicating the standard error) for DOPC/chol (100/0)-GUVs and DOPC/chol (71/29)-GUVs, respectively. The average values of D_{ave} at various cholesterol concentrations are presented in Table 4.1.

4.1.2. Effects of cholesterol on the size distribution of GUVs of charged membranes

In the previous paper, it has been demonstrated that the electrostatic effects influence significantly on the size distribution of GUVs [87]. It is the reason why it has been considered here also the effect of cholesterol on such distribution in case of GUVs contained the charged lipids. The effects of cholesterol in case of charged vesicles membranes on the size distribution of GUVs were investigated upon fixing the surface charge density of membranes (≈ – 0.15 to – 0.16 C/m^2). It has been analyzed the system by varying cholesterol fraction from C_h = 0 to 40 at C = 162 mM. Fig. 4.2 shows the experimental results for DOPG/DOPC/chol (46/39/15) and DOPG/DOPC/chol (40/20/40)-GUVs. A typical experimental result of the phase contrast image of GUVs suspension for DOPG/DOPC/chol (46/39/15)-GUVs is shown in Fig. 4.2(a). The corresponding histogram of the size distribution of GUVs using N = 350 is shown in Fig. 4.2(b). It is seen that as well in case of DOPG/DOPC/chol (46/39/15)-GUVs the histogram is asymmetrical with the positively skewed distributions, i.e., there are a small number of GUVs with diameters greater than 14 μm and a large number of GUVs with diameters 3–14 μm. The similar results were also obtained in other independent experiments. A typical phase contrast image in the same buffer for DOPG/DOPC/chol (40/20/40)-GUVs and the corresponding histogram (using N = 350) are shown in Fig. 4.2(c) and Fig. 4.2(d) correspondently. In this histogram, a large number of GUVs with diameters greater than 15 μm and a small number of GUVs with diameters 3–15 μm are observed. The similar results were obtained from other experiments. Therefore, with the increase of cholesterol the peak of the histogram of the vesicle distribution shifts to the region of the large GUVs. The histograms of Fig. 4.2(b) and 4.2(d) are fitted (blue line) with equation 4.1, and the diameters of the GUVs distribution were obtained 15.6 and 18.5 μm using equation 4.2 for DOPG/DOPC/chol (46/39/15) and DOPG/DOPC/chol (40/20/40)-GUVs, respectively. The average values of the GUVs diameters were obtained (16.0 ± 0.6) and (19.7 ± 1.2) μm for DOPG/DOPC/chol (46/39/15) and DOPG/DOPC/chol (40/20/40)-GUVs, respectively using 2–3 independent experiments. Figs. 4.2(a) and 4.2(b) show a phase contrast image and a size distribution histogram of DOPG/DOPC/chol (46/39/15)-GUVs, respectively. Figs. 4.2(c) and 4.2(d) show a phase contrast image and a size distribution histogram for DOPG/DOPC/chol (40/20/40)-GUVs, respectively. The blue lines show the best fitting theoretical curves corresponding to eq. 4.11. The parameters in Fig. 4.2(b) are μ = 2.66, σ = 0.42, and in Fig. 4.2(d) are μ = 2.74, σ = 0.60. The values of R^2 are obtained 0.88 in Fig. 4.2(b) and 0.84 in Fig. 4.2(d) for the fitted (blue) curves. The red lines show the theoretical curves of equation

4.7. The parameters in Fig. 4.2(b) are K_{ben} =26.6 k_BT, D_{freq} = 8.6 μm, L = 3700, and in Fig. 4.2(d) are K_{ben} = 36.8 k_BT, D_{freq} = 9.5 μm and L = 3600. The values of R^2 in Fig. 4.2(b) and Fig. 4.2(d) are obtained 0.76 and 0.86, respectively for the fitted (red) curves.

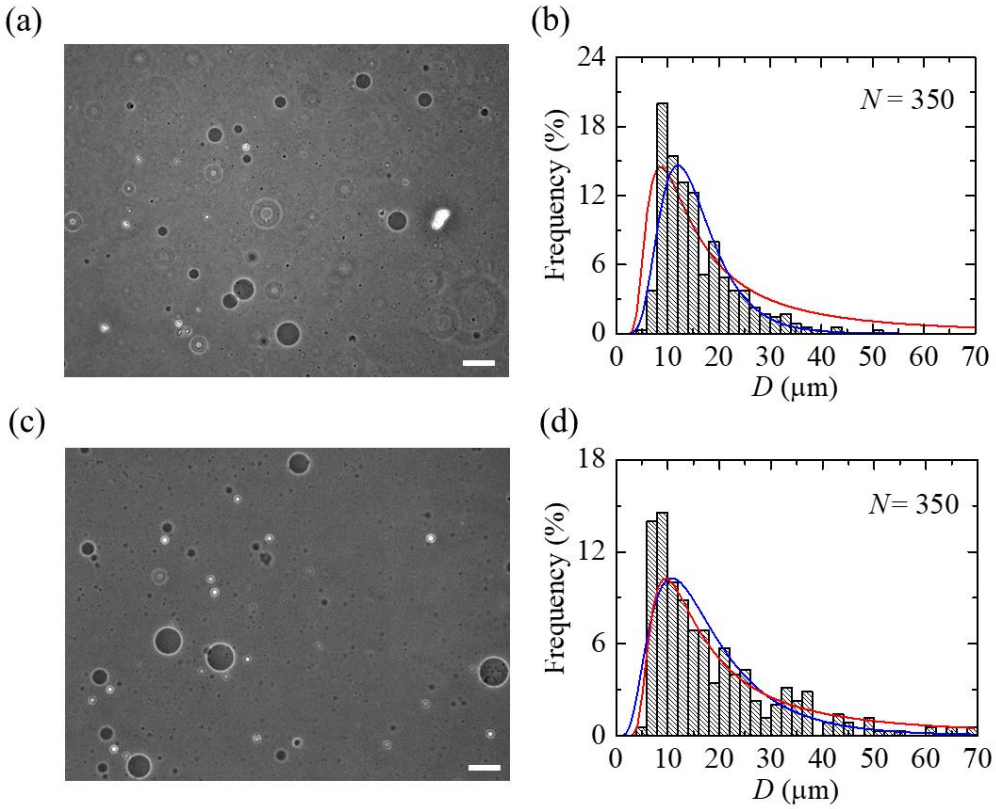

Fig. 4.2 Effects of cholesterol on the size distribution of charged GUVs. The bar in the images corresponds to 50 μm.

The values of D_{ave} and K_{ben} at various cholesterol concentrations in charged membranes are presented in table 4.1. The dependence of D_{ave} on C_h for cholesterol-rich neutral GUVs and cholesterol-rich charged GUVs is shown in Fig. 4.3. The solid lines show the theoretical curve corresponding to the eqs 4.12, 4.13 and 4.14. The fitting parameters for DOPC/chol-GUVs are D_{freqPC} = 15.4 μm, K_{DOPC} = 19.1 k_BT and η = 0.5 k_BT and for DOPG/DOPC/chol-GUVs are D_{freqPC} = 22.8 μm, K_{DOPC} = 19.1 k_BT, η = 0.28 k_BT and γ = 2.5 k_BT/mM$^{3/2}$. The values of R^2 are obtained 0.99 and 0.73 for DOPC/chol-GUVs and DOPG/DOPC/chol-GUVs, respectively.

Table 4.1 The values of average size of GUVs and bending modulus of neutral and charged (surface charge density ≈ – 0.15 to – 0.16 C/m^2 and C = 162 mM) membranes.

DOPC/chol			DOPG/DOPC/chol		
Chol (%)	D_{ave} (μm)	K_{ben} (k_BT)	Chol (%)	D_{ave} (μm)	K_{ben} (k_BT)
0	9.9 ± 0.8	19.1 ± 0.1	0	16.5 ± 0.3	25.9 ± 0.3
15	12.0 ± 0.4	23.1 ± 0.1	15	16.0 ± 0.6	26.8 ± 0.1
29	14.9 ± 0.04	28.6 ± 0.01	29	18.7 ± 0.3	32.1 ± 0.3
40	15.7 ± 0.5	31.0 ± 0.1	40	19.7 ± 1.2	37.1 ± 0.3

It is seen that as the cholesterol concentration in GUVs membrane increases the average size of the GUVs increases for both the neutral and charged membranes. So, the results of this research shows that the sizes of self-assembled neutral and charged GUVs depend on the cholesterol concentration in vesicle membranes. Generalizing these results one can conclude that with the increase of cholesterol the fraction of large GUVs in population of vesicles increases.

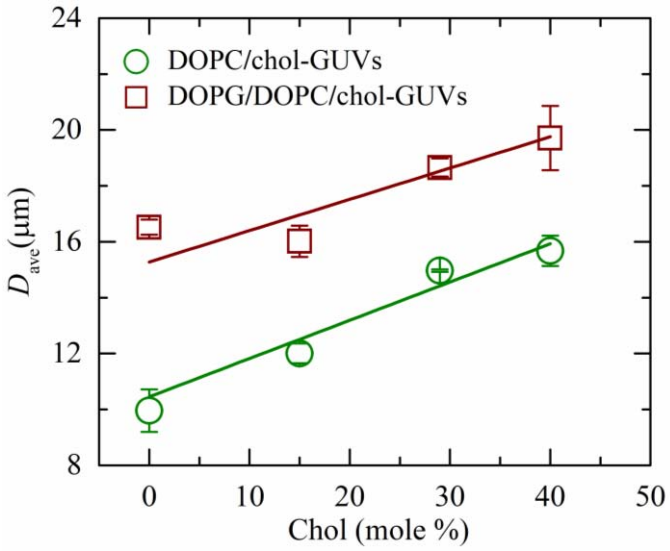

Fig. 4.3 The cholesterol concentration dependent average size of DOPC/chol-GUVs and DOPG/DOPC/chol-GUVs. Average values and standard errors of the size for each membrane were obtained from 2–3 independent experiments using 350 GUVs in each experiment.

It has been discussed that these results in framework of the theory which describes the behavior of the system as interplay between the entropy of the system and bending energy

of lipid membrane. It is worth to note that this results correspond to experimental investigations of the effects of cholesterol on the size of sonicated phospholipid vesicles where the increase of cholesterol from 0 to 30 mole % induced the increase of the vesicle surface area from 7.7 to 14.0 nm was demonstrated [138].

4.2. Theory

Recently, it has been developed the theory of the formation of GUVs in population [30]. Here a short description of this theory is given. We postulate the existence of some initial population of lipid bilayer aggregates which treated as population of N_{init} lipid supramolecular structures. All such aggregates in this initial population are exactly the same. The surface area of each aggregate is S_{init}. The initial population transforms into population of different sizes GUVs in which the final equilibrium distribution of GUVs by the sizes achieves. Each GUV in this population is described by a number of initial aggregates m, which composes it. Because the total surface of m initial aggregates is mS_{init}, the diameter of m-GUV (i.e. composed on m initial aggregates) is $D_{\text{m}} = \sqrt{mS_{\text{inst}} / \pi}$. The state of such system is determined by the Helmholtz's free energy as follows [29, 87]:

$$\frac{G(n_{\text{m}}, m)}{k_{\text{B}}T} = \left(4\pi K_{\text{ben}} \sum_{m=1}^{N_{\text{init}}} n_{\text{m}} \right) - \left[N_{\text{init}} \ln(\phi N_{\text{init}}) - \sum_{m=1}^{N_{\text{init}}} n_{\text{m}} \ln(m\, n_{\text{m}}) \right] \qquad (4.3)$$

Here n_{m} is the number of m-GUVs in the system, K_{ben} is the bending modulus of membranes in $k_{\text{B}}T$ unit where k_{B} is the Boltzmann constant and T is the absolute temperature and ϕ is the volume fraction of initial vesicles in solution. The first term in equation 4.3 describes the bending energy [139] of all vesicles in the GUVs population and the second term is the contribution of configurational entropy. In the general case, the bending energy of the lipid bilayer consists of a number of components [139, 140-142]. In the case of giant unilamellar lipid vesicles considered here, all these components can be described by a single generalized parameter K_{ben}. In our case, there are no problems associated with spontaneous curvature since we consider only unilamellar vesicles (with a symmetric bilayer) for which the total spontaneous curvature is zero. As for the component associated with the Gaussian one, in our case this component is summed up with the component describing the local curvature, since both the radii of GUV's principal curvatures coincide. Equation 4.3 determines the free energy of the GUVs population for

any arbitrary set of $\{n_m, m\}$. The equilibrium state of the population is determined by equation

$$\frac{\partial G(n_m, m)}{\partial n_m} = 0 \quad \text{for } (n_m = n_{m1}, n_{m2}, n_{m3,\ldots\ldots}) \tag{4.4}$$

under condition

$$\sum_{m=1}^{N_{init}} n_m m = N_{init} \tag{4.5}$$

The solution of equation 4.4 and 4.5 is as follows,

$$n_m(D_m) = N_{init}\phi \frac{S_{init}}{\pi D_m^2} \exp\left[-\frac{4S_{init}}{D_m^2} K_{ben}\right] \tag{4.6}$$

The non-measurable parameter m in equation 4.6 is converted to the measurable one, namely to the size of m-GUVs, D_m, by using expressions $D_m = \sqrt{mS_{init}/\pi}$ and $D_{freq} = 2\sqrt{S_{init}K_{ben}}$. The latter expression is obtained from the condition $\frac{\partial n_m}{\partial D_m} = 0$. The parameter D_{freq} is the mode of the distribution or in other words, the most frequent diameter that can be obtained from experimental histograms. Then one can obtain from equation 4.6 the probability density function $f(D_m)$ (i.e. histogram) as follows,

$$f(D_m) = \frac{n_m(D_m)}{\Delta D_m} = \left(\frac{L}{K_{ben}}\right)\left(\frac{D_{freq}}{D_m}\right)^2 \exp\left[-\left(\frac{D_{freq}}{D_m}\right)^2\right], \tag{4.7}$$

where the step of experimental histogram $\Delta D_m = 2$ μm and $L = N_{init}\phi/(4\pi\,\Delta D_m)$. Equation 4.7 has two fitting parameters, D_{freq}, and K_{ben} (L is normalized parameter). The value of K_{ben} can be determined in each specific experiment from the fitting of the corresponding histogram (see also the legends in figure 4.2 and figure 4.3). Using the equation 4.7, one can also determine the average size of GUVs in population as follows [143]:

$$D_{ave} = \int_0^\infty D_m f(D_m)\, dD_m = -\left(\frac{LD_{freq}^2}{2K_{ben}}\right) Ei\left[-\left(\frac{D_{freq}}{D_{max}}\right)^2\right] \tag{4.8}$$

Here $Ei(z)$ is the exponential integral function, D_{max} is the size of the greatest vesicle obtained in experiment. This equation is not convenient for an analysis of the GUV's parameters influence on the D_{ave}. Hence it is worth to present this equation in a form that

will make it relatively easy to analyze the influence of the system parameters on the distribution of vesicles by size. Because the equation 4.7 gives the positively skewed distributions, we approximate the equation 4.7 by lognormal distribution (see equation 4.1), which also gives the positively skewed distributions. By comparing equation 4.1 and 4.7 and using certain conditions we obtained after manipulation as follows [87].

$$D_{\text{ave}} = \exp\left(\mu + \frac{1}{2}\sigma^2\right) = D_{\text{freq}} \exp\left(\frac{3}{2}\sigma^2\right) = D_{\text{freq}} b, \tag{4.9}$$

where $D_{\text{freq}} = \exp\left(\mu - \sigma^2\right)$ and $b = \exp\left(3\sigma^2 / 2\right) = 0.67$. As it was discussed above the key physical parameter influencing on GUVs size distribution (and therefore, on the average size D_{ave}) is K_{ben}. A few words about this parameter we obtained K_{ben} in our experiments for $C_{\text{h}} = 0$ from the fitting of experimental results by theoretical equation 4.7 in the range of 19–37 $k_{\text{B}}T$ (see table 4.1). These values are at the same order as the values of K_{ben} for PC membrane [89] and for PG/PC membrane [87, 139,144]. Therefore, the value of D_{ave} is determined by D_{freq} which in its turn is determined by K_{ben} (see above $D_{\text{freq}} = 2\sqrt{S_{\text{init}} K_{\text{ben}}}$). We postulate for simplicity that S_{init} does not depend on cholesterol concentration at the same time K_{ben} depends on C_{h}. It means that in our model D_{ave} is proportional only to $\sqrt{K_{\text{ben}}}$ i.e.,

$$D_{\text{ave}} = \left(2b\sqrt{S_{\text{init}}}\right)\sqrt{K_{\text{ben}}} = \text{const}\sqrt{K_{\text{ben}}} \tag{4.10}$$

This assumption is supported by our experiments (see Fig. 4.4).

It has been shown early that electrical charge of the vesicle membrane increases the bending modules of membrane K_{ben} [87]. The results of the current research show that the cholesterol also increases K_{ben}. Hence one can consider as a first approximation that the bending modulus of cholesterol-rich membranes can be written as sum of the three components, namely as follows,

$$K_{\text{ben}} = K_{\text{DOPC}} + K_{\text{ben}}^{\text{el}} + K_{\text{ben}}^{\text{ch}}, \tag{4.11}$$

where K_{DOPC} is the bending modulus of pure DOPC membrane (i.e. without cholesterol), $K_{\text{ben}}^{\text{el}}$ indicates the surface charge density term of bending modulus and $K_{\text{ben}}^{\text{ch}}$ indicates the cholesterol term of the modulus. Inserting equation 4.11 in equation 4.10 one obtains the expression for D_{ave} as follows,

$$D_{\text{ave}} = bD_{\text{freq}} = 2b\sqrt{\left(K_{\text{DOPC}} + K_{\text{ben}}^{\text{el}} + K_{\text{ben}}^{\text{ch}}\right)S_{\text{init}}}$$
$$= 2b\sqrt{K_{\text{DOPC}}S_{\text{init}}}\sqrt{1+\frac{K_{\text{ben}}^{\text{el}} + K_{\text{ben}}^{\text{ch}}}{K_{\text{DOPC}}}}$$
$$= bD_{\text{freqPC}}\sqrt{1+\frac{K_{\text{ben}}^{\text{el}} + K_{\text{ben}}^{\text{ch}}}{K_{\text{DOPC}}}} \approx bD_{\text{freqPC}}\left(1+\frac{K_{\text{ben}}^{\text{el}} + K_{\text{ben}}^{\text{ch}}}{2K_{\text{DOPC}}}\right), \qquad (4.12)$$

where, $D_{\text{freqPC}} = 2\sqrt{K_{\text{DOPC}}S_{\text{init}}}$ is the most frequent vesicle size in case of DOPC-GUVs. It was taking into account in equation 4.12 that $\left(K_{\text{ben}}^{\text{el}} + K_{\text{ben}}^{\text{ch}}\right)/K_{\text{DOPC}} < 1$ in the total range of the cholesterol concentrations used in our experiments.

4.3 Discussion on Bending Modulus

4.3.1 Average size of GUVs and the bending modulus of membranes

As it is following from equation 4.10 the average size of GUVs in the population is determined by value of K_{ben}. Fig. 4.4 shows the dependence of D_{ave} on $\sqrt{K_{\text{ben}}}$ drawing on the base on table 4.1. It is seen from this figure that D_{ave} can be approximated by a linear function of $\sqrt{K_{\text{ben}}}$. The appropriate constants are obtained from Fig. 4.4 and which were 2.63 [μm/$(k_{\text{B}}T)^{1/2}$] for cholesterol-rich neutral membranes and 3.17 [μm/$(k_{\text{B}}T)^{1/2}$] for cholesterol-rich charged membranes. Hence, one can conclude that the above-mentioned assumption (see equation 4.10) is valid. More increase of K_{ben} results the increase of the average size of GUVs in population.

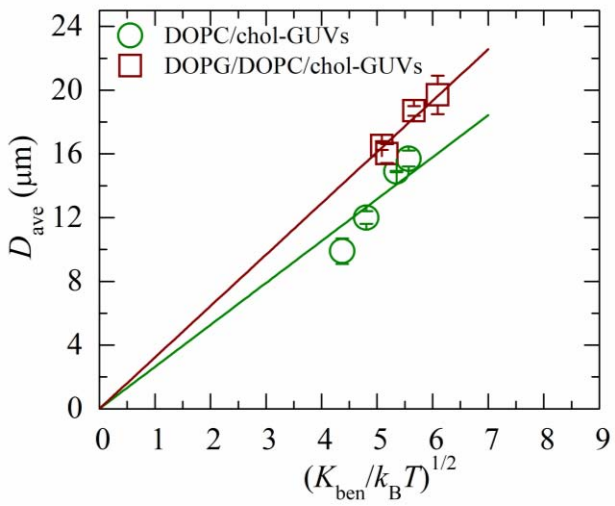

Fig. 4.4 Relationship between the average size and the $\sqrt{K_{ben}}$ of cholesterol containing neutral and charged membranes. Average values and standard errors are determined from 2–3 independent experiments.

The explanation of such behavior of the system under consideration in the following. As it is seen from equation 4.3 increase of K_{ben} means the increase of the total elastic energy of the population. To decrease the free energy in equilibrium, state the system "trends" to increase the number of large vesicles, because the elastic energy of such vesicles is less that the same of small ones.

It is worth to discuss shortly the terms of equation 4.12. The parameter b was obtained above (see equation 4.9), $D_{freqPC} = 2\sqrt{K_{DOPC} S_{init}}$ can be obtained from experimental histograms. As for K_{ben}^{el} we have discussed in detail in our previous paper [30] and we have concluded that this term can be determined as following,

$$K_{ben}^{el} = \text{const}\frac{\Omega_{ch}^2}{\kappa^3} = \frac{\gamma X^2}{\sqrt{C^3}\left(1 - c_h + \beta c_h\right)^2} = \frac{\gamma X^2}{\sqrt{C^3}\left(1 - 0.5 c_h\right)^2}, \qquad (4.13)$$

where $\beta = a_{ch}/a_{DOPG} = 0.5$, Debye length $\kappa^{-1} = \sqrt{\frac{k_B T \varepsilon_s \varepsilon_0}{e^2 C}} = \frac{A}{\sqrt{C}} = 0.76$ [nm] where C = 162 mM is the bulk concentration of NaCl in buffer, ε_S is the dielectric constant of solution, ε_0 is the vacuum permittivity, k_B is the Boltzmann constant and T is absolute temperature. A = 0.304 [nm×mM$^{1/2}$] and κ^{-1} = 0.76 [nm] for C = 162 mM used in our experiment.

It has been used this equation for interpretation and fitting of the results (Fig. 4.3) in which γ = 2.5 k_BT/mM$^{3/2}$ used as a fitting parameter for X = 0.70. To get the information about K_{ben}^{ch} that it is necessary to analyze the experimental results for cholesterol-rich neutral GUVs. Let us describe the dependence of K_{ben} on C_h as following $K_{ben} = K_{DOPC} + \eta C_h$. Based on experiment results one obtains K_{DOPC} =19.1 k_BT and η = 0.5 k_BT. Hence it can be written as follows,

$$K_{ben}^{ch} = \eta C_h \qquad (4.14)$$

4.3.2 Size distribution histograms fitting

In this thesis, it has been considered the cholesterol effect on the size distribution of GUVs during spontaneous vesiculation in the natural swelling method. The cholesterol was varied in both neutral and charged GUVs. All histograms demonstrated a positively skewed distribution, which is described well by the lognormal distribution. Moreover, it is seen from the histograms of Figs. 4.1 and 4.2 that with the increase of cholesterol the histogram peak shifts in the range of larger vesicles, indicating the decrease of histogram asymmetricity.

In Figs. 4.1(b, d) and (b, d), the red lines show the theoretical distribution obtained using equation 4.7. It can be seen that the theoretical curves describe the experimental histograms well. However, as it is seen from a comparison of the theoretical equation with the experimental results, the theoretical distribution overestimates slightly the number of vesicles in the region of vesicle large sizes. This is since the equation 4.7 considers only configurational entropy, but not the orientational one. Since this equation enough well to describe the specific distribution as well as the histogram transformations upon change of cholesterol and to avoid cumbersome mathematical expressions, we do not consider here the orientation entropy. It is to be noted that the energetics is generally contains both the bending modulus and Gaussian modulus (i.e., $2K_{ben}+K_{Gauss}$). Since Gaussian energy makes no difference for shape changes in a single vesicle, as for simplicity we ignored it for the determination of K_{ben} where it was assumed that K_{ben}/K_{Gauss} = -1, which is similar as used before [29]. The average value of K_{ben} are obtained (19.1 ± 0.1) k_BT for DOPC/chol (100/0)-GUVs (i.e., DOPC-GUVs without cholesterol), which is very close to the value (20 ± 0.5) k_BT for DOPC-GUVs obtained in micropipette aspiration technique [89]. In addition, K_{ben} for DOPG/DOPC (70/30)-GUVs is close to the value obtained in the previous study [87]. The average values of K_{ben} at various cholesterol concentrations are provided in table

4.1. Our results demonstrate that, as the cholesterol increases in the DOPC or DOPG/DOPC-GUVs the value of K_{ben} increases.

Taking into account that from one hand it has been shown that the size distribution and average size of GUVs are determined by K_{ben} (equation 4.7 and 4.10) and from another hand our experimental results demonstrated significantly dependences of GUVs size on cholesterol content (see Fig. 4.1 and Fig. 4.2), it can say that the results of this reasearch also exhibit the dependence of the vesicle membrane bending modulus on cholesterol. As it has been discussed above the histograms of Figs. 4.1 and 4.2 show that with the increase of cholesterol concentration in vesicles membranes the histogram peak shifts in the range of larger vesicles. This means that the number of large vesicles in system increases in GUVs population with the addition of cholesterol. As a result, the value of D_{ave} also increases. The physical explanation of such behavior is simple. As it has been discussed above, the cholesterol induces increase of bending modulus of membranes. Hence the energy term of free energy increases (see equation 4.3). However, it is seen that this term does not content the vesicle size explicitly. The question arises: how this term can describe the bending modulus influence on vesicle size distribution. To understand this point it is necessary to consider that this term contains n_m vesicles composed with m initial aggregates. The total number of vesicles in the system $\sum_{m=1}^{N_{init}} n_m = N_{ves}$ is not fixed. The greater fraction of large vesicles in population, the smaller N_{ves}. Hence the system trends to decrease the energy term in equation 4.3 by decreasing the total number of vesicles N_{ves}. Smaller number of vesicles means the greater fraction of large vesicles and consequently larger average size of vesicles in population.

The solid lines in Fig. 4.3 demonstrate the theoretical curves corresponding to equation 4.12, 4.13 and 4.14 for the dependence of D_{ave} on cholesterol for neutral and charged membranes. It is seen the satisfactory fitting of theoretical curves (solid line) to the experimental data. This means once more that the theory describes the real processes in the system under consideration satisfactory. In our investigations, we could measure the GUVs with diameters greater than 3 μm without any difficulties. Hence, we omitted to count the vesicles with diameters less than 3 μm. It is to be noted that the range of the diameters of GUVs were 3.3 – 40.9 μm and 6.3 – 50.2 μm as shown in Figs. 4.1(a, b) and 4.1(c, d), respectively. On the other hand, the range of the diameters of GUVs were 5.6 – 50.9 μm and 5.5 – 72.3 μm as shown in Figs. 4.2(a, b) and 4.2(c, d), respectively. The same

technique was used in the recent papers to measure the similar range of size distribution of GUVs [11, 87]. In addition, Tamba *et al.* was able to measure the GUVs with diameters greater than 2 μm using the similar technique [145].

In these investigations, it has been prepared two types of membranes. One is cholesterol containing neutral membranes such as DOPC/chol-GUVs and another is cholesterol containing charged membranes such as DOPG/DOPC/chol-GUVs. The DOPG/DOPC/chol-GUVs were prepared in PIPIES buffer. The internal solution of the DOPG/DOPC/chol-GUVs was 0.10 M sucrose containing PIPES buffer and the external solution of the same GUVs was 0.10 M glucose containing PIPES buffer. As the preparation of neutral GUVs in PIPES buffer is difficult we used the MilliQ instead of PIPES buffer. The internal solution of the DOPC/chol-GUVs was 0.10 M sucrose containing MilliQ water and the external solution of the same GUVs was 0.10 M glucose containing MilliQ water. So, it has been used 0.10 M glucose in both neutral and charged membranes. It has been compared the bending modulus of cholesterol containing various neutral GUVs. It has been also compared the bending modulus of cholesterol containing various charged GUVs. If the 0.10 M glucose is used with PIPES buffer instead of MilliQ water, the bending modulus may be changed. However, that was not the focus of this research. Our aim was to investigate the change of bending modulus by changing the cholesterol content in the neutral and charged GUVs. Recently, it was investigated the change of bending modulus by changing the salt concentration in PIPES buffer solution and obtained that as the salt concentration in buffer increases the bending modulus of membranes decrease [87].

4.3.3 Estimation of area compressibility modulus of cholesterol-rich neutral membranes

One more interesting characteristic of lipid membranes that must be discussed here is the area compressibility modulus K_A which relates to K_{ben} [89, 146-147]. The polymer brush theory defines this relationship as follows:

$$K_A = \frac{24K_{ben}}{(h-h_e)^2} \tag{4.15}$$

where h is the bilayer thickness (~ 4 nm), h_e is the head group thickness (~ 1 nm). The influence of cholesterol on area compressibility modulus was considered in different studies. Particularly, obtained the increasing trend in area compressibility modulus due to the incorporation of cholesterol in DOPC membranes and the values of K_A for DOPC/chol

(100/0), DOPC/chol (70/30) and DOPC/chol (50/50)-GUVs were obtained 290, 420 and 840 mN/m, respectively. Incorporation of cholesterol in SOPC-GUVs (which is very similar of DOPC-GUVs) increased the area compressibility modulus greatly [60]. The value of area compressibility modulus was obtained (193 ± 20) mN/m for SOPC-GUVs. Upon addition of 14, 28, 38 and 43% cholesterol in SOPC-GUVs the area compressibility modulus increased to (216 ± 12), (244 ± 24), (333 ± 9) and (609 ± 44) mN/m, respectively. Summarizing these results one can conclude that as the cholesterol increases the values of K_A increase. Our results dealing with the estimation of K_{ben} (see table 4.1) give the opportunity to get the K_A in accordance with the equation 4.15. We have done the proper estimations and obtained the following. The values of K_A for DOPC/chol (100/0), DOPC/chol (85/15) and DOPC/chol (71/29) and DOPC/chol (60/40)-GUVs are obtained (209 ± 1), (253 ± 1), (291 ± 0.5) and (340 ± 1) mN/m, respectively. Therefore, the value of K_A for DOPC/chol (100/0) is very similar to that found in micropipette aspiration technique (230 ± 10) mN/m [89]. Hence our estimations of on area compressibility modulus for cholesterol-rich neutral membrane based on our experimental measurements are very similar to the reported ones.

4.4. Probability of Pore Formation in GUVs

Until this section it has been described the results on the effects of cholesterol on the size distribution of vesicles and then estimated the corresponding bending modulus. From this section the effects of cholesterol on the IRE-induced pore formation in charged GUVs is described.

At first, the effect of constant tension of σ_c = 8.0 mN/m on a ‘single DOPG/DOPC/chol (46/39/15)-GUV’ containing 1 mM calcein in 0.10 M sucrose is investigated. Before the application of electric filed (i.e., membrane tension), the GUV had a high contrast in a fluorescence microscopic image as shown in Fig. 4.5(a) at time = 0 s due to the difference in concentrations of calcein containing sucrose and glucose between the inside and the outside of the GUV (i.e., 1 mM calcein containing 0.10 M sucrose in inside and 0.10 M glucose in outside). During the application of σ_c, GUV was also intact with spherical shape until 10.5 s. At time 11 s, GUV is started to rupture and at time 12 s GUV breaks completely (Fig. 4.5(a)). It is to be noted that the spherical structure of GUV is permanently vanished due to the rupture of vesicle. The rupture of vesicle can be explained in the way that at first a nano-sized pore is initiated in the membrane, whose radius rapidly

increases to infinity, leading to complete GUV rupture [18, 69]. The time when the GUV started to rupture indicates the time of pore formation. When we performed the similar experiment using several 'single DOPG/DOPC/chol (46/39/15)-GUVs' (the number of examined GUVs n = 15-24), pore formation occurred stochastically at different times. The stochastic pore formation for several GUVs (n = 16) is shown in Fig. 4.5(b) in which pore formation occurred at different times although σ_c was same. The x-axis of Fig. 4.5(b) indicates the GUV label-number at a particular time. When various σ_c are applied to several 'single DOPG/DOPC/chol (46/39/15)-GUVs', the similar stochastic pore formation are also observed for each σ_c. The probability of pore formation at 60 s, P_{pore} (60), is calculated for various σ_c.

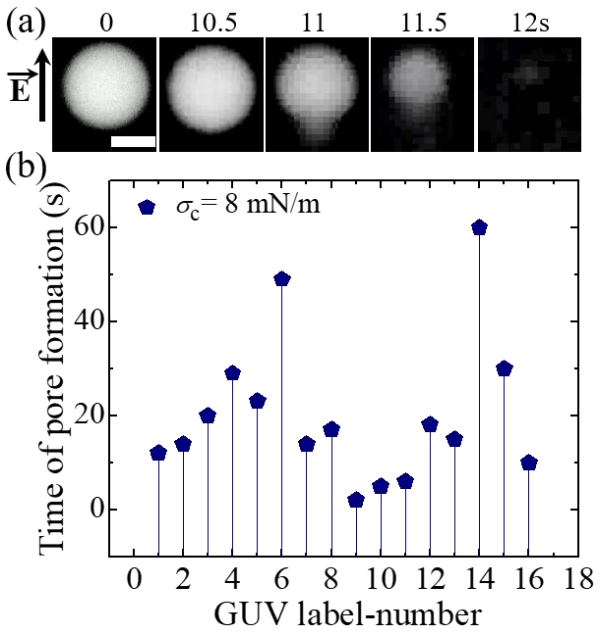

Fig. 4.5 Fluorescence images of pore formation of a 'single GUV' and the stochastic pore formation of several 'single GUVs'. (a) Fluorescent images of pore formation in the membrane of a 'single DOPG/DOPC/chol (46/39/15)-GUV' at σ_c = 8.0 mN/m. The field direction is shown with an arrow in the left side. The numbers above in each image indicate the time in seconds after applying of σ_c due to E. The white bar corresponds to a length of 15 μm. (b) Stochastic pore formation of 16 'single DOPG/DOPC/chol (46/39/15)-GUVs' at σ_c = 8.0 mN/m.

It was performed three independent experiments for DOPG/DOPC/chol (46/39/15)-GUVs at σ_c = 8.0 mN/m.

Table 4.2 shows the time of pore formation for the corresponding GUV level number.

First independent Experiment			Second independent experiment			Third independent experiment		
GUV-label no.	Time of pore formation (s)	Probability of pore formation $P_{pore}(t)$	GUV-label no.	Time of pore formation (s)	Probability of pore formation $P_{pore}(t)$	GUV-label no.	Time of pore formation (s)	Probability of pore formation $P_{pore}(t)$
1	11		1	12		1	22	
2	12		2	14		2	29	
3	20		3	20		3	36	
4	Intact		4	29		4	Intact	
5	5		5	Intact		5	10	
6	28		6	23		6	13	
7	Intact		7	49		7	17	
8	24		8	14		8	22	
9	Intact		9	17		9	40	
10	55		10	Intact		10	Intact	
11	14		11	2		11	60	
12	16		12	5		12	5	
13	3	0.77	13	6	0.86	13	8	0.89
14	Intact		14	18		14	15	
15	5		15	15		15	47	
16	6		16	60		16	Intact	
17	19		17	30		17	20	
18	18		18	10		18	27	
19	60		19	34		19	31	
20	Intact		20	25		20	39	
21	33		21	39		21	57	
22	24		22	Intact		22	43	
						23	28	
						24	32	
						25	60	

It is very clear that the time of pore formation for different GUVs is random though the tension is fixed, such as σ_c = 8.0 mN/m. Such type of random nature of pore formation is observed for different independnt experiments. In the table 4.2, it is presented the data of three independent experiments for DOPG/DOPC/chol (46/39/15)-GUVs' at σ_c = 8.0 mN/m. It is to be mentioned that the similar stochastic nature of pore formation was also observed for different membrane systems at different constant tensions. The stochastic pore formation can be occurred due to the stochastic nature of pre-pore formation in lipid

vesicles. When the radius of pre-pore overcomes the critical value, pre-pore converted to the transmembrane pore.

Fig. 4.6 shows the dependence of the probability of pore formation until 60 s, P_{pore} (60 s) for DOPG/DOPC/chol (46/39/15)-GUVs for various σ_c. At σ_c lower than 5.0 mN/m, P_{pore} (60 s) ≈ 0, at 7.0 mN/m, P_{pore} (60 s) = 0.45 ± 0.07 and at 7.5 mN/m, P_{pore} (60 s) = 0.71 ± 0.09. The value of P_{pore} (60 s) increases with the increase of σ_c and it reaches to 1.0 at σ_c = 8.0 mN/m and above. The similar experiment was performed for DOPG/DOPC/chol (43/28/29)-GUVs and DOPG/DOPC/chol (40/20/40)-GUVs. As a control, we investigated the experiment for the membrane containing without cholesterol such as DOPG/DOPC/chol (70/30/0)-GUVs. The tendency of P_{pore} (60 s) for the 29 and 40 mole% cholesterol is very similar to that observed in DOPG/DOPC/chol (46/39/15)-GUVs. However, the tension required for similar P_{pore} (60 s) using DOPG/DOPC/chol (43/28/29)-GUVs is higher than DOPG/DOPC/chol (46/39/15)-GUVs and similarly for DOPG/DOPC/chol (40/20/40)-GUVs is much higher than DOPG/DOPC/chol (46/39/15)-GUVs.

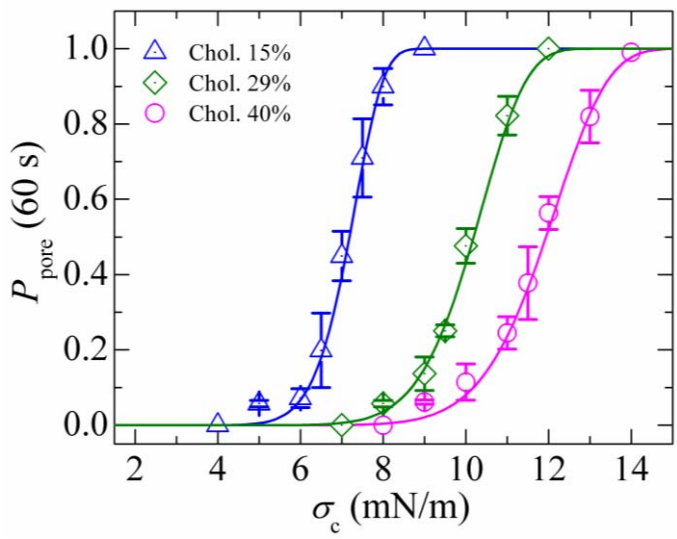

Fig. 4.6 Dependence of P_{pore} (60 s) on σ_c for DOPG/DOPC/chol (46/39/15)-GUVs (triangle), DOPG/DOPC/chol (43/28/29)-GUVs (diamond) and DOPG/DOPC/chol (40/20/40)-GUVs (circle) in IRE experiments. The average values and standard deviations of P_{pore} (60 s) are obtained using 3 independent experiments, each with 15-24 GUVs, for each value of σ_c. The solid lines show the best fitted theoretical curves corresponding to equation (4.21) with same k_p as used in figure 4.8 according to equation (4.20).

As an example, the value of P_{pore} (60 s) is 0.45 ± 0.07 at 7.0 mN/m, 0.48 ± 0.05 at 10.0 mN/m and 0.56 ± 0.04 at 12 mN/m for DOPG/DOPC/chol (46/39/15), DOPG/DOPC/chol (43/28/29) and DOPG/DOPC/chol (40/20/40)-GUVs, respectively. Theoretical equation (4.21) is fitted to the σ_c dependent P_{pore} (60 s) data with the same k_p value as used in Fig. 4.8 according to equation (4.20). The blue, green and red solid lines (Fig. 4.6) are fitted to the experimental data of DOPG/DOPC/chol (46/39/15), DOPG/DOPC/chol (43/28/29) and DOPG/DOPC/chol (40/20/40)-GUVs, respectively.

The tension dependent probability of pore formation with standard deviation for DOPG/DOPC/chol (46/39/15)-GUVs, DOPG/DOPC/chol (43/28/29)-GUVs and DOPG/DOPC/chol (40/20/40)-GUVs are shown in Table 4.3.

Table 4.3. Tension dependent probability of pore formation with standard deviation for different cholesterol containing membranes.

Chol (%)	Tension, σ_c (mN/m)	Probability of pore formation P_{pore} (60 s)	Standard deviation (±)
15	4	0	0
	5	0.05	0.01
	6	0.07	0.02
	6.5	0.19	0.09
	7	0.45	0.07
	7.5	0.71	0.10
	8	0.87	0.05
	9	1	0
29	7	0	0
	8	0.06	0.00849
	9	0.14	0.04434
	9.5	0.25	0.0157
	10	0.48	0.04583
	11	0.82	0.05124
	12	1	0
40	8	0	0
	9	0.06	0.01
	10	0.11	0.05
	11	0.25	0.04
	11.5	0.38	0.09
	12	0.56	0.04
	13	0.82	0.07
	14	0.99	0

4.5 Rate Constant of Pore Formation in GUVs

In order to obtain the rate constant of pore formation in the membranes of GUVs, at first we determine the time course of the fraction of intact GUVs without pore formation among all of the examined GUVs, $P_{\text{intact}}(t)$. It is basically indicating the fraction of GUVs that are still intact after time "t" and is defined as $P_{\text{intact}}(t) = 1 - P_{\text{pore}}(t)$ [71, 148]. Fig. 4.7(a) shows the time course of $P_{\text{intact}}(t)$ for DOPG/DOPC/chol (46/39/15)-GUVs at σ_c = 7.0 mN/m. The time dependent $P_{\text{intact}}(t)$ is well fitted by a single-exponential decay function (black solid line in Fig. 4.7a):

$$P_{\text{intact}}(t) = \exp\left(-k_p t\right) \qquad (4.16)$$

where k_p is the rate constant for pore formation and t is the duration of constant tension applied to a GUV (tension is started at $t = 0$). From the fitted curve, the k_p value is obtained 1.0×10^{-2} s^{-1}. Next, the same experiment is performed at σ_c = 9.0 mN/m.

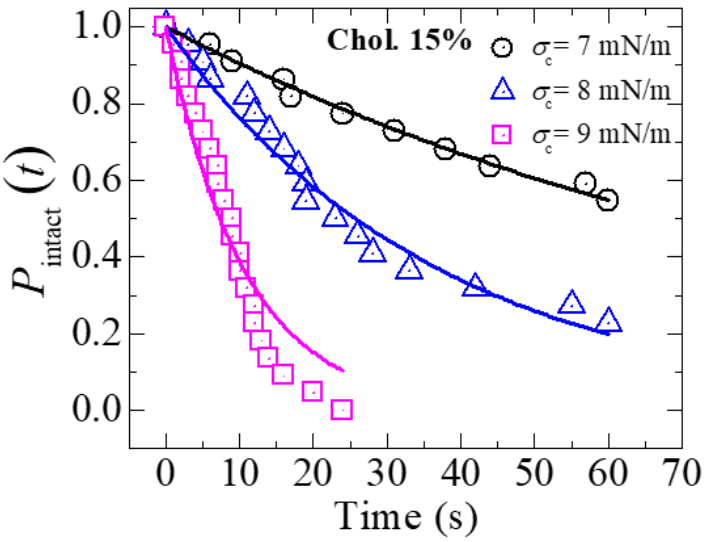

Fig. 4.7 The time course of the fraction of intact DOPG/DOPC/chol (46/39/15)-GUVs at σ_c = 7.0, 8.0 and 9.0 mN/m. The solid lines represent the best fitted single exponential decay function of equation (4.16).

At this σ_c, the decrease in $P_{\text{intact}}(t)$ with time is faster than at 7.0 mN/m, and obtain the value k_p of 11×10^{-2} s^{-1} at 9.0 mN/m. A similar experiment is done for σ_c = 8.0 mN/m, and

obtain the value of k_p of 2.7×10^{-2} s^{-1}. It has been also obtain the k_p values for different membranes at various σ_c. It was performed 3 independent experiments for each tension and obtained the average rate constant with standard deviation. Fig. 4.8 shows the time course of the fraction of intact GUVs containing 29% (A) and 40% (B) cholesterol in the membranes. The solid lines represent the best fitted single exponential decay function of equation (4.16).

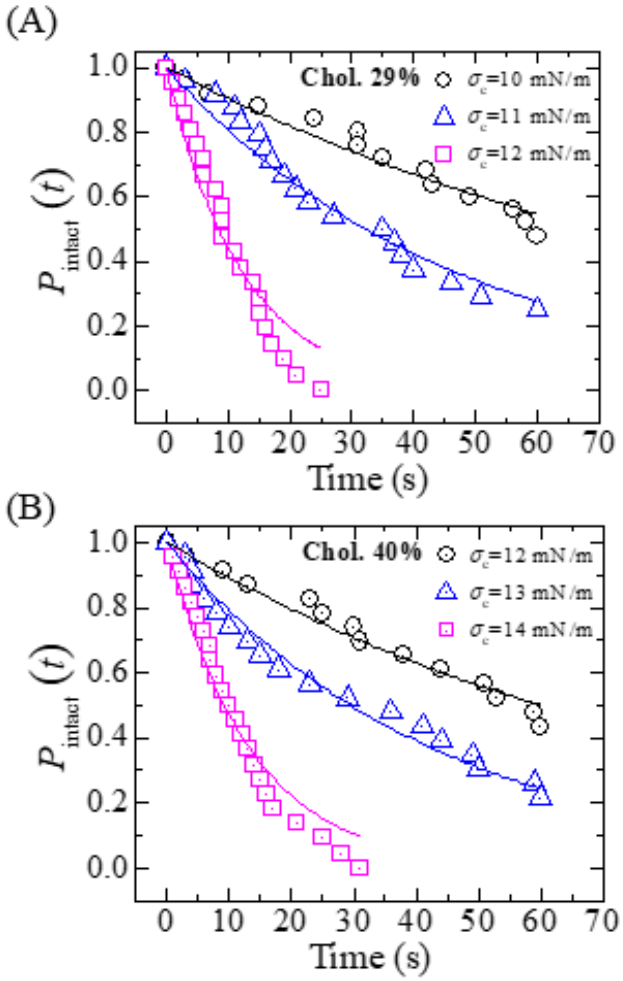

Fig. 4.8 The time course of the fraction of intact GUVs containing 29% (A) and 40% (B) cholesterol in the membranes. The solid lines represent the best fitted single exponential decay function of equation (4.16).

Table 4.4 shows the tension dependent rate constant of pore formation in GUVs containing various concentration of cholesterols. The data is obtained for one independent experiment as shown in Figs. 4.7 and 4.8.

Table 4.4 Tension dependent rate constant of pore formation in GUVs containing various concentrations of cholesterol.

Chol (%)	Tension, σ_c (mN/m)	Rate constant, k_p (s^{-1})
15	7	1.0×10^{-2}
	8	2.7×10^{-2}
	9	11.0×10^{-2}
29	10	1.0×10^{-2}
	11	2.2×10^{-2}
	12	9.0×10^{-2}
40	12	1.2×10^{-2}
	13	2.4×10^{-2}
	14	8.0×10^{-2}

Fig. 4.9 shows the σ_c dependent k_p values for DOPG/DOPC/chol (46/39/15) (Δ), DOPG/DOPC/chol (43/28/29) (◊) and DOPG/DOPC/chol (40/20/40)-GUVs (○). From this figure, it is clear that as the cholesterol content increased in the membranes, the tension required the same k_p is higher. As an example, the value of k_p is $(2.9 \pm 0.3)\times10^{-2}$ s^{-1} at 8.0 mN/m, $(2.5 \pm 0.4)\times10^{-2}$ s^{-1} at 11.0 mN/m and $(2.5 \pm 0.6)\times10^{-2}$ at 13.0 mN/m for DOPG/DOPC/chol (46/39/15), DOPG/DOPC/chol (43/28/29) and DOPG/DOPC/chol (40/20/40)-GUVs, respectively. In all the membranes, σ_c activates the pore formation process, which is observed as an increase of k_p. We have fitted the theoretical equation (4.20) to the experimental data on σ_c vs k_p and obtain the line tension of membranes. The best fit was evaluated from the value of coefficient of determination, R^2, which was 0.95 for DOPG/DOPC/chol (46/39/15)-GUVs, 0.99 for DOPG/DOPC/chol (43/28/29)-GUVs and 0.98 for DOPG/DOPC/chol (40/20/40)-GUVs. The detail result is discussed in the discussion section. The tension dependent average rate constants of pore formation with fitting parameters are shown in Table 4.5. These results indicate that cholesterol inhibits the rate constant of pore formation of GUVs.

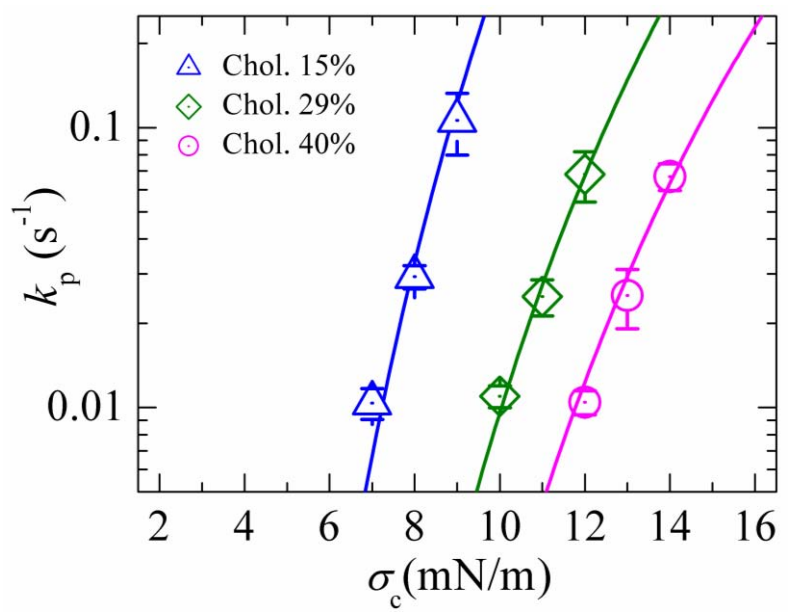

Fig. 4.9 The tension dependent k_p for DOPG/DOPC/chol (46/39/15)-GUVs (triangle), DOPG/DOPC/chol (43/28/29)-GUVs (diamond) and DOPG/DOPC/chol (40/20/40)-GUVs (circle). Average values and standard deviations of k_p for each tension are determined for 3 independent experiments, each with 15-24 GUVs, for each value of σ_c. The solid lines show the best fitted theoretical curves corresponding to equation (4.20).

Table 4.5 Tension dependent average rate constants of pore formation and line tension at various membranes systems.

Chol. (mole %)	Electric tension σ_c (mN/m)	Rate constant of pore formation k_p (s^{-1})	Line tension Γ (pN)	Fitting parameter A_F ($m^2s^{-1}J^{-1}$)	Coefficient of determination R^2
15%	7.0	$(1.0 \pm 0.1) \times 10^{-2}$	12.9	9.3×10^5	0.95
	8.0	$(2.9 \pm 0.3) \times 10^{-2}$			
	9.0	$(11.0 \pm 0.3) \times 10^{-2}$			
29%	10.0	$(1.1 \pm 0.1) \times 10^{-2}$	13.8	1.5×10^5	0.99
	11.0	$(2.5 \pm 0.4) \times 10^{-2}$			
	12.0	$(7.0 \pm 0.1) \times 10^{-2}$			
40%	12.0	$(1.0 \pm 0.1) \times 10^{-2}$	14.6	9.3×10^4	0.98
	13.0	$(2.5 \pm 0.6) \times 10^{-2}$			
	14.0	$(7.0 \pm 0.1) \times 10^{-2}$			

4.6. Analytical Treatment of the Pore Formation in GUVs

Lipid membrane is an ensemble of lipid molecules in which local thermal fluctuations in the lateral density of the bilayer is constantly presented. The local region of a lipid membrane where the lateral density of lipid molecules is lower than their regular one is defined as a local density rarefaction or prepore [149-150]. In the presence of electric field (*E)* in the membranes, the lateral tension σ_c is induced in the membrane. Due to the thermal energy, a lateral density of lipid molecules that is defined as local condensation and local rarefaction exists in the membrane [18, 69, 148]. If the size of such a rarefaction crosses a critical radius r_c, this area transforms into a prepore of radius, r. If $r < r_c$ the prepore closes quickly and if $r \geq r_c$ the prepore transforms into a transmembrane pore. The rupture of vesicles occurred as r goes to infinite within a very short time (~1 s). The free energy of a prepore $U(r, \sigma_c)$ consists of $-\pi r^2\sigma_c$ that is favoring the expansion of prepore and $2\pi r\Gamma$ (Γ is the free energy per unit length of a prepore) that is favoring the closure of prepore. According to the classical theory of pore formation, the free energy of a prepore can be expressed as [18, 69, 148] $U(r, \sigma_c) = 2\pi r\Gamma - \pi r^2\sigma_c$]. A similar equation of a prepore free energy for IRE technique is used in the previous paper [18] where toroidal structure of prepore is considered [151-152] as shown in Fig. 4.10.

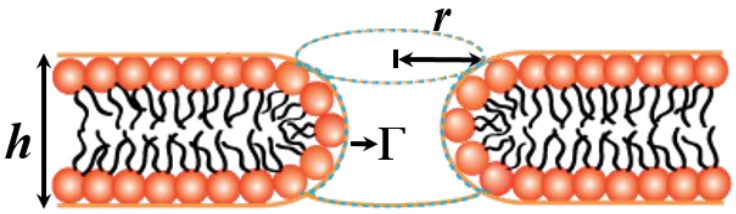

Fig. 4.10 Illustration of toroidal structure of a prepore of radius r. [31]

For cholesterol containing charged membranes, the free energy of a prepore can be written as,

$$U\left(r,\sigma_c\right) = 2\pi\,\Gamma r - \pi r^2(\sigma_c + B) \tag{4.17}$$

The electrostatic effect, B is defined as follows [69, 105],

$$B \approx \left\{4\Omega\left[\frac{1-q}{p} + \ln\left(p+q\right)\right]\frac{k_B T}{e} - \frac{\Omega^2}{\varepsilon_w\varepsilon_0}\omega^2\frac{h}{2}\right\} \tag{4.18}$$

where h is the thickness of membrane, Ω is the membrane surface charge density, ε_w is the

relative dielectric constant of water, ε_0 is the permittivity of free space, $p = 2\pi\lambda_B X/\kappa A_0$ and $q = \sqrt{1+p^2}$, $1/\kappa$ is the Debye length (0.76 nm), Bjerrum length in water at 25 °C is $\lambda_B = e^2/4\pi kT\varepsilon_0\varepsilon_W = 0.716$ nm, k_B is Boltzmann constant, T is absolute temperature, and ω is the fitting parameter. At the critical radius of a prepore, $r = r_c = \frac{\Gamma}{\sigma + B}$, the energy barrier of a prepore free energy is as follows [69, 105]:

$$U_b(r, \sigma_c) = \frac{\pi\Gamma^2}{\sigma_c + B} \tag{4.19}$$

Using the mean first passage time approach the rate constant of the formation of pore in membranes is determined as follows [105, 144]:

$$k_p = A_F\left(\sigma_c + B\right)\exp\left[-\frac{\pi\Gamma^2}{k_B T\left(\sigma_c + B\right)}\right] \tag{4.20}$$

where $A_F = \left(\frac{D_r\sqrt{3}}{k_B T}\right)$ is the pre-exponential factor. The fitting parameters of equation (4.20) are A_F and Γ. By changing these two parameters, this equation is fitted to experimental rate constant data. The fraction of GUVs with pores, among all the examined GUVs at t = 60 s is as follows [18, 148].

$$P_{pore}(\sigma_c, 60\text{ s}) = 1\text{- }\exp\left(-60k_p\right) \tag{4.21}$$

4.7. Discussion on Electroporation

As the membranes charge density is similar, the value of $B \approx 2.03$ mN/m (which corresponds to the best fitting parameter ω = 0.49) according to equation (4.18). The experimental data of k_p vs σ_c was fitted by varying the parameters A_F and Γ. The curves of Fig. 4.8 were fitted using the values of $A_F = 9.3 \times 10^5$ $m^2s^{-1}J^{-1}$ and Γ = 12.9 pN for DOPG/DOPC/chol (46/39/15)-GUVs, $A_F = 1.5 \times 10^5$ $m^2s^{-1}J^{-1}$ and Γ = 13.8 pN for DOPG/DOPC/chol (43/28/29)-GUVs and $A_F = 9.3 \times 10^4$ $m^2s^{-1}J^{-1}$ and Γ = 14.6 pN for DOPG/DOPC/chol (40/20/40)-GUVs. The values of Γ for different membranes are provided in table 4.5. It has been observed that the value of Γ increased with the increase of cholesterol content in the membranes. Recent results on electroporation of vesicles and

analysis of the pore closure dynamics indicated that the addition of 17 mol% cholesterol to the DOPC-GUVs causes an increase of line tension [153]. It was reported the Γ value of 27.7 ± 2.5 pN for DOPC-GUVs and 36.4 ± 1.9 pN for DOPC/cholesterol (5:1)-GUVs. Using the micropipette aspiration and electroporation technique the Γ at the pore region was determined for stearoyloleoylphosphatidylcholine (SOPC) and SOPC with 50 mol% cholesterol, and obtained the Γ value of 9.2 ± 0.7 pN and 30.5 ± 1.2 pN, respectively [154-155]. Using the pore closure dynamics and the light-induced poration technique it was reported that cholesterol (a model of inverted cone-shaped molecule) increases the value of Γ upon addition into the bilayers [156]. It was reported the Γ value of 6.9 ± 0.42 pN for DOPC-GUVs (DOPC supplied from Sigma) and incorporation of cholesterol of upto 31 mol% into DOPC-GUVs increased the Γ value of 9-22 pN [156]. Therefore, these investigations supported our results that as the cholesterol increased in membranes the value of Γ also increase. Taking the same values of k_p as used in figure 4.9, the experimental data of Fig. 4.6 was fitted using equation (4.21). It is very clear that the theoretical equation fitted well to the experimental data (Fig. 4.6). Recent report indicated that cholesterol decreased the rate of entry of cell-penetrating peptide oligoarginine into the lipid vesicles [30], which supported our investigation that as cholesterol increased in the membranes, the probability of pore formation and the rate constant of pore formation decreased. From equation (4.19), the main factor determining the IRE-induced rate constant of pore formation is U_b which depends on the value of σ_c, in which σ_c is controlled by E (equation 3.3 in chapter 3). Fig. 4.11 shows an example of $U(r, \sigma_c)$ for different Γ. As it has been mentioned above that Γ increases with the increase of cholesterol in membrane and therefore $U_b(r, \sigma_c)$ increases as cholesterol increases in the membranes. The similar tendency of prepore energy profile is observed in the cell-penetrating peptide oligoarginine-induced pore formation in the lipid membranes containing cholesterol [30].

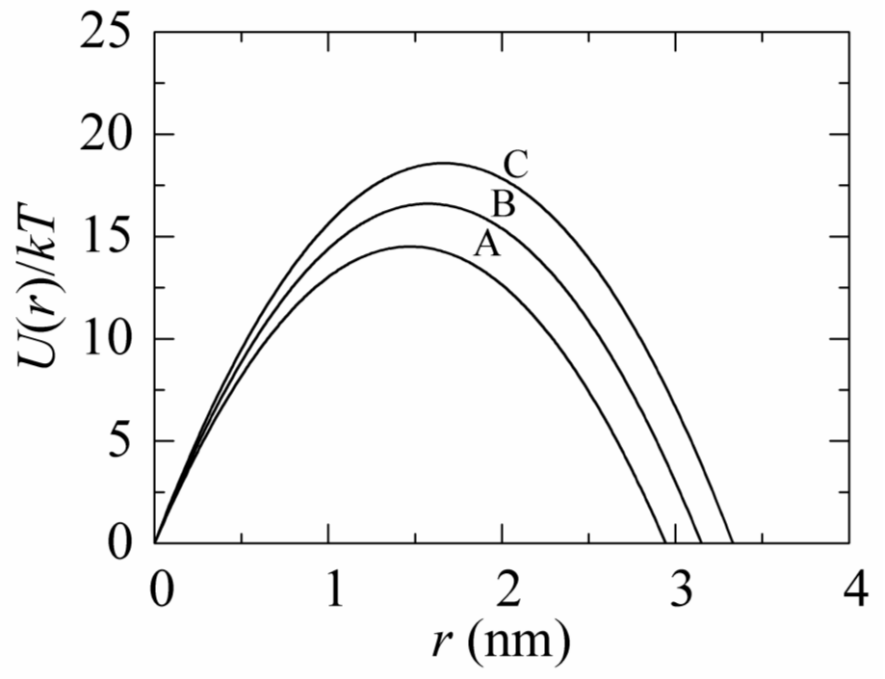

Fig. 4.11 Dependence of the prepore energy profile, U(r) on the pore radius at (A) Γ = 12.9 pN, (B) Γ = 13.8 pN, (C) Γ = 14.6 pN. UI is calculated according to equation (4.17) using σ_c = 7.0 mN/m and $B \approx 2.03$ mN/m.

The free energy of a prepore, $U_b(r, \sigma_c)$ decreases with the decrease of Γ, because $U_b(r,\sigma_c) = \frac{\pi\Gamma^2}{\sigma_c + B}$. The initial slope of UI decreases with a decrease of U_b, so the prepore radius decreases with a decrease of Γ, consequently the rate constant of pore formation increases. Therefore, it is observe that as the value of Γ increases due to the incorporation of cholesterol in the membranes, the rate constant of pore formation decreases which support our investigations.

4.8. General Discussion

It has been observed that the main fitting parameter of the theoretical model is K_{ben}. The value of K_{ben} in our experiments was obtained 19.1-31.0 k_BT for neutral GUVs and 25.9-37.1 k_BT for charged GUVs. According to the theoretical approach, D_{ave} is only proportional to K_{ben} i.e., $D_{ave} = \text{const}\sqrt{K_{ben}}$. When it has been plotted the dependence of D_{ave} (*C, X*) and K_{ben} (*C X*) in the same graph (Fig 4.4), it is observed that D_{ave} is proportional to K_{ben}. The appropriate constants are equal to 2.63 [μm/(kBT)]$^{1/2}$ for cholesterol-rich neutral GUVs and 3.17 [μm/(k_BT)$^{1/2}$] for cholesterol-rich charged GUVs. The average value of

K_{ben} are obtained (19.1 ± 0.1) k_BT for DOPC/chol (100/0)-GUVs (i.e. DOPC-GUVs without cholesterol), which is very close to the value (20 ± 0.5) k_BT for DOPC-GUVs obtained in micropipette aspiration technique [89]. In addition, K_{ben} for DOPG/DOPC (70/30)-GUVs is close to the value as reported earlier [87]. The average values of K_{ben} at various cholesterol concentrations are provided in table 4.1. Our results demonstrate that, as the cholesterol increases in the DOPC-GUVs or DOPG/DOPC-GUVs, the value of K_{ben} increases. Taking into account that from one hand it has been shown that the size distribution and average size of GUVs are determined by K_{ben} and from another hand the experimental results demonstrated significantly dependences of GUVs size on cholesterol content, it can say that these results also exhibit the dependence of the vesicle membrane bending modulus on cholesterol. The increase of K_{ben} means the increase of the total elastic energy of the population. To decrease the free energy in equilibrium, state the system "trends" to increase the number of large vesicles, because the elastic energy of such vesicles is less that the same of small ones, as a result the average size of all vesicles increases.

With the increase of cholesterol, the histogram peak shifts in the range of larger vesicles (Figs. 4.1 and 4.2), which means that the number of larger vesicles in population increases, and therefore, D_{ave} increases. As it has been discussed above, cholesterol increases the bending modulus of membranes, and hence the energy term of free energy increases (see eq. 4.3). However, it is seen that this term does not content the vesicle size explicitly. The question arises: how this term can describe the bending modulus influence on vesicle size distribution. To understand this point it is necessary to consider that this term contains n_m vesicles composed with m initial aggregates. The total number of vesicles in the system $\sum_{m=1}^{N_{init}} n_m = N_{ves}$ is not fixed. The greater the fraction of large vesicles in population, the smaller the N_{ves}. Hence the system trends to decrease the energy term in equation (4.3) by decreasing the total number of vesicles N_{ves}. Smaller number of vesicles means the greater fraction of large vesicles and consequently larger average size of vesicles in population. It has been shown early that electrical charge of the vesicle membrane increases the bending modules of membrane K_{ben} [87]. The results of the current research show that the cholesterol also increases K_{ben}. Hence one can conclude that if the cholesterol concentration increases, the average sizes of GUVs, D_{ave} in the system increases also the K_{ben} increases.

It was also investigated the effects of IRE-induced probability of pore formation and the rate constant of pore formation in GUVs containing various mole% of cholesterol. As the membranes charge density is similar, the value of $B \approx 2.03$ mN/m (which corresponds to the best fitting parameter $\omega = 0.49$) according to equation (4.18). The experimental data of

k_p vs σ_c was fitted by varying the parameters A_F and Γ. The obtained line tension increased from 12.9 to 14.6 pN for the increase of cholesterol from 15 to 40 mole%. Using the micropipette aspiration and electroporation technique the Γ at the pore region was determined for pure SOPC and SOPC with 50 mol% cholesterol, and obtained the Γ value of 9.2 ± 0.7 pN and 30.5 ± 1.2 pN, respectively [154-155]. Using the pore closure dynamics and the light-induced poration technique it was reported that cholesterol increases the value of Γ [156]. It was reported the Γ value of 6.9 ± 0.42 pN for DOPC-GUVs and incorporation of cholesterol of upto 31 mol% into DOPC-GUVs increased the Γ value of 9-22 pN [156]. Therefore, these investigations supported our results that as the cholesterol increased in membranes the value of Γ also increase and therefore $U_b(r, \sigma_c)$ increases as in the membranes. Therefore, it has been observe that as the value of Γ increases due to the incorporation of cholesterol in the membranes, the rate constant of pore formation decreases which support our investigations. Since the bending modulus and rate constant of pore formation dependent with the cholesterol concentrations so, it can say that with the increase of cholesterol concentrations the bending modulus increased, for this reason the rate constant of pore formation in the membranes of vesicles decrease.

CHAPTER 5

CONCLUSIONS

In this thesis, the influence of cholesterol on the size distribution and the IRE-induced pore formation in GUVs is considered. The amount of cholesterol was varied from 0 to 40 mole%. The size distributions of GUVs were presented as a set of histograms. The classical lognormal distribution was well fitted to the histograms from where the average size of vesicle was obtained. With the increase of cholesterol concentration, the peak of the histograms shifted to right, i.e., in the region of large vesicles for both the neutral and charged GUVs. This means that with the increasing of cholesterol, the fraction of large GUVs in population increases. The values of average size (D_{ave}) were obtained (9.9 ± 0.8), (12.0 ± 0.4), (14.9 ± 0.04) and (15.7 ± 0.5) μm for DOPC/chol, DOPC/chol (85/15), DOPC/chol (71/29) and DOPC/chol (60/40)-GUVs, respectively. Similarly, the values of D_{ave} were obtained (16.5 ± 0.3), (16.0 ± 0.6), (18.7 ± 0.3) and (19.7 ± 1.2) μm for DOPG/DOPC/chol (70/30/0), DOPG/DOPC/chol (46/39/15), DOPG/DOPC/chol (43/28/29) and DOPG/DOPC/chol (40/20/40)-GUVs, respectively. Therefore, the increase of cholesterol content in the membranes of GUVs increases the average size of vesicles in population. For theoretical explanation of the obtained results the theory based on Helmholtz's free energy is used. The specific GUVs size distribution was determined by the bending modulus of membranes of vesicles. The values of bending modulus (K_{ben}) of neutral GUVs were obtained (19.1 ± 0.1), (23.1 ± 0.1), (8.6 ± 0.01) and (31.0 ± 0.1) k_BT for DOPC/chol (100/0), DOPC/chol (85/15), DOPC/chol (71/29) and DOPC/chol (60/40)-GUVs, respectively. Also, for charged GUVs, the average values of K_{ben} were obtained (25.9 ± 0.3), (26.8 ± 0.1), (32.1 ± 0.3) and (37.1 ± 0.3) k_BT, for DOPG/DOPC/chol (70/30/0), DOPG/DOPC/chol (46/39/15), DOPG/DOPC/chol (43/28/29) and DOPG/DOPC/chol (40/20/40)-GUVs, respectively. Hence, the value of bending modulus increased with the increase of cholesterol concentration. It was observed a proportional relation between the average sizes of GUVs and the average K_{ben} of those corresponding GUVs. The increase of K_{ben} means the increase of the total elastic energy of the population. To decrease the free energy in equilibrium, state the system "trends" to increase the number of large vesicles, because the elastic energy of such vesicles is less that the same of small ones.

For IRE-induced pore formation in GUVs, it was applied an electric field of pulsating DC of frequency 1.1 kHz. At first, the probability of pore formation until 60 s, P_{pore} (60 s) for DOPG/DOPC/chol (46/39/15)-GUVs for various constant electric tension σ_c was calculated. The value of P_{pore} (60 s) increased with the increase of σ_c and it reached to 1.0. The similar results were also obtained for other cholesterol containing vesicles. The tension required for similar P_{pore} (60 s) using DOPG/DOPC/chol (43/28/29)-GUVs was higher than DOPG/DOPC/chol (46/39/15)-GUVs and similarly for DOPG/DOPC/chol (40/20/40)-GUVs was much higher than DOPG/DOPC/chol (46/39/15)-GUVs. To obtain the rate constant of pore formation in the membranes of GUVs, the time course of the fraction of intact GUVs without pore formation among all the examined GUVs, P_{intact} (t), was determined. The P_{intact} (t) vs time graph was well fitted by a single-exponential decay function, P_{intact} (t) = exp(-$k_p t$), where k_p indicates the rate constant for pore formation in GUVs. The value of k_p increased with the increase of membrane tension. However, the value of k_p decreased with the increase of cholesterol at a particular tension. As the cholesterol content increased, the tension required the same k_p was higher. Theoretical equation fitted well to the tension dependent rate constant which allowed obtaining the line tension of membranes. The obtained line tension increased from 12.9 to 14.6 pN for the increase of cholesterol from 15 to 40 mole%. The increase in the energy barrier of a prepore free energy due to the increase of cholesterol was the main factor for the decrease of rate constant of pore formation in the cholesterol containing membranes. This observation offers the kinetics of irreversible pore formation under constant electric tension in the cholesterol containing membranes of giant vesicles.

From the above discussions, finally it can be concluded that as the bending modulus increased with the increase of cholesterol the rate constant of pore formation in GUVs decrease.

REFERRENCES

[1] Holmberg, K., Jönsson, B., Kronberg, B., Lindman, B., "Surfactants and polymers in aqueous solution," John Wiley & Sons, Ltd, Chichester, UK, 2002.

[2] Kita-Tokarczyk, K., Grumelard, J., Haefele, T., Meier, W., Kita-Tokarczyk, K., Grumelard, J., Haefele, T., Meier, "Block copolymer vesicles-using concepts from polymer chemistry to mimic biomembranes," *Polymer,* vol. 46, pp 3540-3563, 2005.

[3] Segota, S., Tezak, D.," Spontaneous formation of vesicles," *Adv Colloid Interface Sci*., vol. 121, pp 51–75, 2006.

[4] Angelova, M.I., Soléau, S., Méléard, P., Faucon, F., Bothorel, P., "Preparation of giant vesicles by external AC electric fields. Kinetics and applications," In: Helm, C., Lösche, M., Möhwald, H. (eds) Trends in Colloid and Interface Science VI. Steinkopff, Darmstadt, pp 127–131, 1992.

[5] Pavlič, J.I., Genova, J., Popkirov, G., Kralj-Iglič, V., Iglič, A., Mitov, M.D., "Mechanoformation of neutral giant phospholipid vesicles in high ionic strength solution," *Chem Phys Lipids*, vol. 164, pp 727–731, 2011.

[6] Sackmann, E., "Physical basis of self-organization and function of membranes: physics of vesicles," In: Handbook of biological physics. *Elsevier*, pp 213–304, 1995.

[7] Iqbal, U., Albaghdadi, H., Nieh, M-P., Tuor, U.I., Mester, Z., Stanimirovic, D., Katsaras, J., Abulrob, A., "Small unilamellar vesicles: a platform technology for molecular imaging of brain tumors," *Nanotechnology*, vol. 22 pp 195102, 2011.

[8] Dimova, R., "Giant vesicles and their use in assays for assessing membrane phase state, curvature,mechanics, and electrical properties," *Annu. Rev. Biophys.,* vol. 48, pp 93–119, 2019.

[9] Guida, V., "Thermodynamics and kinetics of vesicles formation processes," *Adv Colloid Interface Sci*., vol. 161(1-2), pp 77–88, 2010.

[10] Karal, M.A.S., Alam, J.M., Takahashi, T., Levadny, V., Yamazaki, M., "Stretch Activated Pore of the Antimicrobial Peptide, Magainin 2" *Langmuir,* vol. 31, pp 3391–3401, 2015.

[11] Karal, M.A.S., Rahman, M., Ahamed, M.K., Shibly, S.U.A., Ahmed M., Shakil, M.M., "Low cost non-electromechanical technique for the purification of giant

unilamellar vesicles," *Eur. Biophys J.*, *v*ol. 48 pp 349–359, 2019.

[12] Karal, M.A.S., Ahamed, M.K., Orchi, U.S., Towhiduzzaman, M., Ahmed, M., Ahammed, S., Mokta, N.A., Ullah, M.S., "An investigation into the critical tension of electroporation in anionic lipid vesicles," *Eur Biophys J.*, vol. 50, pp 99–106, 2021.

[13] Reeves, J.P., Dowben, R.M., "Formation and properties of thin-walled phospholipid vesicles," *J Cell Physiol*., vol. 73, pp 49–60, 1969.

[14] Siegel, D.P., Kozlov, M.M., "The Gaussian Curvature Elastic Modulus of N-Monomethylated Dioleoylphosphatidylethanolamine: Relevance to Membrane Fusion and Lipid Phase Behavior," *Biophys J.*, vol. 87, pp 366–374, 2004.

[15] Yamashita, Y., Oka, M., Tanaka, T., Yamazaki, M., "A new method for the preparation of giant liposomes in high salt concentrations and growth of protein microcrystals in them," *Biochim. Biophys. Acta*., vol. 1561, pp 129–134, 2002.

[16] Blosser, M.C., Horst, B.G., Keller, S.L., "cDICE method produces giant lipid vesicles under physiological conditions of charged lipids and ionic solutions," *Soft Matter*, vol. 12, pp 7364–7371, 2016.

[17] Evans, E., Smith, B.A., "Kinetics of hole nucleation in biomembrane rupture," *New J Phys*., vol. 13, pp 095010, 2011.

[18] Karal, M.A.S., Ahamed, M.K., Rahman, M., Ahmed, M., Shakil, M.M, Rabbani, K.S., "Effects of electrically-induced constant tension on giant unilamellar vesicles using irreversible electroporation," *Eur. Biophys. J.*, vol. 48, pp 731–741, 2019.

[19] Pommella, A., Brooks, N.J., Seddon, J.M., Garbin V., "Selective flow-induced vesicle rupture to sort by membrane mechanical properties," *Sci Rep*, vol. 5, pp. 13163, 2015.

[20] Ahamed, M.K., Karal, M.A.S., Ahmed, M., Ahammed, S., "Kinetics of irreversible pore formation under constant electrical tension in giant unilamellar vesicles," *Eur. Biophys. J.,* vol. 49, pp 371–381, 2020.

[21] Karal, M.A.S., Islam, M.K., Mahbub, Z.B., "Study of molecular transport through a single nanopores in the membrane of a giant unilamellar vesicle using COMSOL simulation," *Eur. Biophys. J.*, vol. 49, pp 59–69, 2020.

[22] Karal, M.A.S., Ahammed, S., Levadny, V., Belaya, M., Ahamed, M.K., Ahmed,

M., Mahbub, Z.B., Ullah, A.K.M.A., “Deformation and poration of giant unilamellar vesicles induced by anionic nanoparticles,” *Chem. Phys. Lipids,* vol. 230, pp 104916, 2020.

[23] Karal, M.A.S., Ahamed, M.K., Ahmed, M., Ahamed, S., Mahbub, Z.B., “Location of peptide-induced submicron discontinuities in the membranes of vesicles using ImageJ,” *J. Fluoresc*., vol. 30, pp 735–740, 2020.

[24] Lian, T., Ho, R.J., “Trends and developments in liposome drug delivery systems,” *J. Pharm. Sci*., vol. 90, pp 667–680, 2001.

[25] Malam, Y., Loizidou, M., Seifalian, A.M., “Liposomes and nanoparticles: nanosized vehicles for drug delivery in cancer,” *Trends Pharmacol Sci*., vol. 30, pp 592–599, 2009.

[26] Allen, T.M., Cullis, P.R., “Liposomal drug delivery systems: from concept to clinical applications,” *Adv. Drug. Deliv. Rev.*, vol. 65, pp 36–48, 2013.

[27] Bardania, H., Tarvirdipour, S., Dorkoosh, F., “Liposome-targeted delivery for highly potent drugs,” *Artif Cells Nanomedicine Biotechnol.,* vol. 45, pp 1478–1489, 2017.

[28] Huang, C., Quinn, D., Sadovsky, Y., Suresh, S., Hsia, K.J., “Formation and size distribution of self-assembled vesicles,” *Proc Natl. Acad. Sci*. vol. 114, pp 2910–2915, 2017.

[29] DePierre, J.W., Karnovsky, M.L., “Plasma membranes of mammalian cells,” *J. Cell. Biol.*, vol. 56, pp 275–303, 1973.

[30] Sharmin, S., Islam, M.Z., Karal, M.A.S., Shibly, S.U.A., Dohra, H., Yamazaki, M., “Effects of lipid composition on the entry of cell-penetrating peptide oligoarginine into single vesicles,” *Biochemistry*, vol. 55, pp 4154–4165, 2016.

[31] Karal, M.A.S., Ahamed, M.K., Mokta, N.A., Ahmed, M., Ahammed, S., “Influence of cholesterol on electroporation in lipid membranes of giant vesicles,” *Eur. Biophys. J*., vol. 49, pp 361–370, 2020.

[32] Alam, J.M., Kobayashi, T., Yamazaki, M., “The single-giant unilamellar vesicle method reveals lysenin-induced pore formation in lipid membranes containing sphingomyelin,” *Biochemistry*, vol. 51, pp 5160–5172, 2012.

[33] Marsh, D., “Elastic curvature constants of lipid monolayers and bilayers,” *Chem. Phys. Lipids*, vol. 144, pp 146–159, 2006.

[34] Dimova, R., “Recent developments in the field of bending rigidity measurements on membranes,” *Adv. Colloid Interface Sci*., vol. 208, pp 225–234, 2014.

[35] Evans, E., Rawicz, W., “Entropy-driven tension and bending elasticity in condensed-fluid membranes,” *Phys. Rev. Lett*., vol. 64, pp 2094–2097, 1990.

[36] Duwe, H.P., Kaes, J., Sackmann, E., “Bending elastic moduli of lipid bilayers: modulation by solutes,” *J. Phys*., vol. 51, pp 945–961, 1990.

[37] Song, J., Waugh, R.E., “Bending rigidity of SOPC membranes containing cholesterol,” *Biophys. J.* vol. 64, pp 1967–1970, 1993.

[38] Méléard, P., Gerbeaud, C., Pott, T., Fernandez-Puente, L., Bivas, I., Mitov, M.D., Dufourcq, J., Bothorel, P., “Bending elasticities of model membranes: influences of temperature and sterol content,” *Biophys. J*., vol. 72, pp 2616–2629, 1997.

[39] Chen, Z., Rand, R.P., “The influence of cholesterol on phospholipid membrane curvature and bending elasticity,” *Biophys. J*., vol. 73, pp 267–276, 1997.

[40] Henriksen, J., Rowat, A.C., Brief, E., Hsueh, Y.W., Thewalt, J.L., Zuckermann, M.J., Ipsen, J.H., “Universal behavior of membranes with sterols,” *Biophys. J*., vol. 90, pp. 1639–1649, 2006.

[41] Doktorova, M., Heberle, F.A., Kingston, R.L., Khelashvili, G., Cuendet, M.A., Wen, Y., Katsaras, J., Feigenson, G.W., Vogt, V.M., Dick, R.A., “Cholesterol promotes protein binding by affecting membrane electrostatics and solvation properties,” *Biophys. J*., vol. 113, pp 2004–2015, 2017.

[42] Ashkar, R., Doktorova, M., Heberle, F.A., Scott, H., Kelley, E., Nagao, M., Usery, R., Barrera, F.N., Feigenson, G.W., Katsaras, J., Khelashvili, G., “Cholesterol affects the bending rigidity of DOPC membranes,” *Biophys. J.* vol. 116, pp 328a, 2019.

[43] Pan, J., Mills, T.T., Tristram-Nagle, S., Nagle, J.F., “Cholesterol Perturbs Lipid Bilayers Nonuniversally,” *Phys. Rev. Lett*., vol. 100, pp 198103, 2008.

[44] Pan, J., Tristram-Nagle, S., Nagle, J.F., “Effect of cholesterol on structural and mechanical properties of membranes depends on lipid chain saturation,” *Phys. Rev. E*., vol. 80, pp 021931, 2009.

[45] Gracià, R.S., Bezlyepkina, N., Knorr, R.L., Lipowsky, R., Dimova, R., “Effect of cholesterol on the rigidity of saturated and unsaturated membranes: fluctuation and electrodeformation analysis of giant vesicles,” *Soft Matter*, vol. 6, pp 1472–1482, 2010.

[46] Nagle, J.F., Jablin, M.S., Tristram-Nagle, S., Akabori, K., “What are the true values of the bending modulus of simple lipid bilayers?,” *Chem. Phys. Lipids*, vol. 185, pp 3–10, 2015.

[47] Meer, G.V., Voelker, D.R., Feigenson, G.W., "Membrane lipids: where they are and how they behave," *Nat. Rev. Mol. Cell Biol*., vol. 9, pp 112–124, 2008.

[48] Simons, K., Ikonen, E., "Functional rafts in cell membranes," *Nature,* vol. 387, pp 569–572, 1997.

[49] Silvius, J.R., "Role of cholesterol in lipid raft formation: lessons from lipid model systems," *Biochimica et Biophysica Acta (BBA) – Biomembranes*, vol. 1610, pp 174–183, 2003.

[50] Yeagle, P.L., "Cholesterol and the cell membrane," *Biochim. Biophys. Acta*, vol. 822, pp 267–287, 1985.

[51] Hinzpeter, A., Fritsch, J., Borot, F., Trudel, S., Vieu, D.L., Brouillard, F., Baudouin-Legros, M., Clain, J., Edelman, A., Ollero, M., "Membrane cholesterol content modulates ClC-2 gating and sensitivity to oxidative stress," *J biology Chem*, vol. 282, pp 2423–32, 2007.

[52] Pucadyil, T.J., Chattopadhyay, A., "Role of cholesterol in the function and organization of G-protein coupled receptors," *Prog. Lipid Res*., vol. 45, pp 295–333, 2006.

[53] Holthuis, J.C.M., Meer, G.V., Huitema, K., "Lipid microdomains, lipid translocation and the organization of intracellular membrane transport (Review)," *Mol. Membr. Biol*., vol. 20, pp 231–241, 2003.

[54] Evans, E., Heinrich, V., Ludwig, F., Rawicz, W., "Dynamic tension spectroscopy and strength of biomembranes," *Biophys J*., vol. 85, pp 2342–2350, 2003.

[55] Róg, T., Pasenkiewicz-Gierula, M., Vattulainen, I., Karttunen, M., "Ordering effects of cholesterol and its analogues," *Biochim. Biophys. Acta*, vol. 1788, pp 97–121, 2009.

[56] Evans, E., Smith, B.A., "Kinetics of hole nucleation in biomembrane rupture," *New J Phys.,* vol. 13, pp 095010, 2011.

[57] Semple, S.C., Chonn, A., Cullis, P.R., "Influence of cholesterol on the association of plasma proteins with liposomes,' *Biochemistry*, vol. 35, pp 2521–2525, 1996.

[58] Coderch, L., Fonollosa, J., De Pera, M., Estelrich, J., De La, M.A., Parra, J.L., "Influence of cholesterol on liposome fluidity by EPR. Relationship with percutaneous absorption," *J control release: official journal of the Controlled Release Society*, vol. 68, pp 85–95, 2000.

[59] Vasir, J.K., Labhasetwar, V., "Biodegradable nanoparticles for cytosolic delivery of therapeutics," *Adv. Drug Deliv*. *Rev.*, vol. 59, pp 718–728, 2007.

[60] Needham, D., Nunn, R.S., "Elastic deformation and failure of lipid bilayer membranes containing cholesterol," *Biophys. J*., vol. 58, pp 997–1009, 1990.

[61] Miller, L., Leor, J., Rubinsky, B., "Cancer cells ablation with irreversible electroporation," *Technol. Cancer Res. Treat*, vol. 4, pp 699–705, 2005.

[62] Al-Sakere, B., André, F., Bernat, C., Connault, E., Opolon, P., Davalos, R.V., Rubinsky, B., Mir, L.M., "Tumor ablation with irreversible electroporation," *PloS ONE*, vol. 2, pp e1135, 2007.

[63] Lian, T., Ho, R.J., "Trends and developments in liposome drug delivery systems," *J. Pharm. Sci*., vol. 90, pp 667–680, 2001.

[64] Malam, Y., Loizidou, M., Seifalian, A.M., "Liposomes and nanoparticles: nanosized vehicles for drug delivery in cancer," *Trends. Pharmacol. Sci.*, vol. 30, pp 592–599, 2009.

[65] Allen, T.M., Cullis, P.R., "Liposomal drug delivery systems: from concept to clinical applications," *Adv. Drug Deliv. Rev*., vol. 65, pp 36–48, 2013.

[66] Islam, M.Z., Alam, J.M., Tamba, Y., Karal, M.A.S., Yamazaki, M., "The single GUV method for revealing the functions of antimicrobial, pore-forming toxin, and cell-penetrating peptides or proteins," *Phys. Chem. Chem. Phys*., vol. 16, pp 15752–15767, 2014.

[67] Hasan, M., Karal, M.A.S., Levadnyy, V., Yamazaki, M., "Mechanism of initial stage of pore formation induced by antimicrobial peptide magainin 2," *Langmuir,* vol. 34, pp 3349–3362, 2018.

[68] Karal, M.A.S., Yamazaki, M., "Communication: Activation energy of tension-induced pore formation in lipid membranes," *J Chem Phys*, vol. 143, pp 081103, 2015.

[69] Karal, M.A.S., Levadnyy, V., Yamazaki, M., "Analysis of constant tension-induced rupture of lipid membranes using activation energy," *Phys. Chem. Chem. Phys.,* vol. 18, pp 13487–13495, 2016.

[70] Tsong, T.Y., "Electroporation of cell membranes. In: Neumann E., Sowers A.E., Jordan C.A. (eds) Electroporation and electrofusion in cell biology," *Springer*, Boston, MA, 1989.

[71] Sukharev, S.I., Klenchin, V.A., Serov, S.M., Chernomordik, L.V., Chizmadzhev, Y.A., "Electroporation and electrophoretic DNA transfer into cells. The effect of DNA interaction with electropores," *Biophys J.*, vol. 63, pp 1320–1327, 1992.

[72] Orlowski, S., Mir, L.M., "Cell electropermeabilization: a new tool for biochemical

and pharmacological studies," *Biochimica. Et. Biophysica. Acta. (BBA) — Reviews on Biomembranes*, vol. 1154, pp 51–63, 1993.

[73] Akimov, S.A., Volynsky, P.E., Galimzyanov, T.R., Kuzmin, P.I., Pavlov, K.V., Batishchev, O.V., "Pore formation in lipid membrane II: Energy landscape under external stress," *Sci. Rep*. vol. 7, pp 12509, 2017.

[74] Böckmann, R.A., de Groot, B.L., Kakorin, S., Neumann, E., Grubmuller, H., "Kinetics, statistics, and energetics of lipid membrane electroporation studied by molecular dynamics simulations," *Biophys J.*, vol. 95, pp 1837–1850, 2008.

[75] Levine, Z.A., Vernier, P.T., "Life cycle of an electropore: Field-dependent and field-independent steps in pore creation and annihilation," *J. Membrane Biol*., vol. 236, pp 27–36, 2010.

[76] Tarek, M., "Membrane electroporation: A molecular dynamics simulation," *Biophys. J*., vol. 88, pp 4045–4053, 2005.

[77] Tieleman, D.P., "The molecular basis of electroporation," *BMC Biochemistry,* vol. 5, pp 10, 2004.

[78] Cunill-Semanat, E., Salgado, J., "Spontaneous and stress-induced pore formation in membranes: Theory, experiments and simulations," *J. Membrane Biol*., vol. 252, pp 241–260, 2019.

[79] Tsong, T.Y., "Electroporation of cell membranes," *Biophys. J*., vol. 60, pp 297–306, 1991.

[80] Dev, S.B., Rabussay, D.P., Widera, G., Hofmann, G.A., "Medical applications of electroporation," *IEEE Transactions on Plasma Science*, vol. 28, pp 206–223, 2000.

[81] Koronkiewicz, S., Kalinowski, S., "Influence of cholesterol on electroporation of bilayer lipid membranes: chronopotentiometric studies," *Biochimica. Et. Biophysica. Acta (BBA) – Biomembranes*, vol. 1661, pp 196–203, 2004.

[82] Fernández, M.L., Marshall, G., Sagués, F., Reigada, R., "Structural and kinetic molecular dynamics study of electroporation in cholesterol-containing bilayers," *J. Phys. Chem. B.*, vol. 114, pp 6855–6865, 2010.

[83] Casciola, M., Bonhenry, D., Liberti, M., Apollonio, F., Tarek, M., "A molecular dynamic study of cholesterol rich lipid membranes: comparison of electroporation protocols," *Bioelectrochemistry*, vol. 100, pp 11–17, 2014.

[84] Jurkiewicz, P., Olżyńska, A., Cwiklik, L., Conte, E., Jungwirth, P., Megli, F.M., "Biophysics of lipid bilayers containing oxidatively modified phospholipids:

insights from fluorescence and EPR experiments and from MD simulations," *Biochim. Biophys. Acta*., vol. 1818, pp 2388–2402, 2012.

[85] Claessens, M.M.A.E., van Oort, B.F., Leermakers, F.A.M, Hoekstra, F.A., Cohen Stuart, M.A., "Charged Lipid Vesicles: Effects of salts on bending rigidity, stability, and size," *Biophys. J*. vol. 87, pp 3882–3893, 2004.

[86] Claessens, M.M.A.E., van Oort, B.F., Leermakers, F.A.M., Hoekstra, F.A., Cohen Stuart, M.A., "Bending rigidity of mixed phospholipid bilayers and the equilibrium radius of corresponding vesicles," *Phys Rev. E.*, vol. 76, pp 011903, 2007.

[87] Karal, M.A.S., Ahmed, M., Levadny, V., Belaya, M., Ahamed, M.K., Rahman, M., Shakil, M.M., "Electrostatic interaction effects on the size distribution of self-assembled giant unilamellar vesicles," *Phys. Rev. E*., vol. 101, pp 012404, 2020.

[88] Johnson, N.L., Kotz, S., Balakrishnan, N., "Continuous univariate distributions, 2nd ed," New York Wiley, 1994.

[89] Rawicz, W., Olbrich, K.C., McIntosh, T., Needham, D., Evans, E., "Effect of chain length and unsaturation on elasticity of lipid bilayers," *Biophys. J*., vol. 79, pp 328–339, 2000.

[90] Pan, J., Tristram-Nagle, S., Nagle, J.F., "Effect of cholesterol on structural and mechanical properties of membranes depends on lipid chain saturation," *Phys Rev. E*, vol. 80, pp 021931, 2009.

[91] Genova, J., Kralj-Iglic, V., Iglic, A., Marinov, R., Bivas, I., "Influence of cholesterol on the elastic properties of lipid membranes," *J Phys.*, vol. 398, pp 012037, 2012.

[92] Neumann, E., Schaefer-Ridder, M., Wang, Y., Hofschneider, P.H., "Gene transfer into mouse lyoma cells by electroporation in high electric fields," *The EMBO J.*, vol. 1 (7), pp 841–845, 1982.

[93] Chang, D.C., "Electroporation and Electrofusion", in Meyers, Robert A. (ed.), *Encyclopedia of Molecular Cell Biology and Molecular Medicine*, *Wiley-VCH Verlag GmbH & Co. KgaA*, 2006.

[94] Rubinsky, B., Onik, G., Mikus, P., "Irreversible electroporation: a new ablation modality—clinical implications," *Technol Can Res Treat*, vol. 6 (1), pp 37–48, 2007.

[95] Ringel-Scaia, V.M., Beitel-White, N., Lorenzo, M.F., Brock, R.M., Huie, K.E., Coutermarsh-Ott, S., "High-frequency irreversible electroporation is an effective

tumor ablation strategy that induces immunologic cell death and promotes systemic anti-tumor immunity," *EbioMedicine,* vol. 44, pp 112–125, 2019.

[96] Gissel, H., Lee, R.C., Gehl, J., "Electroporation and Cellular Physiology*," In Kee ST, Gehl J, Lee EW (eds.). Clin Asp Electrop., New York, NY: Springer New York*, pp 9–17, 2011.

[97] Zhang, Y., Lyu, C., Liu, Y., Lv, Y., Chang, T.T., Rubinsky, B., "Molecular and histological study on the effects of non-thermal irreversible electroporation on the liver," *Biochem Biophys Res Commun.*, vol. 500 (3), pp 665–670, 2018.

[98] "Outcomes of Ablation of Unresectable Pancreatic Cancer Using the NanoKnife Irreversible Electroporation (IRE) System," *https://www.clinicaltrials.gov/show/NCT02041936ClinicalTrials.gov*.

[99] Bulvik, B.E., Rozenblum, N., Gourevich, S., Ahmed, M., Andriyanov, A.V., Galun, E., Goldberg, S.N., "Irreversible Electroporation versus Radiofrequency Ablation: A Comparison of Local and Systemic Effects in a Small-Animal Model," *Radiology*, vol. 280 (2), pp 413–24, 2016.

[100] Scheffer, H.J., Stam, A.G., Geboers, B., Vroomen, L.G., Ruarus, A., de Bruijn, B., "Irreversible electroporation of locally advanced pancreatic cancer transiently alleviates immune suppression and creates a window for antitumor T cell activation," Oncoimmunology, vol. 8 (11), pp 1652532, 2019.

[101] Calvet, C.Y., Mir, L.M., "The promising alliance of anti-cancer electrochemotherapy with immunotherapy," *Cancer Metastasis Rev*, vol. 35 (2), pp 165–77, 2016.

[102] Pandit, H., Hong, Y.K., Li, Y., Rostas, J., Pulliam, Z., Li, S. P., Martin, R.C., "Evaluating the Regulatory Immunomodulation Effect of Irreversible Electroporation (IRE) in Pancreatic Adenocarcinoma," *Ann Surg Oncol.,* vol. 26 (3), pp 800–806, 2019.

[103] Rubinsky, B., Onik, G., Mikus, P., "Irreversible Electroporation: A New Ablation Modality — Clinical Implications," *Tech. Can. Res. Treat.*, vol. 6, pp 37–48, 2007.

[104] Riske, K.A., Knorr, R.L., Dimova, R., "Bursting of charged multicomponent vesicles subjected to electric pulses," *Soft matter,* vol. 5, pp. 1983–1986, 2009.

[105] Karal, M.A.S., Levadnyy, V., Tsuboi, T.A., Belaya, M., Yamazaki, M., "Electrostatic interaction effects on tension-induced pore formation in lipid membranes," *Phys Rev. E*, vol. 92, pp 012708, 2015.

[106] Levadny, V., Tsuboi, T.A., Belaya, M., Yamazaki, M., "Rate constant of tension-induced pore formation in lipid membranes," Langmuir, vol. 29, pp 3848-52, 2013.

[107] Israelachvili, J.N., Intermolecular and Surface Forces, Academic Press, New York, 1992.

[108] Karal, M.A.S., Orchi, U.S., Towhiduzzaman, M., Ahamed, M.K., Ahmed, M., Ahammed, S., Mokta, N.A., Sharmin, S., Sarkar, M.K., "Electrostatic effects on the electrical tension-induced irreversible pore formation in giant unilamellar vesicles," *Chem. Phys. Lipids*, vol. 231, pp 104935, 2020.

[109] Liu, J., Kaksonen, M., Drubin, D.G., Oster, G., "Endocytic vesicle scission by lipid phase boundary forces," *Proc. Natl. Acad. Sci. U.S.A.*, vol. 103, pp 10277, 2006.

[110] McMahon, H.T., Gallop, J.L., *Nature*, vol. 438, pp 590, 2005.

[111] Chernomordik, L., Kozlov, M., Zimmerberg, J., "Lipids in biological membrane fusion," *J. membr. Biol.*, vol. 146, pp 1, 1995.

[112] Helfrich, W., "Elastic properties of lipid bilayers theory and possible experiments," *Z Naturforsch*, vol. 28, pp 693–703, 1973.

[113] Helfrich, W., Servuss, R.M., "Undulations, steric interaction and cohesion of fluid membranes," *Il nuovo cimento*, vol. 3, pp 137–151, 1984.

[114] Hianik, T., "Structure and physical properties of biomembranes and model membranes," *Acta Physica Slovaca*, vol. 56, pp 687 – 805, 2006.

[115] Walde, P., Cosentino, K., Engel, H., Stano, P., "Giant Vesicles: Preparations and Applications", *Chem. Bio. Chem.,* vol**.** 11, pp 848–865 2010.

[116] Shohda, K., Takahashi, K., Suyama, A., "A method of gentle to hydration prepare oil free giant unilamellar vesicles that can confine enzymatic reactions", *Biochem. Biophys. Rep.*, vol. 3, pp 76–82, 2015.

[117] Altamura, E., Carrara, P., D'Angelo, F., Mavelli, F., Stano, P., "Extrinsic stochastic factors (solute partition) in gene expression inside lipid vesicles and lipid-stabilized water-in-oil droplets: a review*", Synth. Biol. J.*, vol. 3, 2018.

[118] *https://www.bioexplorer.net/phospholipid-bilayer.html/*

[119] Pautot, S., Frisken, B.J., Weitz, D.A., "Production of Unilamellar Vesicles Using an Inverted Emulsion", *Langmuir,* vol. 19, pp 2870–2879, 2003.

[120] Kagan, B.L., Selsted, M.E., Ganz, T., Lehrer, R.I., "Antimicrobial Defensin Peptides Form Voltage-Dependent Ion-Permeable Channels in Planar Lipid Bilayer Membranes", *Proc. Natl. Acad. Sci. U. S. A*., vol. 87, pp 210–214, 1990.

[121] "Phospholipid Bilayer." *BioNinja, ib.bioninja.com.au/standard-level/topic-1-cell-biology/13-membrane-structure/phospholipid-bilayer.html*.

[122] Sadava, D., Hillis, D.M., Heller, H.C., Berenbaum, M.R., "Life: The Science of Biology," vol. 9, pp. 105–114, 2011.

[123] Mishra, G.P., Bagui, M., Tamboli, V., Mitra, A.K., "Recent applications of liposomes in ophthalmic drug delivery", *J Drug Deliv*., vol. 2011, pp. 863734, 2011.

[124] Dimova, R., Aranda, S., Bezlyepkina, N., Nikolov, V., Riske, K.A., Lipowsky, R., "A practical guide to giant vesicles. Probing the membrane nanoregime via optical microscopy," *J. Phys. Condens Matter Inst. Phys. J*. vol. 18, pp 1151-1176, 2006.

[125] Falck, E., Patra, M., Karttunen, M., Hyvönen, M.T., Vattulainen, I., "Lessons of slicing membranes: interplay of packing, free area, and lateral diffusion in phospholipid/cholesterol bilayers," *Biophys. J*. vol. 87, pp 1076–1091, 2004.

[126] Alwarawrah, M., Dai, J., Huang, J., "A molecular view of the cholesterol condensing effect in DOPC lipid bilayers," *J. Phys. Chem. B*, vol. 114, pp 7516–7523, 2010.

[127] Armstrong, C.L., Marquardt, D., Dies, H., Kučerka, N., Yamani, Z., Harroun, T. A., Katsaras, J., Shi, A.C., Rheinstädter, M.C., "The observation of highly ordered domains in membranes with cholesterol," *PLOS ONE*, vol. 8, pp 66162, 2013.

[128] Magarkar, A., Dhawan, V., Kallinteri, P., Viitala, T., Elmowafy, M., Róg, T., Bunker, A., "Cholesterol level affects surface charge of lipid membranes in saline solution," *Sci. Rep.,* vol. 4, pp 1–5, 2014.

[129] De Meyer, F., Smit, B., "Effect of cholesterol on the structure of a phospholipid bilayer," *Proc. Natl. Acad. Sci. USA*, vol. 106, pp 3654–3658, 2009.

[130] Kheyfets, B., Mukhin, S., "Area per lipid in DPPC-cholesterol bilayers: Analytical Approach," 2015.

[131] Dimova, R., Bezlyepkina, N., Jordö, M.D., Knorr, R.L., Riske, K.A., Staykova, M., Vlahovska, P.M., Yamamoto, T., Yang, P., Lipowsky, R., "Vesicles in electric fields: Some novel aspects of membrane behavior," *Soft Matter*, vol. 5, pp 3201, 2009.

[132] Abidor, I.G., Arakelyan, V.B., Chernomordik, L.V., Chizmadzhev, Y.A., Pastushenko, V.F., Tarasevich, M.R., "Electric breakdown of bilayer lipid membranes: I. The main experimental facts and their qualitative discussion," *J Electroanal Chem Interf Electrochem*, vol. 104, pp 37–52, 1979.

[133] Riske, K.A., Dimova, R., "Electro-deformation and poration of giant vesicles viewed with high temporal resolution," *Biophysical Journal*, vol. 88, pp 1143–1155, 2005.

[134] Lisin, R., Ginzburg, B.Z., Schlesinger, M., Feldman, Y., "Time domain dielectric spectroscopy study of human cells. I. Erythrocytes and ghosts," *Biochim Biophys Acta (BBA)*, vol. 1280, pp 34–40, 1996.

[135] Simon, S.A., McIntosh, T.J., "Depth of water penetration into lipid bilayers. In: Methods in Enzymology," *Academic Press*, pp 511–521, 1986.

[136] Dimova, R., Riske, K.A., Aranda, S., Bezlyepkina, N., Knorr, R.L., Lipowsky, R., "Giant vesicles in electric fields," *Soft Matter*, vol. 3, pp 817, 2007.

[137] Zupanc, J., Drašler, B., Boljte, S., Kralj-Iglič, V., Iglič, A., Erdogmus, D., Drobne, D., "Lipid vesicle shape analysis from populations using light video microscopy and computer vision," *PLOS ONE*, vol. 9, pp 113405, 2014.

[138] Johnson, S.M., "The effect of charge and cholesterol on the size and thickness of sonicated phospholipid vesicles," *Biochim. Biophys. Acta. BBA – Biomembr.,* vol. 307, pp 27–41, 1973.

[139] Marsh, D., "Intrinsic curvature in normal and inverted lipid structures and in membranes," *Biophys. J.*, vol. 70, pp 2248–55, 1996.

[140] Fischer, T.M., "Bending stiffness of lipid bilayers. II. Spontaneous curvature of the monolayers," *J. Phys. II*, vol. 2, pp 327–336, 1992.

[141] Fischer, T.M., "Bending stiffness of lipid bilayers. V. Comparison of two formulations," *J. Phys. II*, vol. 3, pp 1795–1805, 1993.

[142] Faizi, H.A., Frey, S.L., Steinkühler, J., Dimova, R., Vlahovska, P.M., "Bending rigidity of charged lipid bilayer membranes," *Soft Matter*, vol. 15, pp 6006–6013, 2019.

[143] Landau, L.D., Lifshitz, E.M., "Statistical physics," *Pergamon press*., 1969.

[144] Marsh, D., "Renormalization of the tension and area expansion modulus in fluid membranes," *Biophys. J.*, vol. 73, pp 865–869, 1997.

[145] Tamba, Y., Terashima, H., Yamazaki, M., "A membrane filtering method for the purification of giant unilamellar vesicles," *Chem. Phys. Lipids*, vol. 164, pp 351–

358, 2011.

[146] Goetz, R., Gompper, G., Lipowsky, R., “Mobility and elasticity of self-assembled membranes,” *Phys. Rev. Lett*., vol. 82, pp 221–224, 1999.

[147] Boal, D., Boal, D.H., “Mechanics of the cell,” *Cambridge University Press*, 2002.

[148] Levadny, V., Tsuboi, T., Belaya, M., Yamazaki, M., “Rate constant of tension-induced pore formation in lipid membranes,” *Langmuir*, vol. 29, pp 3848–3852, 2013.

[149] Litster, J.D., “Stability of lipid bilayers and red blood cell membranes,” *Physics Letters A*, vol. 53, pp 193–194, 1975.

[150] Taupin, C., Dvolaitzky, M., Sauterey, C., “Osmotic pressure-induced pores in phospholipid vesicles,” *Biochemistry*, vol. 14, pp 4771–4775, 1975.

[151] Tieleman, D.P., Leontiadou, H., Mark, A.E., Marrink, S.J., “Simulation of pore formation in lipid bilayers by mechanical stress and electric fields,” *J. Am Chem. Soc.*, vol. 125, pp 6382–6383, 2003.

[152] Wohlert, J., den Otter, W.K., Edholm, O., Briels, W.J., “Free energy of a trans-membrane pore calculated from atomistic molecular dynamics simulations,” *J. Chem. Phys*., vol. 124, pp 154905, 2006.

[153] Portet, T., Dimova, R., “A New Method for Measuring Edge Tensions and Stability of Lipid Bilayers: Effect of Membrane Composition,” *Biophysical Journal*, vol. 99, pp 3264-73, 2010.

[154] Needham, D., Hochmuth, R.M., ‘Electro-mechanical permeabilization of lipid vesicles. Role of membrane tension and compressibility,” *Biophys J.*, vol. 55, pp 1001–1009, 1989.

[155] Zhelev, D.V., Needham, D., “Tension-stabilized pores in giant vesicles: determination of pore size and pore line tension,” *Biochim. Biophys. Acta*., vol. 1147, pp 89–104, 1993.

[156] Karatekin, E., Sandre, O., Guitouni, H., Borghi, N., Puech, P.H., Brochard-Wyart, F., “Cascades of transient pores in giant vesicles: line tension and transport,” *Biophys. J.,* vol. 84, pp 1734–1749, 2003.

APPENDIX

PUBLICATIONS

Peer Reviewed Journals

1. Effects of cholesterol on the size distribution and bending modulus of lipid vesicles [Under review]

Authors: Mohammad Abu Sayem Karal, **Nadia Akter Mokta**, Victor Levadny, Marina Belaya, Marzuk Ahmed, Md. Kabir Ahamed, and Shareef Ahammed.

2. Influence of cholesterol on electroporation in lipid membrane of giant vesicles

Authors: Mohammad Abu Sayem Karal, Md. Kabir Ahamed, **Nadia Akter Mokta**, Marzuk Ahmed , Shareef Ahammed.

Journal: European Biophysics Journal (Springer Nature), Vol. 49, pp. 361-370, 2020

Conference Presentations:

2. Nadia Akter Mokta, Marzuk Ahmed, Shareef Ahammed, Md. Kabir Ahamed, Malay Kumar Sarkar, Mohammad Abu Sayem Karal; Estimation of Bending Modulus of Cholesterol-rich Membranes Using the Size Distribution of Self-Assembled Vesicle (PP-11) International Conference on Physics, Organized by BPS, Dhaka, Bangladesh, 05-07 March, 2020,(Poster Presentation), page. 129

2. **Nadia Akter Mokta**, Marzuk Ahmed, Md. Kabir Ahamed, Shareef Ahammed, Malay Kumar Sarkar, Mohammad Abu Sayem Karal: Estimation of Bending and Elastic Modulus of Cholesterol Containing Membranes using Size Distribution of Self-Assemble Vesicles (CP-22) International Conference on Physics in Medicine, Organized by BAEC, BMPA and BMPT-DU, Dhaka, Bangladesh, 06-07 February, 2020 (Oral Presentation), page. 49

3. **Nadia Akter Mokta**, Malay Kumar Sarkar, Marzuk Ahmed, Md. Kabir Ahamed, Shareef Ahammed, Mohammad Abu Sayem Karal: Effects of Cholesterol on the Size Distribution and Average size of Giant Unilamellar Vesicles (Abstract-PP-47) National Conference on Electronics and Informatics, Organized by BEIS and BAEC, Dhaka, Bangladesh, 04-05 December, 2019 (Poster Presentation), page. 95